Title

Who gets infected and why: Confronting models with data to determine drivers of pathogen susceptibility at the individual and population-level

Author

Gostic, Katelyn M

Publication Date

2019

Peer reviewed|Thesis/dissertation

UNIVERSITY OF CALIFORNIA

Los Angeles

Who gets infected and why: Confronting models with data to determine drivers of pathogen susceptibility at the individual and population-level

A dissertation submitted in partial satisfaction

of the requirements for the degree

Doctor of Philosophy in Biology

by

Katelyn Marie Gostic

2019

ABSTRACT OF THE DISSERTATION

Who gets infected and why: Confronting models
with data to determine drivers of pathogen susceptibility
at the individual and population-level

by

Katelyn Marie Gostic
Doctor of Philosophy in Biology
University of California, Los Angeles, 2019
Professor James O. Lloyd-Smith, Chair

Host susceptibility is a foundational concept in infectious disease dynamics. Susceptible individuals are the fuel that allows outbreaks to grow and spread. Once an epidemic takes hold, depletion of susceptible hosts (through new infections) eventually drives the effective reproduction number (R_{eff}) below 1*, causing the outbreak to stutter and fade. Eventually, the demographic buildup of new susceptible hosts (via new births) creates conditions hospitable to a

* R_{eff} is defined as the expected number of new cases caused by a single infectious individual in a partially immune population, and is proportional to the fraction of susceptible individuals. When R_{eff} falls below 1, new cases do not replace themselves, on average, and the outbreak ceases to grow.

new epidemic cycle. Ultimately, the fraction of the population susceptible to a given pathogen, and heterogeneity in individual susceptibility by age, by birth year or by physiological status, determine whether a pathogen can spread and persist in a given host population.

Despite its crucial importance, understanding how host susceptibility is distributed across populations is a perennial challenge. Many pathogens of humans and animals have complex strain structure, with partial cross-protection acting among a variety of serotypes. Immunity to other pathogens may wane over time, or may reduce disease severity without entirely preventing infection. For the myriad pathogens with these characteristics, host susceptibility can be difficult to model and difficult to measure, even when serological data on antibody titers is available.

Individual susceptibility is an emergent property of within-host interactions between pathogens and immune effectors. The specific immune interactions that determine susceptibility are often pathogen-specific, and difficult to observe. However, individual-level data on infection outcomes, or population-level epidemiological data are abundant. Statistical analysis of these existing data can help identify host-level factors that govern individual susceptibility. In turn these insights can be used to improve our understanding of how susceptibility is distributed across the population, and predictions of epidemic spread. These inferences can also provide clues to the underlying molecular drivers of host immunity against specific pathogens.

In chapter 1, I compile publicly available data on two avian influenza viruses, H5N1 and H7N9, which have each spilled over to cause hundreds of human cases. I perform likelihood-based model comparison on these data to show that individuals gain exceptionally strong, lifelong protection against avian influenza subtypes in the same phylogenetic group as the first influenza virus encountered in childhood. These results show that susceptibility varies

systematically with birth year, and challenge the long-standing assumption that antigenically novel, zoonotic or pandemic influenza viruses escape pre-existing immunity when they spill over to cause cases in humans. These results can help explain why certain birth years have been spared during past influenza pandemics, and may help improve birth year-specific forecasts of future pandemic risk. Further, these results suggest an antigenic basis for naturally-occurring, broadly protective influenza immunity.

In chapter 2, I analyze a large epidemiological surveillance data set to ask whether the same patterns of broadly protective childhood immune imprinting shape birth year-specific risk from the seasonal influenza viruses that cause wintertime epidemics in humans. Model selection shows that seasonal influenza risk from subtypes H1N1 and H3N2 is indeed tied to birth year, and shaped by childhood immune imprinting. However, unlike for avian influenza, immune cross-protection acts more narrowly. Individuals only gain imprinting protection against seasonal influenza viruses of the very same antigenic subtype as the first virus encountered in childhood.

Together, results from chapters 1 and 2 provide a partial proof of concept for development of universal influenza vaccines. Chapter 1 illustrates that the sort of broadly protective immune responses that universal vaccines would aim to elicit can already act naturally in human populations, and in certain epidemic contexts, already seem to shape population susceptibility. But chapter 2 highlights the difficulty of deploying these broadly protective immune responses against familiar, high-burden seasonal strains. Taken alongside recent immunological evidence, these results suggest that the breadth of immune cross-protection against influenza viruses is not fixed, but instead is an emergent property of within-host competition between B cell (antibody-producing) clones. On exposure to a familiar, seasonal

influenza virus, narrowly-protective B cell clones competitively exclude broadly protective clones, and the antibody response provides only narrow immune cross-protection, against a single viral subtype. But on exposure to a novel, avian influenza virus, the host may only recognize conserved viral epitopes, and more broadly protective B cell clones are transiently released from competition.

In chapter 3, I shift my focus from childhood imprinting history to explore another dimension of host susceptibility, the role of physical immune barriers in infection resistance. I develop a mechanistic dose-response model to identify factors that limit the spillover of an environmentally abundant bacterial pathogen, *Leptospira interrogans.* Hosts living in contaminated environments may be exposed to low doses of *Leptospira* on a daily basis, yet not all become infected. Using data from animal challenge experiments, we show that broken skin is most likely necessary for low-dose environmental exposures to cause infection.

Together, these studies illustrate that heterogeneity in host susceptibility can be linked to measurable, underlying drivers. Demographic factors like year of birth, and immune history predictably modulate susceptibility to specific influenza virus subtypes. Physiological factors, like the presence of wounds and abrasions, predictably modulate susceptibility to environmentally persistent bacterial pathogens like *Leptospira*. By developing models based on biological principles and then confronting those models with data, we can identify specific risk factors that govern individual susceptibility against specific pathogens. Scaling these insights up to the population level can improve our ability to estimate key epidemiological parameters and can help guide the distribution of limited treatment or prevention resources during outbreaks.

The dissertation of Katelyn Marie Gostic is approved.

Priyanga A. Amarasekare

Van Maurice Savage

Michael Worobey

James O. Lloyd-Smith, Committee Chair

University of California, Los Angeles

2019

To my parents, who gave me the world.

TABLE OF CONTENTS

LIST OF FIGURES

LIST OF SUPPLEMENTARY FIGURES

LIST OF TABLES

LIST OF SUPPLEMENTARY TABLES

ACKNOWLEDGEMENTS

To my advisor, Jamie Lloyd-Smith, for his patience, guidance and mentorship across the past six years. I am so lucky to have found a mentor who cares about his students both as scientists and as people. Thank you for all you've taught me, for your unwavering support through the ups and the downs, and for all the doors you've helped me open.

I also owe a huge thank you to Mike Worobey, who first realized that childhood exposures might shape immunity against emerging, avian influenza viruses. Thank you Mike for generously sharing your brilliant idea, and for helping me build a dissertation around it.

To my committee members, Van Savage and Priyanga Amarasekare, and my reading committee member, Pamela Yeh. Together, you taught me so much, you helped me find a postdoc, and your examples helped me see that successful scientists don't all fit the same mold.

I am grateful to all the past and current members of the Lloyd-Smith lab, who have been great friends and who helped me learn. Monique Ambrose, my lab sister. You are one of the kindest, smartest people I've ever met. I'm so lucky to have shared an office with you. Katie Prager, you have been my rock, and an endless fountain of good advice.

To all my collaborators and co-authors, especially those who were patient with me at the beginning. To Adam Kucharski, who bravely helped me write my first paper ever, and then guided me through my first peer review. To Bryan Grenfell, who for reasons I still don't fully understand, started advocating for me back when I was still just a naïve undergraduate and helped me figure out how to become a scientist. To Cecile Viboud, who has always made me feel welcome, and who is always willing to read my drafts. Thank you to anyone who has ever

written me a letter of recommendation. There are so many of you. I applied for so many things (and was rejected from most of them) but you kept coming through for me.

To friends who made LA feel like home. To Annabel Beichman and Jeff Potts for bad dinner parties and incredible friendship. To Jackie Liu, Emily Ryznar, Alex Zarem and Tyler McCraney, for filling my life with frothiness, optimism and good times.

Thank you to my family. To my dad who taught me to love science, and to my mom who warned me that I was choosing a hard path, but who supported me anyway when I decided to do a PhD. To my grandmother, who taught me the "at" family, and my grandfather, who loved to brag about his grandkids. I could not have made it this far without you behind me.

Thank you to Andy and Gaye, for taking me in and becoming my second family. At first, you fed me dinners and helped me find my feet in a big strange city. Eventually, you gave me a home to come back to as I was finishing my degree. I can't thank you enough for all your generosity, your gardening advice, and for the use of your magic parking permit. Seeing you has made me look forward to each of my treks back to LA over the past year, and I can't wait for more adventures in the future.

And finally, thank you to Charlie. You believed in me even when I didn't believe in myself. You pushed me forward whenever I started to flounder, but also taught me the importance of hobbies and weekends off. You encourage me to chase after exciting opportunities, and even when the path ahead looks unclear, you convince me that I don't have to choose between my career and our relationship. I am a better person, and a better scientist, with you by my side.

Chapter 1 is the accepted version of a manuscript, now published as: Gostic KM, Ambrose M, Worobey M, Lloyd-Smith JO. Potent protection against H5N1 and H7N9 influenza via childhood hemagglutinin imprinting. *Science*. 2016, Nov 11;354(6313):722–6. DOI: 10.1126/science.aag1322. MW conceived of the idea for the study. KG compiled the data with help from MRA, as well as two undergraduate volunteers, Thais Mega and Samuel Wu. JLS and KG developed the modeling analyses. KG analyzed the avian influenza data and MRA simulated projected impacts on pandemic age distributions of infection. MW analyzed genetic similarities between strains. All authors helped interpret the results and write and revise the manuscript. We thank the Lloyd-Smith lab and the Worobey lab for helpful comments, C. Viboud for providing insight into historic influenza data, T. Mega and S. Wu for assistance compiling data, B. Cowling for sharing poultry exposure data, and P. Horby for sharing Vietnam contact data.

Chapter 2 is a version of a manuscript currently in peer review: **Gostic, K.M**., Bridge, R., Brady, S., Viboud, C. Worobey, M., Lloyd-Smith, J.O. (2019) Childhood immune imprinting to influenza A shapes birth year-specific risk during seasonal H1N1 and H3N2 epidemics. *PLoS Pathogens*. Submitted. Pre-print on medRxiv. https://doi.org/10.1101/19001834. MW, KG and JLS conceived of the questions and modeling analysis. CV and MW provided crucial assistance with data access and study design. SB and RB supervised data curation and advised the modeling arm of our team about compatibility between the data and analysis strategy. KG wrote the code and performed analyses, with supervision from JLS, and drafted the manuscript. All authors provided input on analysis and interpretation of the results, and helped revise and edit the manuscript text. We are grateful to Ken Komatsu and Kristen Herrick for their assistance with

data access, and to Trevor Bedford for assistance accessing and interpreting antigenic distance data from *Nextstrain*. We thank Lone Simonsen for helpful discussions.

Chapter 3 is the accepted version of a manuscript in press: **Gostic, K.M**., Wunder, E.A. Jr., Bisht, V., Hamond, C., Julian, T.R., Ko, A.I., Lloyd-Smith, J.O. Mechanistic dose-response modeling of animal challenge data shows that intact skin is a crucial barrier to leptospiral infection. *Phil. Trans. B.* In press. DOI: 10.1098/rstb.2019.0367. EAWJ and AIK conceived the study. EAWJ, VB, and CH developed the experimental protocol and collected the data. TJ, JLS, and KG developed the modeling methods. KG wrote the code and analyzed the data with guidance from JLS. KG and EAWJ drafted the manuscript. All authors critically revised the manuscript, gave final approval for publication and agree to be held accountable for the work performed therein.

This dissertation would not have been possible without funding from the Eugene V. Cota-Robles Foundation, from the UCLA Dean's Scholar program, and from the National Institutes of Health (F31AI134017, T32-GM008185). I also gratefully acknowledge funding from the UCLA Department of Ecology and Evolutionary Biology, and from UCLA Graduate Division for travel and research expenses. The funders had no role in data analysis, study design or interpretation of results. These findings do not necessarily represent the views of the US Government.

VITA

EDUCATION

AB, Ecology & Evolutionary Biology, Princeton University, Princeton, NJ. (2013)

FELLOWSHIPS AND AWARDS

1) **James S. McDonnell Foundation: Understanding Dynamic and Multi-scale Systems Postdoctoral Fellowship**, $200,000 (planned 2019-2021)
2) **NRSA Predoctoral Fellowship** (NIAID F31AI134017), $55,125+fees (2017-2019)
3) **Scherbaum Award**, outstanding research by a graduate student, UCLA EEB, $200 (2018)
4) **Invited session co-chair,** 6th European Scientific Working Group on Influenza Conference, Riga, Latvia, (travel and accommodations) (2017)
5) **Charles E. and Sue K. Young Award**, UCLA Graduate Division, $10,000 (2016)
6) **Carol Newton Legacy Poster Prize**, UCLA Dept. Biomathematics, $100 (2015)
7) **Systems and Integrative Biology Training Grant**, $48,000+fees (2014-2016)
8) **Eugene V. Cota-Robles Foundation Fellowship**, $56,000+fees (2013, 2016)

PUBLICATIONS

* Authors contributed equally

1) **Gostic, K.M***., Wunder, E.A*. Jr., Bisht, V., Hamond, C., Julian, T.R., Ko, A.I., Lloyd-Smith, J.O. Mechanistic dose-response modeling of animal challenge data shows that intact skin is a crucial barrier to leptospiral infection. *Phil. Trans. B.* In press. DOI: 10.1098/rstb.2019.0367.
2) Morris, D.H.,* **Gostic, K.M.**,* Pompei, S.,* Bedford, T., Łuksza, M., Neher, R.A., Grenfell, B.T., Lässig, M., McCauley, J.W. (2018) Predictive modeling of influenza shows the promise of applied evolutionary biology. *Trends in Microbiology.* **26,** 102-118. DOI: https://doi.org/10.1016/j.tim.2017.09.004
3) **Gostic, K.M.,** Ambrose, M., Worobey, M., Lloyd-Smith, J.O. (2017) Maternal antibodies' role in immunity -- Response. *Science.* **355**, 705. DOI: 10.1126/science.aam7389
4) **Gostic, K.M.,** Ambrose, M., Worobey, M., Lloyd-Smith, J.O. (2016) Potent protection against H5N1 and H7N9 influenza via childhood hemagglutinin imprinting. *Science.* **354,** 722-726. DOI: 10.1126/science.aag1322
5) Buhnerkempe M.G.*, **Gostic K.M.***, Park M., Ahsan P., Belser J.A., Lloyd-Smith J.O. (2015) Mapping influenza transmission in the ferret model to transmission in humans. *eLife.* 4:e07969. DOI: 10.7554/eLife.07969
6) **Gostic, K.M.*** Kucharski, A*. Lloyd-Smith, J. O. (2015) Natural history of infection influences effectiveness of screening measures for emerging pathogens. *eLife*. 4:e05564. DOI: 10.7554/eLife.05564

SELECT PRESENTATIONS

1) Ecology and Evolution of Infectious Diseases, Princeton University (Talk) 2019
2) Workshop on Immunity, Aging and the Arrow of Time, Santa Fe Institute (Talk) 2019
3) Theoretical Biology Group, Los Alamos National Laboratory (Seminar) 2019
4) NIH Workshop on Universal Influenza Vaccines (Talk) 2018
5) NIH Vaccine Research Center, Bethesda MD (Seminar) 2017
6) European Scientific Working Group on Influenza 6th Conference, Riga, Latvia (Talk) 2017
7) Occidental College, Los Angeles, CA (Invited Seminar) 2017
8) Joint Training Grant Research Symposium, UCLA, Los Angeles, CA (Talk) 2015
9) Ecological Society of America 2016 Annual Meeting, Ft. Lauderdale, FL (Talk) 2016
10) WHO workshop on models for influenza vaccine design, Princeton, NJ (Talk) 2016

TEACHING AND SERVICE

1) **Teaching assistantships**: Math for Life Scientists, UCLA Division of Life Sciences, (2018); Modeling in Ecological Research, UCLA Ecology and Evolutionary Biology (2016); Research Immersion Lab, UCLA Microbiology, Immunology and Molecular Genetics (2014) 2018; Volunteered as a summer teaching assistant in 5th Grade Math at KIPP DC AIM Academy, Anacostia DC (2010)
2) **Outreach activities**: Developed and led an activity at DNA Day, (on-campus event for LA middle school students), UCLA Dept. of Human Genetics, (2015, 2016, 2017, 2018); Developed and led an activity at EmpowHer STEM Day (on-campus event for LA middle school girls), UCLA Empowering Women in Science, (2014, 2015); Visiting scientist, Science Lunch Friday, University High School, Los Angeles, CA (2013)
3) **Department service:** Founded and coordinated Eco-Evo Careers, (career discussion series for UCLA EEB Graduate Students) (2016, 2017); Organized UCLA EEB Graduate Student Seminar Series (Eco-Evo Pub) (2014-2015); Assisted at R Boot Camp for incoming graduate students (2014-2019)
4) **Peer review**: I have reviewed scholarly articles for PLoS Computational Biology, the Journal of the Royal Society Interface, the American Journal of Epidemiology, and Epidemiology and Infection.

PRESS

My research has been featured by several major news outlets, including the Economist, the Atlantic, NBC, CNN, AAAS Science Podcast, the NIH Director's Blog & the BBC Word Service. Links found at kgostic.github.io.

Chapter 1: Potent Protection against H5N1 and H7N9 Influenza via Childhood Hemagglutinin Imprinting

ABSTRACT

Two zoonotic influenza A viruses (IAV) of global concern, H5N1 and H7N9, exhibit unexplained differences in age distribution of human cases. Using data from all known human cases of these viruses, we show that an individual's first IAV infection confers lifelong protection against severe disease from novel hemagglutinin (HA) subtypes in the same phylogenetic group. Statistical modeling shows protective HA imprinting is the crucial explanatory factor, providing 75% protection against severe infection and 80% protection against death for both H5N1 and H7N9. Our results enable us to predict age distributions of severe disease for future pandemics and demonstrate that a novel strain's pandemic potential increases yearly when a group-mismatched HA subtype dominates seasonal influenza circulation. These findings open new frontiers for rational pandemic risk assessment.

ONE SENTENCE SUMMARY

Influenza strains encountered during early childhood provide powerful long-term protection against novel HA subtypes of the same phylogenetic group.

MAIN TEXT

The spillover of novel influenza A viruses (IAV) is a persistent threat to global health. H5N1 and H7N9 are particularly concerning avian-origin IAVs, each having caused hundreds of severe or fatal human cases (*1*). Despite commonalities in their reservoir hosts and epidemiology, these viruses show puzzling differences in age distribution of observed human cases (*1*,*2*). Existing explanations, including possible protection against H5N1 among older birth-year cohorts exposed to the neuraminidase of H1N1 as children (*3*,*4*) or age biases in exposure to infected poultry (*5–7*), cannot fully explain these opposing patterns of severe disease and mortality. Another idea is that severity of H5N1 and H7N9 differs by age, leading to case ascertainment biases (*1*), but no explanatory mechanism has been proposed.

The key antigenic determinants for IAV susceptibility are the virus's two surface glycoproteins, hemagglutinin (HA) and neuraminidase (NA), where different numbered subtypes canonically indicate no cross-immunity. However, recent experiments have revealed that broadly-protective immune responses can provide cross-immunity between different HA subtypes, particularly subtypes in the same phylogenetic group (*8–14*). (HA group 1 contains (human seasonal) subtypes H1, H2 and avian H5, while group 2 contains seasonal H3 and avian H7; Fig. 1-1A, Fig. 1-S1). Combining these insights into heterosubtypic immunity with the concept of 'original antigenic sin' (*15*) or 'antigenic seniority' (*16*), we hypothesized that individuals imprint on the HA group of their first IAV exposure and thereby experience a reduced risk of severe disease from novel IAVs within that same phylogenetic group. This hypothesis predicts that the 1968 pandemic, which marked the transition from an era of group 1 HA circulation (1918-1968) to a group 2-dominated one (1968-present) (Fig. 1-1B), caused a

major shift in population susceptibility that would explain why H5N1 cases are generally detected in younger people than H7N9 (*2*,*17*–*19*). Our analysis of human cases of H5N1 and H7N9 revealed strong evidence that childhood HA imprinting indeed provides profound, lifelong protection against severe infection and death from these viruses. These findings allowed us to develop new approaches for IAV pandemic risk assessment, preparedness and response, but also raise possible challenges for future vaccination strategies.

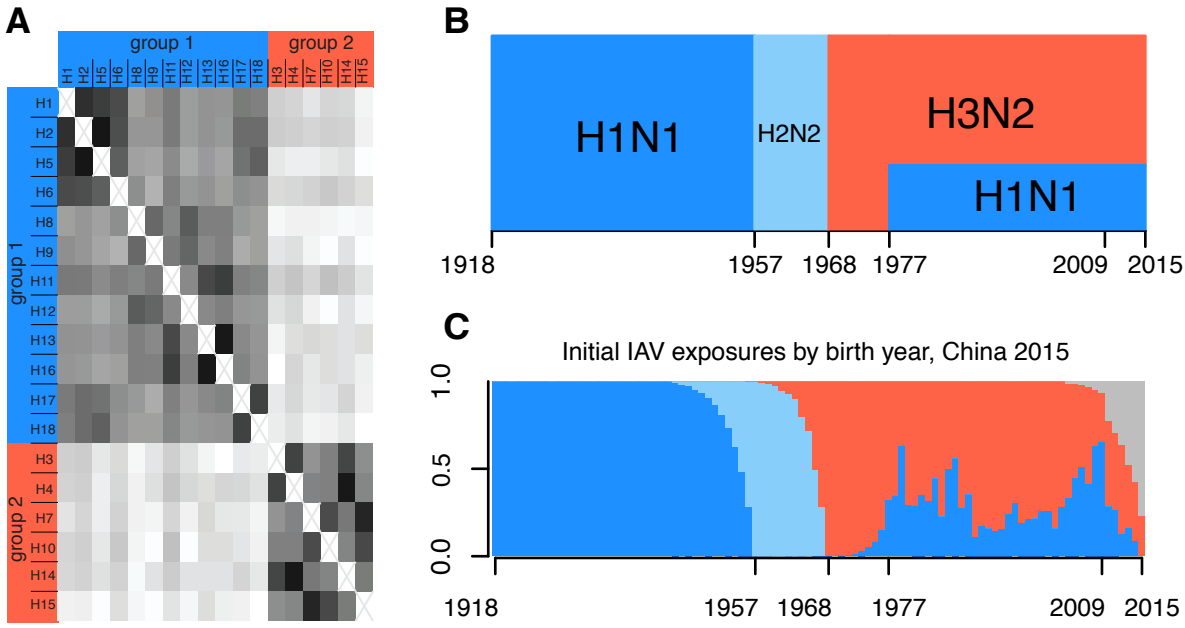

Figure 1-1: HA groups and reconstruction of 20th century HA imprinting.

(A) HA groups 1 and 2, and pairwise amino acid similarities in the HA stem region. Darker colored cells indicate higher similarity (see Fig. 1-S1). Each within-group subtype pair is more similar (83.2%-97.8%) than any between-group pair (75.9%-81.7%). (B) History of seasonal IAV circulation, and (C) estimated fraction of each birth cohort in China with initial exposure to each subtype. Estimated patterns in other countries (not shown) are identical up to 1977, and very similar thereafter. Pandemic years are marked on the horizontal axis. Blue represents group 1 HA viruses, red represents group 2, and grey represents naïve children who have not yet experienced an IAV infection.

Reconstructing IAV exposure history by birth year

To investigate whether an individual's initial childhood exposure to IAV influences later susceptibility to H5 and H7 viruses, we estimated the fraction of each birth-year cohort from 1918 to 2015 with first exposure to H1, H2, or H3 – or the fraction still naïve – for each country in our study (China, Egypt, Cambodia, Indonesia, Thailand, Vietnam). We estimated the annual probability of IAV infection in children using published age-seroprevalence data (*20*,*21*) and then rescaled this baseline attack rate to account for year-to-year variability in IAV circulation intensity (Supplementary Text).

One resulting country-specific reconstruction of HA history is depicted in Fig. 1-1C. While H3N2 has dominated since 1968, a non-negligible fraction of many birth-year cohorts from the 1970s onwards was exposed first to H1N1 viruses, with notable peaks near the re-emergence of H1N1 in 1977 and the 2009 pandemic.

H5N1 and H7N9 cases track HA imprinting patterns

Next, we compiled data on all known human cases of H5N1 and H7N9 with reported patient age (Fig. 1-2A,B). These data encompass mostly clinically severe and fatal cases; total incidence remains unknown. Thus, our analysis focused on the determinants of severe cases. The possible existence of many undetected mild cases, as hypothesized for H7N9 (*1*), is consistent with HA imprinting since broadly-protective immune responses are expected to provide partial protection (*8*,*14*), i.e., reduce severity without preventing infection altogether (*4*,*12*,*22–25*).

The preponderance of observed H7N9 cases among older cohorts, and H5N1 cases among younger cohorts, is clear (Fig. 1-2A,B). These patterns reflect birth year, not age: H5N1 cases occurred over 19 years from 1997-2015, yet cases from all years exhibit similar

dependence on birth year. Analysis of 361 H5N1 cases in Egypt, the one country with many cases across the last decade, shows no trend in case birth years through time, while case age increased steadily (p=0.0003, Spearman's correlation; Fig. 1-S2). So, on average, the same birth cohorts remained at high risk of severe infection, even as members grew ten years older.

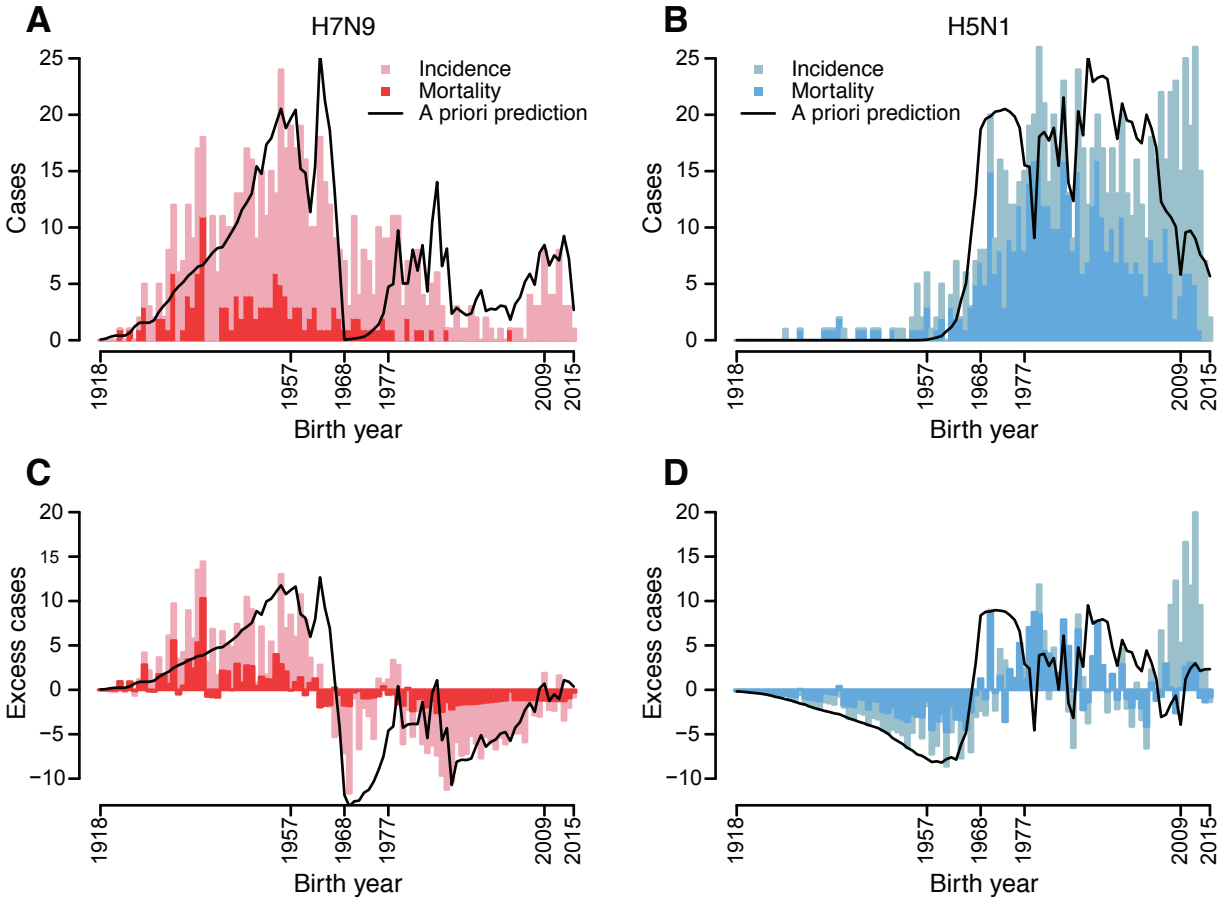

Figure 1-2: H7N9 and H5N1 observed cases and deaths by birth year.

Black lines show *a priori* prediction based on demographic age distribution and reconstructed patterns of HA imprinting. (A) 680 H7N9 cases, from China, 2013-2015. (B) 835 H5N1 cases, from Cambodia, China, Egypt, Indonesia, Thailand and Vietnam, 1997-2015. (C, D) Case data normalized to demographic age distribution from appropriate countries and case observation years.

Fig. 1-2C and D depict the case data normalized to demographic age distributions in affected countries. (If all birth cohorts had equal risk of severe infection, case incidence would be proportional to age distribution.) Bars above the midline thus represent birth years showing excess risk, while bars below indicate a shortfall. This normalization highlights two points: first, excess incidence and mortality data for H5N1 and H7N9 are near-mirror images of each other. Second, the group 1 to group 2 HA transition in 1968 is the key inflection point, with those born before the emergence of H3N2 showing protection against severe cases of H5N1 but not H7N9, and those born after 1968 showing the opposite pattern. For H7N9 severe case incidence also spikes in birth years around 1977 and 2009, when resurgent H1N1 circulation would have caused considerable mismatched imprinting. One-sided binomial exact tests showed excess H5N1 incidence had a lower probability of occurring in cohorts born before 1968 ($p<1e^{-10}$), while excess H7N9 incidence was more probable in these same cohorts ($p<1e^{-9}$). The same pattern held for excess mortality (Supplementary Text). These patterns suggest that the immune system imprints on conserved HA epitopes from the first-ever exposure to IAV, resulting in heterosubtypic (but within-group) protection against severe infection.

Even more striking is the tight correspondence of observed H5N1 and H7N9 incidence and mortality with *a priori* predictions based on HA imprinting patterns and demographic age distributions (Fig. 1-2). We emphasize that the black lines in Fig. 1-2 are not fitted to the case data, but are independent predictions (Fig. 1-1C). Differences between the predictions and data are remarkably small—some noise arises from generalization across time and countries (e.g. attack rates for the reconstruction came from German data, but focal populations are largely Asian), and from small case numbers. Incorporating additional epidemiological factors and estimating the protective efficacy of imprinting further improved correspondence between

predictions and data (Fig. 1-S3). In contrast, NA imprinting patterns (which fully capture patterns of childhood exposure to N1) are a poor fit to H5N1 and H7N9 data from 1957-1968 cohorts (Fig. 1-S4), and NA-mediated protection is not supported by statistical modeling.

HA imprinting explains age distributions

To formally assess the HA imprinting hypothesis alongside previous explanations (*1*,*3*–*7*) for observed H5N1 and H7N9 age distributions, we developed a set of multinomial models. These models related the probability that a case occurred in a given birth cohort to country- and year-specific demography, and risk factors including age-based risk of exposure to poultry, age-based risk of severe disease or case ascertainment, and reconstructed patterns of first exposure (and hence potential immunological imprinting) to HA or NA subtypes (Table 1-S1). Model comparison showed HA imprinting was the dominant explanatory factor for observed incidence and mortality patterns for both H5N1 and H7N9. It was the only tested factor included in all plausible models for both viruses (i.e. all models with Akaike weights greater than $4e^{-5}$).

The best models also included age-based risk of severe disease, echoing patterns known from seasonal influenza epidemiology. Age-based poultry exposure risk (estimated based on contact data from China (*6*, *7*)) was included for H7N9 but not H5N1, perhaps reflecting that age-specific poultry exposures vary across the multiple countries affected by H5N1 or that humans interact differently with ill (H5N1-infected) versus asymptomatic (H7N9-infected) poultry. In models including HA imprinting, NA imprinting never showed any significant effect (Table 1-S2). Remarkably, despite differences between the viruses and age cohorts involved, the estimated protective effects of HA imprinting were nearly identical for H7N9 and H5N1. In all

models, protective HA imprinting reduced the risk of severe infection with H5N1 or H7N9 by ~75%, and the risk of death by ~80% (Table 1-1, Figs. 1-S5-S7, Table 1-S2).

Table 1-1: Estimated protection from HA imprinting.

D=Demography, E=Exposure to poultry, A=High-risk age groups, H=HA imprinting, N=NA imprinting (see Methods, Table 1-S1).

Factors in model*	HA imprinting protection (95% CI)	ΔAIC	Akaike weight
	H5N1		
DAH	0.75 (0.65-0.82)	0.00	0.9994
DEAH	0.83 (0.76-0.88)	15.35	4.65E-4
DEANH	0.83 (0.73-0.88)	17.32	1.74E-4
DH	0.80 (0.71-0.85)	69.18	9.50E-16
DEH	0.87 (0.80-0.90)	103.31	3.69E-23
DENH	0.86 (0.78-0.90)	105.29	1.37E-23
	H7N9		
DEAH	0.76 (0.67-0.82)	0.00	1.00
DAH	0.81 (0.74-0.87)	42.87	4.09E-10
DEH	0.84 (0.78-0.88)	61.59	4.23E-14
DENH	0.83 (0.75-0.88)	62.26	3.02E-14
DH	0.88 (0.84-0.92)	138.40	8.83E-31

Antigenic seniority across influenza subtypes

Most individuals born before the emergence of H3N2 in 1968, and exposed first to group 1 HA antigens (Fig. 1-1), have also been exposed to H3N2 after 1968—probably multiple times. Yet these seasonal group 2 exposures later in life evidently fail to override group 1 HA imprinting from childhood (Fig. 1-2). The birth-year specific protection seen for human H5N1 and H7N9 thus clearly indicates that clinically relevant antigenic seniority—preferential recall of immunological reactivities to antigens encountered earlier in life upon later exposure to cross-reactive antigens (*16*)—can act across HA subtypes of the same HA group, not just within subtypes as often assumed.

While the precise mechanism underlying antigenic seniority in this context remains to be determined, antibodies directed against conserved HA epitopes provide a plausible explanation for protection at the level of HA groups. For example, research following the 2009 H1N1 pandemic drew attention to the fact that primary exposure to a novel IAV can preferentially boost broadly-protective antibodies that bind conserved HA head or stem epitopes shared by different HA subtypes (*8–14*), even though immune memory against more variable epitopes on the novel HA head may be absent. This absence may in fact enable robust expression of otherwise subdominant, broadly-protective responses to conserved epitopes such as those on the HA stem (*8*). In particular, primary exposure to H5N1 or H7N9 can activate HA stem-specific reactivities induced by previous infection by H1 or H3, respectively (*12*,*13*,*26*). Indeed, others have suggested that heterosubtypic antibodies might attenuate disease from other IAV strains and may be imprinted to some degree by childhood exposure, though their serological assays provided no ability to detect or predict actual patterns of protection relevant to H5N1 and H7N9 in human populations (27).

Given the immunodominant nature of HA head reactivities (*13*,*14*,*26*,*28*), conserved HA head epitopes shared within, but not between, HA groups (*29*) may play a role in these patterns of protection. Cross-reactive HA-specific CD4+ or CD8+ T cell responses should also be investigated, since they too are likely to be disproportionately shared within HA groups (given the sequence similarities within each clade) and might be especially capable of facilitating the sort of long-term immunity indicated by the data.

Nevertheless, current data, including the high degree of sequence conservation of stem domains within each HA group (Fig. 1-1A, Fig. 1-S1), seem most consistent with a stem-directed mechanism for the antigenic seniority acting at the HA-group level (*13*). Divergence in HA stem amino acid sequences within each phylogenetic *group* is comparable to divergence in globular head sequences within a single HA *subtype* (i.e. the scale at which antigenic seniority is already known to act (*16*); Fig. 1-S1), but stem divergences between the two HA groups are markedly higher. Notably, H3 and H7 are as divergent as any pair of group 2 HAs; since H3 childhood exposure provides protection against H7 it may thus protect as well or better against the other group 2 HAs (H4, H10, H14, H15), but perhaps not at all against more divergent group 1 HAs (Fig. 1-S1C). Similarly, the joint consideration of protein sequence conservation patterns (Fig. 1-1A, Fig. 1-S1) along with immunological and epidemiological data suggests that H1 or H2 childhood exposure may protect generally against zoonotic group 1—but not group 2—HAs.

The putative generality in HA imprinting protection patterns for novel HA subtypes other than H5N1 or H7N9 is tentatively supported by the preponderance of HA group-mismatched childhood exposures among the small number of clinically significant human cases detected to date: pooling data from 28 human cases of H5N6, H6N1, H7N7, H9N2, H10N7 and H10N8, age patterns are consistent with HA imprinting ($p=0.019$; see Supplementary Text), but case numbers

are insufficient to investigate particular subtypes. Immunological experiments (e.g. using chimeric HA proteins (*12*)) are needed to systematically map HA cross-protection patterns across all HA subtypes, both within and between HA groups.

Rational projections of future pandemic risk

For any new pandemic IAV strain capable of efficient human-to-human transmission, HA imprinting patterns would combine with age-based mixing patterns (*30–32*) to determine the epidemiological impacts of the first pandemic wave. We created projections for a putative pandemic-capable strain of subtype H5 or H7—such as a gain-of-function strain or a natural variant with mutations increasing human-to-human transmissibility. The data on observed H7N9 and H5N1 cases enabled us to quantify how matched HA imprinting reduces the probability of developing a severe infection, but not how matched imprinting affects an individual's probability of acquiring a milder infection or the infectivity of such mild infections. People who become infected despite prior immunity likely transmit influenza at reduced rates owing to diminished viral titers and viral shedding, as observed in humans and in animal models (*4*,*12*,*22–25*). We thus assumed, conservatively, that imprinting does not change the probability of acquiring infection upon exposure, but can reduce severity and infectivity in individuals with protective HA imprinting.

Fig. 1-3A illustrates the projected age-structured attack rate of severe cases for hypothetical pandemics of H5 or H7 IAV occurring in 2015 in the United Kingdom. The projected risk profiles for severe infection are shaped strongly by HA imprinting, including the prediction that individuals above 50 years of age (i.e. born well before 1968 and first exposed to

a group 1 HA) would experience much lower morbidity than younger age groups in an H5 pandemic.

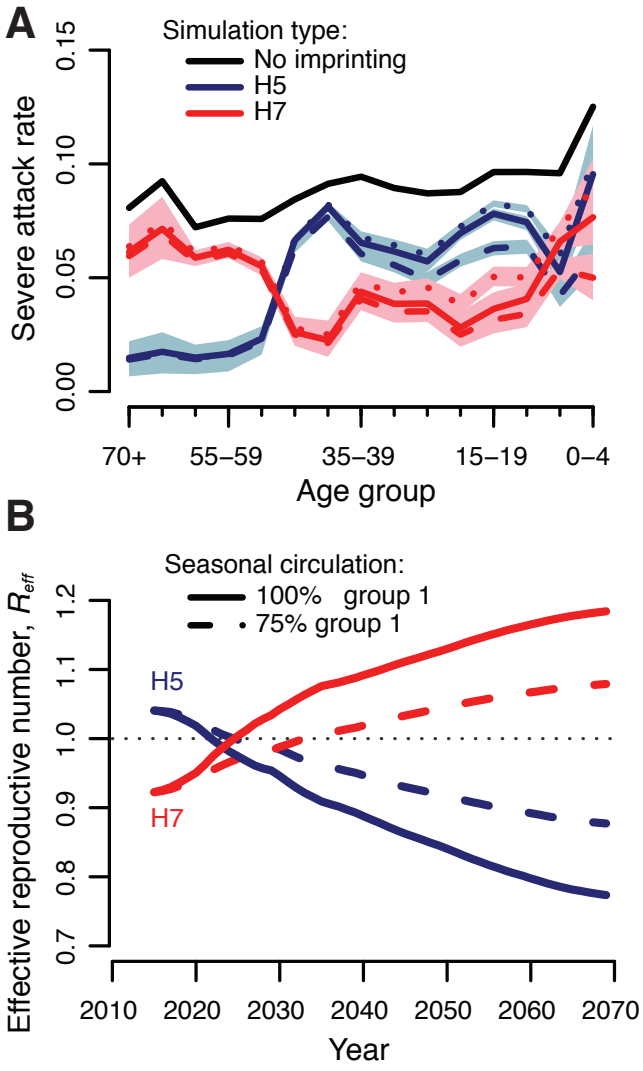

Figure 1-3: Projected effects of HA imprinting on future pandemics.

(A) Attack rate of severe cases, by age group, for hypothetical H5 (blue) and H7 (red) IAV pandemics in 2015 (R_0=2.5, relative infectiousness of imprinting-protected individuals (α)=0.5), assuming UK demography and age-structured mixing (Supplementary Text). Lines show the average of 100 simulated outcomes, and shaded regions show the central 95%. Three vaccination scenarios explored: vaccination of IAV-naïve children could cause dual imprinting to both HA groups (dashed lines), prevent imprinting to both groups (dotted lines), or have no effect on imprinting (solid lines). (B) Projected change in R_{eff}, for

hypothetical H5 (blue) or H7 (red) IAV with R_0=1.2 and α=0.5, if group 1 IAVs make up 100% or 75% of seasonal circulation after 2015.

Similar projections for China and Vietnam reveal the influence of demographic differences between countries (Fig. 1-S8). The qualitative patterns in projected age impacts are robust to a wide range of assumptions about how seasonal influenza vaccination might affect imprinting (Fig. 1-3A), and to the assumed infectivity of mild cases arising in individuals with protective HA imprinting (Fig. 1-S8A).

Projections for pandemics occurring a decade from now highlight predictable shifts in severe disease risk patterns as the imprinted population ages, with the key pivot point around birth years near 1968 shifted to older ages (Fig. 1-S8). Impacts in the youngest age groups would depend on patterns of IAV circulation in the coming decade. All pandemic projections that account for HA imprinting exhibit markedly lower severe attack rates than projections assuming no imprinting protection (Fig. 1-3A, Fig. 1-S8). Total attack rates (including mild and subclinical cases) would be higher and more evenly distributed across age groups than the severe attack rates shown here.

Over any prolonged period when IAV circulation is dominated by one HA group, imprinting generates growing herd immunity against zoonotic IAV strains from that group. Conversely, zoonotic strains from the mismatched HA group benefit from the rising proportion of humans without protection. So long as mild cases arising in people with group-matched imprinting contribute any less to transmission than unprotected cases, or if some fraction of infection events is prevented by imprinting-derived immunity, imprinting will alter the transmissibility of zoonotic IAV strains in the human population. This is summarized by the effective reproductive number, R_{eff}, which quantifies transmission in a partially immune

population (Fig. 1-3B). Crucially, a zoonotic strain that is initially subcritical (i.e. with $R_{eff} < 1$ and therefore unable to spread sustainably) could—due solely to susceptibility changes in the human population—emerge as supercritical, and hence as a pandemic threat, if the mismatched HA group dominates IAV circulation for a sufficient period (Fig. 1-3B).

Our work implies that we have never seen a true 'virgin soil' influenza pandemic, and that all prior estimates of R_0 for pandemic IAVs are systematic underestimates since they do not account for protection induced by HA imprinting. Conversely, we see that imprinting raises the threshold R_0 necessary for a novel subtype to invade. Interestingly, the co-circulation of group 1 and 2 HAs since 1977 has balanced herd immunity in a way that increases the inherent transmissibility needed for a novel subtype from either HA group to invade. As a generality, R_{eff} for zoonotic influenza strains will change through time depending on seasonal influenza patterns and demographic background, and the magnitude of change will depend on the infectivity of imprinting-protected cases (Fig. 1-S9).

DISCUSSION

Our findings show that major patterns in zoonotic IAV epidemiology, previously attributed to patient age, are in fact driven by birth year. IAV strains circulating during an individual's childhood confer long-term protection against novel HA subtypes from the same phylogenetic group. Hence, antigenic seniority extends across IAV subtypes, introducing previously unrecognized generational structure to influenza epidemiology. These immune imprinting effects have implications for public health and highlight that influenza virulence

represents a joint phenotype between virus and host—even for strains not yet adapted to the human population.

These findings support the hypothesis that the unusually high mortality in young adults during the 1918 H1N1 (group 1) pandemic may have arisen primarily from mismatched H3 (group 2) imprinting in the cohort born between ~1880 and 1900 (*19*). This same cohort was strongly affected during the (group 1) 1957 pandemic (*33*); yet they suffered no excess mortality when they were even older, during the (group 2) 1968 pandemic (*34*). The possibility that mismatched HA imprinting currently contributes to the greater health impacts of seasonal H3N2 (relative to H1N1) in today's older age classes is worth investigating. And a diagnostic assay to determine whether an individual was imprinted on a group 1 or group 2 HA may be useful for individualized clinical care and vaccine design strategies, both for pandemic and seasonal IAVs.

Our findings raise questions about whether seasonal influenza vaccination might boost broadly-protective anti-HA responses (*27*) or alter imprinting from natural infection in IAV-naïve children. By exposing IAV-naïve children simultaneously to group 1 (H1N1) and group 2 (H3N2) antigens, vaccination might confer dual imprinting to both HA groups, or prevent strong imprinting against either HA group—or it could have no effect beyond delaying the age of imprinting via the first natural infection. Our sensitivity analyses demonstrated that, given the low IAV vaccination coverage in H5N1- and H7N9-affected countries, none of these effects would change our study's conclusions (Fig. S7). However, to properly inform early childhood vaccine policy, future research must determine which, if any, of these effects occur.

HA group imprinting also might complicate 'universal' vaccination approaches targeting conserved HA epitopes. Our findings indicate potent, long-lasting cross-protection between subtypes, putatively based on such responses. However, universal vaccination may have to

outperform natural infection in its ability to induce broad immunity in the face of previous imprinting. The persistence of group 1 imprinting in older adults, despite decades of natural exposure to H3N2 after 1968 (Fig. 2), and the relative weakness of group 2 anti-HA stem reactivities in these older cohorts (*11*), suggest HA exposures later in life do not readily alter broadly-protective responses in individuals already imprinted to a particular HA group. To be effective, would bivalent (group 1 and group 2 HA stem) universal vaccines need to be delivered to infants prior to natural IAV infection? Or, might universal vaccines even impair natural, long-term protection of the sort we have detected against H5N1/H7N9 if received prior to an individual's first natural IAV infection?

Our findings are consistent with the known potential for repeated infection by seasonal IAV subtypes. Group-matched imprinting, like other broadly-protective IAV immune responses, is expected to protect against severe disease but not necessarily against infection (*8,12,14*). This parallels the reduced severity observed for repeat infections with seasonal strains (*22*,*23*,*25*). Furthermore, re-exposure to a seasonal subtype typically elicits memory responses against the immunodominant HA head, which mask subdominant broadly-protective responses involved in group-level imprinting (*26*).

For any country with suitable contact and demographic data, the methods shown here can provide rolling estimates of which age groups would be at highest risk for severe disease, should particular novel HA subtypes emerge. Such projections could guide cohort- or region-specific prevention, preparation, or control. Quantitative projections of changes in R_{eff}, and hence pandemic risk, will require further research into the protection arising from matched imprinting: is some fraction of cases prevented entirely, and by what factor is infectivity reduced in mild cases arising in protected individuals?

Our findings show that emergence risk cannot be considered in isolation, even for 'novel' pathogens that have not circulated in humans before. These pathogens are commonly assumed to have a blank slate of immunologically naïve humans to infect, but cross-protection from related pathogens can generate substantial population immunity. When this community of related pathogens undergoes major shifts, as during influenza pandemics, the landscape of population immunity changes accordingly. Thus emergence of novel pathogens can be governed by bottom-up control, with population immunity acting in an important and predictable manner to modulate the widely-recognized effects of virological and ecological risk factors. This perspective opens new frontiers for quantitative and mechanistic analysis of emergence risk.

MATERIALS AND METHODS

Case data

We compiled data describing all reported human cases of H7N9 (2013-Nov. 2015) and H5N1 (1997-Nov. 2015) influenza. We obtained case data from three previously published H5N1 line lists, one spanning 1997 *(35)* and the other spanning Sept. 2006-Aug. 2010 *(36)*. We obtained data from one H7N9 line list spanning Jan.-Sept. 2013 *(37)*. For all other cases, we compiled original line lists using reports from the WHO as our primary resource and the Hong Kong Centre for Health Protection as a secondary resource. We incorporated additional cases or case details from Flu Trackers (https://flutrackers.com/forum/). Our newly compiled line lists are available as supplementary data files within the published version of this article (DOI: 10.1126/science.aag1322). Hyperlinks to information sources for each case are provided within.

We included confirmed, suspected and probable cases in our final analysis, but verified that our results are robust to the exclusion of unconfirmed cases (Fig. 1-S7). We excluded cases for which patient age was not reported. Our H7N9 database contained 686 confirmed, suspected or probable cases, which were reported between April 1, 2013 and Nov. 13, 2015. All occurred in China. We excluded 6 cases for which patient age was not available, and used the remaining 680 cases, including 132 deaths, in our analysis (676 were confirmed and 4 were suspected or probable). In the same time period, WHO reported 681 confirmed cases of H7N9, so at most we are missing information on 5 confirmed cases (or fewer if some of these cases were included among our suspected and probable cases).

In total, our H5N1 database contained 927 confirmed, suspected or probable cases. These cases were reported in the 1997 Hong Kong outbreak, or in any country globally between Feb. 19, 2003 and Nov. 13, 2015. Over 94% of H5N1 cases occurred in Cambodia, China, Egypt, Indonesia, Thailand, and Vietnam, so we focused on these six countries and excluded 54 cases that occurred elsewhere. From the remaining 873 cases, we excluded an additional 38 cases for which patient age was not reported. Thus, we analyzed a total of 835 H5N1 cases, including 440 deaths (755 were confirmed and 80 were suspected or probable). In the same time period, WHO reported 823 confirmed cases of H5N1 in our study's six countries of interest, so at most we are missing information on 68 confirmed cases. Most of these additional confirmed cases were included in aggregate reports of H5N1 cases that lacked any accompanying details, making it impossible to determine whether case details reported elsewhere should be linked to WHO-confirmed case reports. Thus, it is possible that some of these WHO-confirmed cases were included in our database (based on information from Flu Trackers or other sources), but were listed as suspected or probable.

Mild or asymptomatic cases of both infections may not be ascertained *(1)*, so our results should be interpreted only as predictors of severe, symptomatic infection. We used simulated data to verify that our study's core findings should be robust to case ascertainment biases (see Supplementary Text, section 7).

Normalization of data to demographic age distribution

If all birth years were at equal risk of severe infection, we would expect the observed age distribution of cases to be proportional to the demographic age distribution. To examine excess incidence of severe infection or death, relative to this demographic null expectation, we normalized the observed data to the demographic age distribution (Fig. 1-2C, D). We tabulated the observed and expected number of cases occurring in each birth year, i, for each country, c, in each case observation year, y. To determine birth year, we subtracted case age from the year in which case onset occurred. To estimate the expected number of cases in each birth year, Exp_{yci} we used the following formula:

$$Exp_{yci} = D_{yci} I_{Total,yc} \tag{1-1}$$

Here D_{yci} describes the fraction of the total population, in country c, year y, that belongs to birth year i. $I_{Total,yc}$ describes the total number of cases or fatalities that occurred in year y, country c.

Finally, we defined normalized values within each birth year, N_i, as the unweighted sum, across all possible country-years, of differences between observed and expected numbers of cases or fatalities:

$$N_i = \sum_y \sum_c (Obs_{yci} - Exp_{yci})$$

(1-2)

Model formulation

We used multinomial models to describe the probability distribution of H5N1 or H7N9 cases or fatalities across birth years. The multinomial distribution requires a set of parameters, p_{yci}, which described the probability that an infection observed in year *y*, country *c*, occurred in birth cohort *i*. Within each model, a unique combination of factors, including age-based risk of severe infection, poultry exposure risk, HA imprinting, and NA imprinting, determined p_{yci}. For each virus (H5N1 and H7N9), we fitted models independently for each case outcome (infection or death).

For each candidate model, we computed maximum likelihood parameter estimates to quantify the effects of relevant explanatory factors on birth-cohort risk (Table 1-S1). Parameters H_m and N_m described the relative risk of severe infection or mortality for those with protective HA or NA imprinting, while parameters A_c and A_e described relative risk for young children (<5 years old) and the elderly (>65 years old).

We performed model comparison using AIC to determine which combination of factors best explained observed distributions of H5N1 or H7N9 incidence or mortality across birth years. We calculated Akaike weights, w_z, which can be interpreted as the proportional evidence in support of model *z* as the best of all models tested. Weights are calculated using the expression, $w_z = \frac{e^{\left(\frac{-\Delta AIC_z}{2}\right)}}{\sum_z e^{\left(\frac{-\Delta AIC_z}{2}\right)}}$*(38)*. In many cases, when we added NA imprinting to models already considering HA imprinting, the maximum likelihood estimate of the N_m parameter was 1. In these cases, NA

imprinting had no effect, and the new, more complex model became identical to the simpler model. We excluded these degenerate models from Akaike weight calculations.

Factors tested

Demography (D)

If all individuals were at equal risk of infection, regardless of birth year, the number of cases occurring in a given birth year would be proportional to the fraction of the population born in that year, as given by the country's demographic age distribution. Thus, for every country, c, and case observation year, y, a vector, D_{yc}, described the demographic age distribution and served as the null predictor of infection risk in each birth cohort. Vector D_{yc} was normalized to sum to 1, so that each element described the fraction of the population born in a particular year. Using the US Census Bureau's International Database *(39)*, we obtained publicly available demographic data for each country and year of case observation. Demography was included as a factor in every model tested (Supplementary Text).

Exposure to poultry (E)

Though limited human-to-human transmission is thought to occur, the majority of H7N9 and H5N1 infections are caused by spillover from infected poultry *(2, 6)*.To build models incorporating age-based patterns of exposure to poultry (E), we obtained published data from six surveys conducted in provinces that have experienced at least five cases of H5N1 or H7N9. These data were collected in three cities, Guangzhou, Shanghai and Shenzhen, and two non-urban locations, subrural Guangzhou and Xiuning, in China *(6, 7)*. Note that we included data

from two independent surveys conducted in urban Guangzhou, for a total of six survey data sets. No poultry exposure data were available for other affected countries.

Although poultry exposure patterns vary by location, even within China, large reported uncertainties and geographic constraints on the available data prohibited a statistically valid effort to match cases with geographically specific exposure patterns. Instead we computed an average exposure rate for each birth cohort and year of H5N1 or H7N9 case observation, as follows. Each survey reported poultry exposure rates by age group. We used these values to assign each birth cohort an age-specific poultry exposure rate, based on their ages in each possible year of case observation. If exposure rates were not reported explicitly for young children, we substituted the rate reported for the youngest available age group. We then normalized across birth cohorts to determine the proportional risk of exposure at each survey location. Normalization ensured that survey locations reporting higher overall rates of exposure did not disproportionately influence model inputs. Finally, for each birth year, we took the average proportional exposure rate across all six poultry exposure surveys. These normalized exposure scores are shown in Fig. 1-S10 B.

Age-based risk of severe infection (A)

A basic principle of influenza epidemiology is that children under 5 and elderly adults over 65 are high-risk groups for severe influenza infection *(40-42)*. These groups may be more susceptible to severe influenza infections, or may seek healthcare at an increased rate, leading to case-ascertainment biases. Models including the age-based risk factor (A) introduced two parameters that allowed each high-risk age group to experience increased risk of severe infection relative to adults and children ages 5-64. Parameter A_c quantified the relative risk of young

children, while parameter A_e quantified the relative risk of the elderly (Table 1-S1). Both parameters are constrained take a minimum value of 1 so as to represent elevated risk of severe infection.

For mortality analyses, we noted that case-fatality rates are not always elevated in children, despite their elevated risk of severe infection *(41)*. Thus, for mortality analyses we relaxed the constraint on parameter A_c, allowing the data to inform whether young children exhibit increased ($A_c > 1$) or decreased ($A_c < 1$) risk of death from H7N9 or H5N1 infections, relative to the general population.

Hemagglutinin imprinting (H)

Models that considered hemagglutinin imprinting (H) divided the population into two exposure groups: those with group-matched first IAV exposures (protective HA imprinting), and all others (non-protective HA imprinting or naïve children). We calculated the fraction of each birth cohort with first exposure to either HA group using methods described below (see Reconstructing immune imprinting patterns). We initially separated naïve children from adults with non-protective HA imprinting, but our results consistently indicated no difference in risk between these groups (results not shown), leading us to combine naïve children and mismatched HA imprinting into a single reference group.

Hemagglutinin imprinting models introduced a single parameter, H_m, which allowed the group with protective HA imprinting to experience decreased risk relative to all others in the population.

Neuraminidase imprinting (N)

As for HA imprinting, models that considered NA imprinting divided the population into two groups: one with matched (protective) first IAV exposures, and a reference group that included all others. Models containing factor N introduced one parameter, N_m, which allowed the group with protective NA imprinting to experience decreased risk. Two phylogenetic groups have been identified for NA, as for HA. We are not aware of experimental evidence of cross-protection between NA subtypes within the same phylogenetic group (without which NA history could not explain incidence patterns for H7N9, since N9 is not known to have circulated in the human population). However, given that N9 and N2 fall in the same NA group, we considered the possibility that imprinting on N2 might be protective against N9. H5N1 is clearly matched to seasonal H1N1, as they share the N1 subtype—so this analysis fully captures patterns of first exposure to N1, which have been proposed previously as a driver of H5N1's infection age distribution *(3, 4)*.

Models tested

We tested models that considered all possible combinations of the above four factors, as well as demographic age structure. Our full set of 16 models included: D, DE, DA, DH, DN, DNH, DAH, DAN, DANH, DEA, DEH, DEN, DEAH, DEAN, DENH, and DEANH. For each model, we fit relevant parameters to the appropriate data before performing model comparison. We repeated each model analysis using both incidence and mortality data for H7N9 and H5N1. See Supplementary Text for model equations and likelihood functions.

Reconstructing immune imprinting patterns

To inform hemagglutinin and neuraminidase imprinting models, we estimated the fraction of each birth cohort with first IAV exposure to seasonal subtypes H1N1, H2N2 or H3N2, and the fraction that remained naïve. We first used a truncated geometric model to estimate the baseline probability that first IAV infection occurs at a given age. Because age-seroprevalence studies report that 98-100% of children have been infected with IAV by age 12 *(20, 21, 43)*, we set 12 as the maximum possible age of first infection. Let ε_{ij} be the probability that an individual with birth year *i* has his or her first IAV infection in calendar year *j*. Then:

$$\varepsilon_{ij} = \frac{(1-a)^{j-i}a}{\sum_{j=i}^{i+12}(1-a)^{j-i}a} \quad (1\text{-}3)$$

where *a* is the annual probability of infection (the baseline annual attack rate on seronegative children), and *j* takes values from *i* to *i+12*. Using published age-seroprevalence data *(20, 21)*, the maximum likelihood estimate for *a* was 0.28 (95% CI 0.26-0.30), consistent with other IAV attack rates estimated in children *(43-45)*.

To account for variability in the annual attack rate between years, we compiled an index of IAV circulation intensity from 1918-2015 (Supplementary Text). We defined the scaled annual attack rate as $a_m = aI_m$, where *m* is the calendar year, I_m represents that year's intensity score and *a* represents the baseline annual attack rate estimated above.

Finally, we modified equation 3 to account for variable annual attack rates and the possibility that some children have not yet been exposed:

$$\varepsilon_{ij|y} = \begin{Bmatrix} \frac{a_j}{N_{i|y}} & i = j \\ \frac{\left[\prod_{k=i}^{j-1}(1-a_k)\right]a_j}{N_{i|y}} & i < j \leq i+12 \end{Bmatrix}$$

(1-4)

Here, $\varepsilon_{ij|y}$ is the probability that individuals in birth cohort *i* experienced their first infection in calendar year *j*, given that H5N1 or H7N9 case observation occurs in year *y*. Note that because birth cohorts are very large, the fraction of birth cohort *i* with first exposure in year *j* converges to probability $\varepsilon_{ij|y}$. The expression, $\frac{a_j}{N_{i|y}}$ represents the probability of infection in the first year of life (at age 0), and the expression, $\frac{\left[\prod_{k=i}^{j-1}(1-a_k)\right]a_j}{N_{i|y}}$ represents the probability of infection at ages 1-12. The normalizing factor, $N_{i|y}$, reflects the assumption that all individuals have had their first infection by age 12, and is used to ensure that all relevant probabilities for an age group sum to 1. It is taken as:

$$N_{i|y} = \begin{Bmatrix} a_i + \sum_{j=i+1}^{i+12}\left[\prod_{k=i}^{j-1}(1-a_k)\right]a_j & y \geq i+12 \\ 1 & y < i+12 \end{Bmatrix}$$

(1-5)

When the birth cohort is older than 12 in the year of observation, $N_{i|y}$ always falls within the range (0.98-1.00) and minimally affects the final outcome. For birth cohorts that are younger than 12 at the year of observation ($y<i+12$), normalization is not appropriate because some individuals in the age group have not had their first exposure; in these instances we set $N_{i|y} = 1$ and calculate the naïve fraction as the complement of the cumulative probability of first exposure (equation 7).

Finally, we combined the age of first infection probabilities with seasonal circulation patterns to determine the fraction of age group *i* with first exposure to subtype *S* in year *j* and country *c* ($w_{S,i|y,c}$). We scaled $\varepsilon_{ij|y}$ by the fraction $f_{S|j,c}$ of circulating IAVs belonging to subtype *S* (where *S* could represent H1N1, H3N2 or H2N2):

$$w_{S,i|y,c} = \sum_{j=i}^{y} f_{S|j,c}\varepsilon_{ij|y} \quad (1\text{-}6)$$

For birth cohorts younger than 12 in the year of case observation ($y<i+12$), a portion of the cohort had not yet experienced a first IAV exposure. The fraction of cohort *i* that remained naïve in year *y* was given by:

$$w_{n,i|y,c} = 1 - \sum_{j=i}^{y} \varepsilon_{ij|y} \quad (1\text{-}7)$$

Values of $f_{S|j,c}$ were determined by IAV circulation history, and for all *j*, $f_{H1N1|j,c} + f_{H2N2|j,c} + f_{H3N2|j,c} = 1$. Prior to 1977, a single IAV subtype circulated each year, and pandemic years marked circulation of a new seasonal subtype. Thus, in years 1918-1976, $f_{S|j,c}$ was set equal to 1 for the circulating subtype, and 0 for all other subtypes.

For years 1977-2015, when H1N1 and H3N2 have circulated simultaneously, we estimated $f_{S|j,c}$ using influenza surveillance data reported by WHO collaborating laboratories *(46, 47)*. For each year of interest, we defined relative incidence as follows: $\frac{Positive\ specimens\ of\ subtype\ S}{All\ positive\ specimens\ of\ subtype\ H1N1\ or\ H3N2}$. Whenever possible (1997-2015), we used surveillance data from the country of interest (China, Egypt, Cambodia, Indonesia, Thailand or Vietnam) to estimate country-specific relative incidence. When fewer than 50 specimens were

reported for a given country in a given year, we substituted surveillance data from the same year, across all other countries of interest with adequate data. For years in which no surveillance data was available from any H5N1 or H7N9 affected country (1977-1996), we substituted surveillance data from laboratories in the United States *(47)*. From 1997-2015, the relative incidence of H3N2 or H1N1 in the United States was significantly correlated with subtype-specific relative incidence in our study's six countries of interest (Pearson's $r = 0.70$, $p < 0.001$), suggesting that US data is a reasonable proxy.

A priori predictions

The *a priori* predictions in Fig. 1-2 illustrate how the observed total number of cases would be distributed across birth years if individuals with protective HA imprinting never experienced severe infection, but risk is otherwise identical for everyone. Thus, the distribution of observed cases across birth years was expected to be proportional to the distribution of unprotected individuals across birth years (i.e. to the demographic age distribution, after individuals with protective HA imprinting had been removed). For each country and year in which cases were observed, this *a priori* prediction is:

$$P_{yci} = \frac{D_{yci} w_{o,i|y,c}}{\sum_i D_{yci} w_{o,i|y,c}} \tag{1-8}$$

Here, P_{yci} is the fraction of all cases observed in country c, year y predicted to occur in birth year i. D_{yci} represents the demographic age distribution as defined in equation 1. Building from equations 6 and 7, $w_{o,i|y,c}$ represents the fraction of each birth cohort with first exposure to a subtype in the opposite HA group as the challenge strain, or naïve to IAV. For the predictions shown in Figs. 1-2A and B, we scaled P_{yci} by the number of cases, $I_{Total,yc}$ observed in year y,

country *c,* and then summed across all affected countries and years: $\sum_y \sum_c \left[I_{Total,yc} P_{yci} \right]$. For the predictions shown in Figs. 1-2C and D, we subtracted the demographic null expectation (as in equations 1 and 2), to obtain the prediction: $\sum_y \sum_c \left[(I_{Total,yc} P_{yci}) - Exp_{yci} \right]$.

Sensitivity analyses

We verified that our conclusions are robust to model assumptions by repeating model fitting and model comparison on twelve variations of the main model described above (Fig. 1-S7). First, to test for robustness against uncertainty on annual intensity of seasonal IAV circulation, we repeated all model analyses assuming a constant annual attack rate ($a_j = a$ for all years j). Second and third, we considered uncertainty on the baseline attack rate, a, by setting this parameter equal to its upper and lower 95% confidence bounds. Fourth, we checked for robustness to the estimated annual dominance of H1N1 and H3N2 by fixing the relative incidence of each to its average from 1977 to 2015 (0.34 for H1N1, 0.66 for H3N2). Fifth and sixth, to generate upper and lower bound estimates of either subtype's seasonal dominance, we increased the observed relative incidence of H1N1 or H3N2 by 0.05 for all years from 1977-2015, while simultaneously decreasing the relative incidence of the complementary subtype by the same amount. Seventh and eighth, we considered two alternate poultry-risk distributions, using data exclusively from Urban Shenzhen *(6)* and Shanghai *(7)* as data from these surveys respectively reported the highest and lowest poultry exposure rates in cohorts born before 1968. Ninth through eleventh, although overall influenza vaccine coverage is low in all six countries considered (approaching 10% in Thailand and <5% elsewhere) *(48)*, we tested whether our analysis is robust to childhood vaccination effects. We considered three scenarios, in which vaccination of naïve children could

prevent imprinting and leave the child fully susceptible to both HA groups, replace imprinting and leave the child protected against both HA groups or delay imprinting via delay of the first natural infection. To be conservative, these models considered an upper-bound case for IAV vaccination coverage, and assumed childhood coverage levels beyond what is actually achieved in H5N1- and H7N9-affected countries (Supplementary Text). Finally, to verify that our results were robust to the exclusion of data from probable or suspected cases, we repeated model analyses using only laboratory-confirmed cases.

Phylogenetic and amino acid sequence analyses

We aligned amino acid sequences of representative H1 strains (HA globular head) and group 1 and group 2 HA strains (stem domain) in Geneious v9.0.4 *(49)* (global alignment with free end gaps, BLOSUM62 cost matrix). Maximum likelihood phylogenies were estimated in RAxML version 7.2.8 *(50)* using the aligned amino acid sequences and a GAMMA LG protein model (rapid hill-climbing algorithm). We generated a heat map of HA stem amino acid sequences with percent similarities (BLOSUM62 matrix with threshold 0) calculated in Geneious version 9.0.4 *(49)*.

Projections of future pandemics

We used a discrete-time stochastic model to create projections of the age-specific severe attack rates in a hypothetical future H7 or H5 pandemic. We conducted simulations for the United Kingdom, China, and Vietnam in 2015 and 2025. For the 2025 simulations, we considered two scenarios for seasonal IAV circulation between 2015 and 2025: 25% group 1 and 75% group 1 circulation. Demography and imprinting patterns for each country and year were

obtained as described in Methods (see 'Normalization to demographic data' and 'Reconstructing immune imprinting patterns').

In the model, individuals with matched imprinting have probability $(1 - H_m)$ of experiencing a 'protected' course of infection and a probability H_m of experiencing the same 'unprotected' infection as individuals with mismatched imprinting. 'Protected' individuals have some degree of acquired immune protection and do not experience severe disease; to be conservative, we assume that they still become infected but their lower viral loads lead to reduced infectiousness relative to their 'unprotected' counterparts (mediated by a relative infectiousness parameter, α). As discussed in the main text, this assumption mirrors data from experimental infections in humans and non-human animals, which show that infections in partially-protected individuals exhibit lower viral titers, lower and more short-lived viral shedding, and lower rates of transmission than infections in naïve individuals *(22, 24, 25)*. In our analyses, we tested values of α spanning from 0.1 to 0.9, representing the full range of possible reductions in transmission. We expect that the true value for a given situation would depend on specific properties of the focal IAV strain as well as the past strains that generated the imprinted responses.

An 'unprotected' infected individual in age group i exposes a total of X_{ij} individuals from age group j to the virus, where X_{ij} follows a negative binomial distribution with dispersion parameter $k = 0.94$ *(51)* and mean M_{ij}. For 'protected' infected individuals, the mean number of new infections is instead αM_{ij}. The matrix $\mathbf{M}$ (with entries M_{ij}) is the next generation matrix with dominant eigenvalue equal to the pathogen's basic reproductive number (R_0). R_0 was set at 2.5 so that the effective reproductive number (R_{eff}), which accounts for protection from matched

imprinting, was approximately 1.9 at the beginning of the 2015 simulations. This value aligns with the R_{eff} calculated at the beginning of previous pandemics *(52-56)*.

An unscaled next generation matrix **M** was constructed from data on contact rates between age groups. Separate contact matrices giving the relative rates of contacts between individuals in different age groups were used for each country. For the UK, we used the matrix of all reported physical and non-physical contacts in Great Britain reported by Mossong et al. *(30)*; for China, we used data on individual-level contacts reported by Read et al. *(31)*; and for Vietnam, we used contact diary data from Horby et al. (individual-level data provided by Peter Horby) *(32)*. We converted the China and Vietnam contact data from the reported age bins into the age bins needed for simulations by disaggregating the reported data (scaled by demography) into separate age years and then reaggregating the data into the appropriate age bins. All elements of this matrix were rescaled by a constant factor so that its dominant eigenvalue was equal to the desired R_0.

The X_{ij} exposures caused by an infectious individual were assumed to occur after a serial interval of T days from the source case, where T was distributed according to a Weibull distribution with mean 3.6 (shape = 2.3 and scale = 4.1) *(57)*. Given exposure on day t, the probability that an individual in age group j developed the disease was equal to the proportion of age group j susceptible on day t.

Each individual that experienced an 'unprotected' course of infection had a chance of developing a severe infection. The probability of severe infection is a property of a given viral strain (roughly, its virulence) and will vary among scenarios; we chose a baseline value of 0.1, and note that different choices for this value simply rescale the results and do not alter any qualitative patterns. To account for the elevated risk of severe infection in children (0-4 years)

and the elderly (65+), the probability of severe infection in these age groups was multiplied by the age-specific risk parameters A_c and A_e. We used consensus parameter estimates for A_c and A_e, which should most robustly represent the behavior of pandemic strains that cause large numbers of cases in both old and young age groups. To obtain these values, we set H_m at 0.245 (the midpoint value from our main analyses; see Table 1-1), constrained A_c and A_e to be identical for H5N1 and H7N9, and estimated the parameter values by maximizing the constrained likelihood.

We used three sets of assumptions to explore how vaccination of naïve children might affect imprinting for the 2015 UK simulation. In the first set, we assumed that vaccination had no impact on imprinting patterns in the population (this assumption is used in the simulations for all other years and countries). In the second set, we assumed that children who were vaccinated against seasonal influenza before experiencing their first natural IAV infection obtained full imprinting protection against both HA group 1 and 2 IAVs. In the third set, we assumed that children who were vaccinated before experiencing their first natural IAV infection were blocked from imprinting on either HA group and experienced no imprinting protection.

Seasonal influenza vaccination was first recommended in the UK for individuals in certain high risk groups in the late 1960s *(58)*. Before 2013, influenza vaccination was only recommended for children in certain clinical risk groups, and vaccine coverage across all children was rarely measured. Beginning in 2013, the UK began a phased introduction of influenza vaccination in children, and regular surveys measuring the vaccine coverage rates became available *(59, 60)*. For the model, we assumed a linear rate of increase between 1966 and 2012, assuming 0% coverage in 1966 and using the estimated 13.4% coverage of children aged 0-2 in 2007 to calibrate the rate of coverage increase between 1966 and 2012 *(61)*. For 2013,

2014, and 2015, the maximal coverage values reported in age groups 0-5 were used: these were 42.6%, 41.3%, and 54.4%, respectively *(60, 62)*.

One hundred simulations were run for each pandemic scenario. To appropriately represent all sources of uncertainty, each simulation was run with independent values of H_m, A_c, and A_e drawn from the relevant sampling distributions.

Projections of R_{eff} (Fig. 1-3B, Fig. 1-S9) were created for the UK, China, and Vietnam, assuming that a group 1 HA had constant seasonal dominance of 0%, 25%, 75%, or 100% from 2015 to 2060. For a given country, seasonal dominance scenario, and year, the fraction of each birth-year cohort with first exposure to each HA group was calculated as described in Methods (Reconstructing immune imprinting patterns) and used in conjunction with H_m to calculate the proportion of each birth-year cohort that would experience a 'protected' versus 'unprotected' course of infection with H5 or H7 IAV. The next generation matrix for a fully naïve population **M** (described in the previous section) was modified to separate 'protected' and 'unprotected' individuals, and account for the reduced infectiousness of 'protected' individuals (governed by α), and R_{eff} was calculated as the dominant eigenvalue of this matrix.

SUPPLEMENTARY TEXT

Likelihood Functions

The probability density function for the multinomial distribution is:

$$P(x_1, x_2, \ldots x_n) = \frac{n!}{\prod x_i!} \prod {p_i}^{x_i} \quad \text{(S1)}$$

In our analysis, for a given country in a given year, we considered the multinomial probability of observing a certain number of cases or fatalities, x_i, in each birth year, i. Each of our models assumes different factors may influence p_i, the probability that any case has birth year i.

To find the likelihood of the full data, which comes from several countries in several case observation years, we multiply the multinomial probabilities from all relevant countries, c, and all relevant years of case observation, y. The full likelihood is:

$$L = \prod_y \prod_C \left[\frac{n_{yc}!}{\prod x_{yci!}} \prod p_{yci}^{x_{yci}} \right] \quad \text{(S2)}$$

From equation S2, we obtain the full log likelihood:

$$L = \sum_y \sum_c \left[\log(n_{yc}!) - \sum_i \log(x_{yci}!) + \sum_i x_{yci} \log(p_{yci}) \right] \quad \text{(S3)}$$

Maximum likelihood estimation was performed in R (version 3.2.0) and the optim() function was used to minimize the negative log likelihoods of candidate models. Code for model fitting is provided as a supplementary data file within the published version of this article (DOI: 10.1126/science.aag1322).

Model equations

Each model below assumes that a unique combination of five possible factors determine p_{yci}, the probability that an infection or death observed in year y, country c, occurred in birth cohort i (Methods, Table 1-S1). Demography (D) serves as the null hypothesis for the

distribution of cases across birth years, and appears in every model. We assume all additional factors act independently. In all models, we normalize the probabilities to ensure $\sum_{i=1918}^{y} p_{yci} = 1$.

Demography (D)

This model assumes incidence in each birth year should be proportional to the fraction of the population of country *c*, year *y*, born in the year of interest.

$$p_{yci} = D_{yci} \tag{S4}$$

D_{yci} = Fraction born in year *i*, of the total population of country *c* born between 1918 and the case observation year (*y*).

Demography + exposure (DE)

This model adds a factor describing poultry exposure risk across age groups.

$$p_{yci} = D_{yci} E_{yi} \tag{S5}$$

E_{yi} = Proportional risk in each birth year cohort, based on the frequency with which individuals of a given age (birth year *i*, in year *y*) contact poultry.

Demography + age-based risk (DA)

This model introduces parameters that allow children ages 0-4 or the elderly ages 65+ to experience increased risk relative to other children and adults.

$$p_{yci} = D_{yci}(u_{c_{yi}}A_c + u_{e_{yi}}A_e + u_{a_{yi}})$$

(S6)

Group indicators

- $u_{c_{yi}}$ = Indicator of membership in the age group representing high-risk children, taking value 1 for birth year cohorts of age 0-4 in year *y*, and 0 for all others.
- $u_{a_{yi}}$ = Indicator of membership in the reference age group, taking value 1 for birth year cohorts of age 5-64 in year *y*, and 0 for all others.
- $u_{e_{yi}}$ = Indicator of membership in the high-risk, elderly age group, taking value 1 for birth year cohorts of age 65+ in year *y*, and 0 for all others.

Parameters

- A_c = Proportional increase in risk for children ages 0-4, relative to the reference age group.
- A_e = Proportional increase in risk for the elderly, ages 65+, relative to the reference age group.

Demography + hemagglutinin imprinting (DH)

This model introduces parameter H_m, which allows individuals with group-matched first hemagglutinin exposures to experience decreased risk relative to all others.

$$p_{yci} = D_{yci}(w_{m,i|y,c}\, H_m + w_{o,i|y,c})$$

(S7)

Group indicators

- $w_{m,i|y,c}$= Faction of each birth cohort with protective HA imprinting (group-matched to the challenge strain). This group should experience reduced risk under the HA imprinting hypothesis.
- $w_{o,i|y,c}$ = Fraction of each birth cohort without protective HA imprinting. This group includes both IAV-naïve children and all individuals with HA-mismatched first exposures.

  Parameters
- H_m = Proportional risk for individuals with group-matched first hemagglutinin exposures, relative to all others. H_m takes values in the range [0, 1], where 0 indicates full protection and 1 indicates no additional protection relative to the reference group.

Demography + neuraminidase imprinting (DN)

This model introduces parameter N_m, which, similarly to the DH model above, allows those with group-matched first neuraminidase exposures to experience decreased risk.

$$p_{yci} = D_{yci}(w_{m,i|y,c}N_m + w_{o,i|y,c}) \quad \text{(S8)}$$

Group indicators

- $w_{m,i|y,c}$= Fraction of each birth cohort with NA imprinting group-matched to the challenge strain.
- $w_{o,i|y,c}$ = Fraction of each birth cohort without protective NA imprinting.

  Parameters

- N_m = proportional reduction in risk for individuals with group-matched first hemagglutinin exposures, relative to all others. N_m takes values in the range [0, 1], where 0 indicates full protection and 1 indicates no additional protection relative to the reference group.

Demography + neuraminidase imprinting + hemagglutinin imprinting (DNH)

This model includes protection from first exposure to a group-matched HA (as in the DH model) as well as a group-matched NA (as in the DN model).

$$p_{yci} = D_{yci}(H_m N_m w_{mm,i|y,c} + H_m w_{mo,i|y,c} + N_m w_{om,i|y,c} + w_{oo,i|y,c}) \quad \text{(S9)}$$

Group indicators

- $w_{mm,i|y,c}$ = Fraction of each birth cohort with matched imprinting to HA and NA.
- $w_{mo,i|y,c}$ = Fraction of each birth cohort with matched HA imprinting and mismatched NA imprinting.
- $w_{om,i|y,c}$ = Fraction of each birth cohort with mismatched HA imprinting and matched NA imprinting.
- $w_{oo,i|y,c}$ = Fraction of each birth cohort with mismatched imprinting to HA and NA, or that is naïve to IAV infection.

Demography + age-based risk + hemagglutinin imprinting (DAH)

This model assumes that demography, age-based risk and HA imprinting determine overall risk.

$$p_{yci} = D_{yci}(w_{m,i|y,c}H_m + w_{o,i|y,c})(u_{c_{yi}}A_c + u_{e_{yi}}A_e + u_{a_{yi}})$$

(S10)

Demography + age-based risk + neuraminidase imprinting (DAN)

This model assumes that demography, age-based risk and neuraminidase imprinting, determine overall risk.

$$p_{yci} = D_{yci}(w_{m,i|y,c}N_m + w_{o,i|y,c})(u_{c_{yi}}A_c + u_{e_{yi}}A_e + u_{a_{yi}})$$

(S11)

Demography + age-based risk + neuraminidase imprinting + hemagglutinin imprinting (DANH)

This model assumes that demography, age-based risk, neuraminidase imprinting and hemagglutinin imprinting determine overall risk.

$$p_{yci} = D_{yci}\left(H_m N_m w_{mm,i|y,c} + H_m w_{mo,i|y,c} + N_m w_{om,i|y,c} + w_{oo,i|y,c}\right)(u_{c_{yi}}A_c + u_{e_{yi}}A_e + u_{a_{yi}})$$

(S12)

Demography + exposure + age-based risk (DEA)

This model assumes that demography, exposure frequency and age-based risk determine overall risk.

$$p_{yci} = D_{yci}E_{yi}(u_{c_{yi}}A_c + u_{e_{yi}}A_e + u_{a_{yi}})$$

(S13)

Demography + exposure + hemagglutinin imprinting (DEH)

This model assumes that demography, exposure frequency and hemagglutinin history determine overall risk.

$$p_{yci} = D_{yci}E_{yi}(w_{m,i|y,c}H_m + w_{o,i|y,c})$$

(S14)

Demography + exposure + neuraminidase imprinting (DEN)

This model assumes that demography, exposure frequency and neuraminidase history determine overall risk.

$$p_{yci} = D_{yci}E_{yi}(w_{m,i|y,c}N_m + w_{o,i|y,c})$$

(S15)

Demography + exposure + age-based risk + hemagglutinin imprinting (DEAH)

This model assumes that demography, exposure frequency, age-based risk and hemagglutinin imprinting determine overall risk.

$$p_{yci} = D_{yci}E_{yi}(w_{m,i|y,c}H_m + w_{o,i|y,c})(u_{c_{yi}}A_c + u_{e_{yi}}A_e + u_{a_{yi}})$$

(S16)

Demography + exposure + age-based risk + neuraminidase imprinting (DEAN)

This model assumes that demography, exposure frequency, age-based risk and neuraminidase imprinting determine overall risk.

$$p_{yci} = D_{yci}E_{yi}\left(w_{m,i|y,c}N_m + w_{o,i|y,c}\right)\left(u_{c_{yi}}A_c + u_{e_{yi}}A_e + u_{a_{yi}}\right)$$

(S17)

Demography + exposure + neuraminidase imprinting + hemagglutinin imprinting (DENH)

This model assumes that demography, exposure frequency, hemagglutinin imprinting and neuraminidase imprinting determine overall risk.

$$p_{yci} = D_{yci}E_{yi}(H_m N_m w_{mm,i|y,c} + H_m w_{mo,i|y,c} + N_m w_{om,i|y,c} + w_{oo,i|y,c}) \quad \text{(S18)}$$

Demography + exposure + age-based risk + neuraminidase imprinting + hemagglutinin imprinting (DEANH)

This model assumes that demography, exposure frequency, age-based risk, neuraminidase imprinting and hemagglutinin imprinting determine overall risk.

$$p_{yci} = D_{yci}E_{yi}(H_m N_m w_{mm,i|y,c} + H_m w_{mo,i|y,c} + N_m w_{om,i|y,c} + w_{oo,i|y,c})(u_{c_{yi}}A_c + u_{e_{yi}}A_e + u_{a_{yi}}) \quad \text{(S19)}$$

Reconstructing HA imprinting patterns with vaccination

When IAV-naïve children receive the seasonal influenza vaccine, the effect on HA imprinting in these children is unknown. We chose not to consider childhood vaccination in our main analysis, but instead to consider its possible effects via subsequent sensitivity analyses. Our rationale for omitting childhood vaccination in our main analysis was based on three main arguments.

First, childhood vaccination coverage is low in all H5N1- and H7N9-affected countries, so any effects of childhood vaccination on our results would be small. China and Thailand have

recently launched public health initiatives to encourage early childhood influenza vaccination. However, even in these countries, recent estimates of childhood vaccine coverage are relatively low (and quite variable), ranging from 1% *(63)* to 30% *(64)* in Thailand, and from 26% *(65)* in China to <9% *(66)* in Hong Kong. For all other countries in our study, conservative estimates based on the number of vaccine doses purchased *(48)* show that even in the upper-bound limit that all vaccine doses were administered, and were distributed exclusively among children ages 0-9 years, childhood coverage would remain well below 5% in these countries (details below).

Second, early childhood influenza vaccination has only been widely recommended since the mid-late 2000's *(64, 67)*. Thus, the great majority of birth cohorts in our study would not have been affected at all. Since our study's conclusions are driven most strongly by the dramatic change from group 1 to group 2 HA imprinting around the 1968 birth year, our conclusions are robust to variation in HA imprinting patterns in the very young birth cohorts that could have been affected by very recent, moderate increases in early childhood vaccination.

Third, for naïve children, single-dose influenza vaccine efficacy is exceptionally low, so the coverage estimates stated above strongly overestimate the effective vaccine coverage levels relevant to our analysis. IAV-naïve individuals require a series of two vaccine doses for effective protection *(67, 68)*. However, in the United States, CDC data shows that only about 60% of children aged 6-24 months complete the two-dose course. We have not found equivalent data for H5N1- or H7N9-affected countries, but two-dose compliance is unlikely to be drastically better than in the US.

Given these arguments, we expected that childhood vaccination would have a minimal impact on our main findings, no matter how vaccination of IAV-naïve children affects HA imprinting at the individual scale. To test this expectation, we performed sensitivity analyses that

considered three possible effects of imprinting: 1, vaccination of naïve children could prevent imprinting to either HA group, 2, vaccination of naïve children could cause dual imprinting to both HA groups or 3, vaccination of naïve children could delay the first natural infection and hence delay imprinting.

All of these sensitivity analyses required estimates of childhood vaccination coverage and efficacy for each country and year. Because reported estimates of childhood vaccine coverage vary considerably among studies, we estimated conservative, upper-bound limits on the true coverage to test the maximum effect childhood vaccination might have on our findings. We used data from Palache et al. *(48)* to determine the total number of vaccine doses distributed in each country of interest over time. For each year, we made the conservative assumption that all doses within the country were administered, and distributed uniformly among children ages 0-9. In reality, not all doses are administered, and administered doses are actually distributed across all age groups, not exclusively in young children. Furthermore, while some naïve children would in reality receive two vaccine doses, we estimated upper-bound coverage levels as though all children required only one dose. We assumed vaccine efficacy was 60% in all non-pandemic years. This upper-bound efficacy estimate reflects that, as discussed above, at most 60% of naïve children complete the required two-dose course *(67).* This efficacy estimate is further conservative because even among children that receive two doses, the vaccine will not be perfectly protective due to antigenic drift.

In our first sensitivity analysis, we assumed that vaccination of IAV-naïve children delays the first natural infection, and hence delays imprinting, but does not affect imprinting otherwise. To estimate the fraction of each birth cohort with imprinting to particular seasonal

subtypes, we incorporated the assumed vaccine-induced delay of imprinting by revising the definition of the annual attack rate on children, a_j (see equation 4 in Methods):

$$a_j' = \left(1 - v_j e_j\right) a I_j \tag{S20}$$

Here v_j describes childhood IAV coverage in year j, e_j describes IAV vaccine efficacy, a represents the baseline attack rate on children and I_j represents the year's intensity score. With these modifications, we estimated vaccine-influenced imprinting patterns and performed model analyses as described in the Methods (Reconstructing immune imprinting patterns).

In our second and third sensitivity analyses, we assumed vaccination would prevent or replace imprinting in IAV-naïve children, so all children vaccinated before their first natural infection would either remain fully susceptible to both HA groups, or would simultaneously imprint to both groups. Here, it became necessary to keep track of the fraction first exposed via natural infection, the fraction first exposed via vaccination, and the fraction that remained naïve in the first 12 years after the birth year. We computed these using a recursive approach:

$$\varepsilon_{ij}{}' = n_{i,j-1}\left(1 - v_i e_j\right) a I_j \tag{S21}$$

$$\lambda_{ij} = n_{i,j-1}\, v_i e_j \tag{S22}$$

$$n_{ij} = n_{i,j-1}\left(1 - v_i e_j\right)\left(1 - a I_j\right) \tag{S23}$$

Here, as in equation 3 and 4, $\varepsilon_{ij}{}'$ represents the fraction of birth cohort i that was first naturally infected in year j (prime indicates modification of the main text definition). λ_{ij}

represents the fraction of birth cohort *i* that was first vaccinated (prior to their first natural exposure) in year *j*. n_{ij} represents the fraction of cohort *i* that remained naïve at the beginning of year *j,* and was thus eligible for first infection or vaccination as year *j* progressed. In the first year of life (when $j = i$), n_{ii} is set to 1, indicating that all newborns are initially naïve. In all subsequent years, *j,* probabilities of first vaccination or natural infection were only applied to the naïve fraction of the cohort. Parameters v_j, e_j, a and I_j are as defined above.

After calculating relevant raw values of $\varepsilon_{ij}{}'$ and λ_{ij}, we applied a normalizing factor, $N_{i|y}{}'$ to all $\varepsilon_{ij}{}'$ and $\lambda_{ij.}$ As discussed in equation 4, the normalizing factor reflects the assumption that all individuals have their first natural infection or vaccination by age 12, and ensures that all relevant probabilities for a birth year sum to 1. It is given by:

$$N_{i|y}{}' = \begin{cases} \sum_{j=i}^{i+12}(\varepsilon_{ij} + \lambda_{ij}) & y \geq i+12 \\ 1 & y < i+12 \end{cases} \quad \text{(S24)}$$

Finally, in the analysis assuming that vaccination of IAV-naïve children prevents imprinting, we always assigned the fraction of each cohort that was vaccinated before the first natural infection, $\sum_j \lambda_{ij,}$ to the mismatched-imprinting group, $w_{o,i|y,c}$, as defined in equation 6 above. In the analysis assuming that vaccination of IAV-naïve children causes dual imprinting, we always assigned fraction $\sum_j \lambda_{ij}$ to the matched-imprinting group, $w_{m,i|y,c}$. Even at the upper limits of plausible vaccination coverage rates, our main results remained robust in all three sensitivity analyses (Fig. 1-S7).

Annual intensity of influenza circulation from 1918-2015

Before 1977, the annual intensity of influenza circulation (which scales the annual attack rate) has minimal influence on imprinting patterns, since the dominant HA group changed only once, during the 1968 pandemic. To model the post-1977 era of H3N2 and H1N1 co-circulation, when the dominant HA group could change on yearly rather than pandemic timescales, we obtained virological surveillance data from WHO collaborating laboratories. These data are available from 1977-2015, providing a direct measure of annual IAV incidence. In years prior to 1977, the best estimates of the annual influenza burden come from pneumonia and influenza (P&I) excess mortality data from the United States *(69)*. Thus, to estimate annual IAV intensity, we compiled estimates of incidence from virological surveillance data in years 1977-2015, and P&I excess mortality data in years 1918-1976. Sensitivity analyses (Fig. 1-S7) confirmed that our study's results are quantitatively and qualitatively robust to uncertainty in the intensity index, and the results also remained robust when we replaced the intensity index with a constant value.

For 1997-2015 we obtained influenza surveillance data from our study's six countries of interest. To shield against local biases in case ascertainment and small sample sizes, we aggregated data across all six countries to model annual intensity. We defined raw annual incidence as: $\frac{Total\ IAV\ positive\ specimens\ in\ all\ countries}{Total\ IAV\ specimens\ processed\ in\ all\ countries}$. In years when the total number of reported specimens processed across all six affected countries was less than 50 (1997, 2000 and 2001), we substituted surveillance data from the United States. For 1977-1996 we could not find influenza surveillance data from countries affected by H5N1 and H7N9. Thus, we also substituted data from the United States for this time period *(47)*.

After aggregating influenza surveillance data for all years from 1977-2015, we found that the observed annual incidence of influenza has increased predictably over time. A linear regression showed that the proportion of positive IAV specimens increased by about 0.0019/year (SE = 0.0006, p = 0.005). We assume this trend reflects a steady improvement in case detection efficiency, perhaps due to improved diagnostics or more targeted sampling, rather than a true increase in the annual influenza incidence proportion. Thus, we used this linear model to define yearly, expected incidence values for 1977-2015, and then defined annual circulation intensity as the ratio of observed to expected incidence.

For 1918-1976, we compiled published estimates of pneumonia and influenza (P&I) excess mortality rates, per 100,000 population, for each year *(69-74).* Because northern hemisphere influenza seasons occur in the winter, estimates were not always reported on a calendar year basis. Instead, rates were often reported for a defined outbreak period, beginning and ending in specified months. In these cases, to adjust to the calendar year basis on which we defined birth cohorts, we first determined the fraction of outbreak months occurring within each calendar year, and then allocated the appropriate fraction of the season's total excess mortality to either relevant year. By definition, excess mortality takes only non-negative values, but intensity values informed by surveillance data could be positive or negative (Fig. 1-S10 A). To verify that our results are robust to this discrepancy, we performed a sensitivity analysis in which we shifted all P&I scores down by their mean (thus allowing the P&I series to also take positive and negative values). This did not change the results of model selection, or notably change the maximum likelihood value of parameter H_m. Because we used our intensity time series to inform IAV imprinting patterns, we set excess mortality equal to zero in years dominated by type B

influenza. In years when types A and B were co-dominant, we attributed half the total reported excess mortality to influenza A.

When verifying the comparability of excess mortality and incidence data, we found that the variance in post-1977 intensity estimates (informed by virological surveillance data) was greater than the variance in 1918-1976 estimates (informed by excess mortality data). To correct this discrepancy, we scaled the variance in the older P&I data set to match the variance of non-negative values in more recent surveillance-based estimates (thus giving the two series similar amplitude). We allowed a maximum intensity score of 2.5, to maintain a reasonable maximum annual attack rate of 0.75 or less. The maximum score applied only in years 1918, 1919, 1944 and 2009, all of which are recognized as years of intense influenza circulation. Annual intensity values and corresponding attack rates are shown in Fig. 1-S10.

Country-specific model fits and model selection

We conducted the full maximum likelihood estimation and model comparison analysis for each of the six countries in our study, in isolation. We found that strong support for HA imprinting effects was maintained in these country-specific analyses. In the four countries with the most cases (China, Egypt, Indonesia and Vietnam, $n \geq 75$), the best models all included HA imprinting, with estimates of protective efficacy (H_m) very similar to the estimate in the main text. In Thailand ($n = 28$), and Cambodia ($n = 57$), despite very low numbers of cases, models including HA imprinting effects were the second most preferred in model selection, and were statistically indistinguishable from the best models, with ΔAIC of 0.45 and 0.47, respectively. Country-specific case distributions, model fits and the results of country-specific model comparison are shown in Fig. 1-S11.

These analyses show that patterns in all countries are qualitatively consistent with core findings presented in the main text: in each of the countries, very few H5N1 cases are observed in cohorts born before 1968. The major distinction among countries is the difference in number of H5N1 cases reported in children (i.e. birth-years since 2005). Relative to the consensus model, excess cases are observed in children in Cambodia and Egypt, but a shortfall of cases in children is observed in Indonesia, China and Vietnam. Country-specific variation in poultry contact, access to healthcare, or case reporting for children could explain these differences. Variation in imprinting patterns (resulting from different experiences with the 2009 pandemic in different regions) could also be at play. While we do not have data to test these potential explanations, we note that children are not under-represented for H7N9 in China (the one country where we can make a direct comparison), which weighs against the former explanations in this one country at least.

Cross-validation analysis

To verify that our data sets are large enough to produce robust model comparison results, and to assess the out-of-sample predictive capability of our models, we performed two-fold cross-validation. We performed these analyses for H5N1 and H7N9 data. Each trial consisted of the following steps:

i. Randomly partition the data set (of H5N1 or H7N9 cases) into two equal subsets. Designate one half of the data as the training set, and the other half as the test set.

ii. Fit all 16 models (D, DR, DH, DN, …etc.) to the training set, determining maximum-likelihood estimates of all model parameters. Calculate AIC values to determine which fitted model performs best on the training set.

iii. Find the likelihood of the test data, given all models and their maximum-likelihood parameter estimates (determined in step ii, using the training set). Determine which model is the best fit to the test data based on likelihood.

iv. Test for robustness to reduced sample size: Are HA imprinting effects included in the best model from step ii, after fitting to a data set of half the size used in the main text analysis? Does the best model match the preferred model from the main text?

v. Test the best model's performance on out-of-sample data: Does the best model for the test data contain HA imprinting effects? Does it match the preferred model from the main text?

vi. Now, switch the subset assignments, so the original test set becomes the new training set, and vice versa. Repeat steps ii-v.

We performed 100 cross-validation trials for each of the H5N1 and H7N9 data sets (so 200 unique training sets were used, see step vi). For H5N1, DRH (the preferred model in the main text analysis) remained the best model for 99% of the training sets. The median and central 95% of H_m estimates were 0.25 (0.17-0.32). For H7N9, DERH (the preferred model in the main text analysis) remained the best model for 100% of the training sets. The median and central 95% of H_m estimates were 0.24 (0.17-0.33). For both H5N1 and H7N9, these H_m values are statistically indistinguishable from estimates obtained using the full data set (see Table 1-S2). Thus, for both H5N1 and H7N9, our core results are robust to the exclusion of half of our available data.

These same models were also strongly preferred by the test sets—DRH was the best model for 92% of H5N1 test sets and DERH was the best model for 97.5% of H7N9 test sets. In

all cases, the best model for the test set included HA imprinting effects. Thus, barring major changes to the biology or epidemiology of these viruses, the best models presented in the main text are suitable for approximate prediction of the birth year distributions of newly arising cases, and HA imprinting effects remain an important predictor in all cases.

Robustness to age biases in case ascertainment

Epidemiological data sets are always subject to possible biases in case ascertainment. As discussed above, we introduced age-based risk parameters A_c and A_e to allow for the increased risk of severe infection (and associated increase in case ascertainment) for children and the elderly, a known pattern from seasonal influenza epidemiology *(41)*. However, other forms of age-specific bias might be present in the data sets we analyzed. Given the centrality of age-related patterns to our findings (insofar as they are connected to birth year), we undertook an extreme test of whether our core results are robust to a hypothetical worst-case bias in case ascertainment. Specifically, we tested the effect of a hypothetical bias that systematically degraded the strongest signal of HA imprinting in the data, i.e. the 1968 shift from group 1 to group 2 dominance in seasonal IAV strains. Thus we used simulations to consider scenarios in which severe H5N1 cases born before 1968, or severe H7N9 cases born after 1968, had lower probabilities of being ascertained, relative to cases in other birth years.

We note that this is a 'perfectly bad' reporting bias, and is based on birth year rather than age (and hence would require the bias to drift systematically over nearly two decades, for H5N1). Also, we emphasize that our work focuses on the influence of imprinting on severe cases of disease, which are much less likely to be subject to reporting bias than mild or subclinical cases. A recent review of H5N1 and H7N9 epidemiology by Qin et al *(1)* did highlight the

potential for under-ascertainment of milder cases of H7N9, which are disproportionately found in younger individuals (and are often found in the course of cluster investigations, following severe index cases). Crucially, this is exactly the pattern that our findings would predict, since younger individuals are more likely to be imprinted on group 2 HA and hence protected from severe H7 disease. Qin et al. did not find any evidence of substantial under-ascertainment of H5N1 cases, and do not suggest any age bias in reporting.

For H5N1, we considered scenarios where severe cases occurring in older, pre-1968 birth cohorts were 50%, 33% or 25% as likely to be observed as cases in younger, post-1968 cohorts. Thus, we used simulation to add hypothetical unobserved cases into the data set, increasing the number of H5N1 cases by a factor of 2, 3 or 4 in the pre-1968 cohorts where these cases are rare in the real data. Effectively, this decreased differences in apparent risk between pre- and post-1968 birth cohorts, systematically diminishing the signature of HA imprinting effects.

Similarly, for H7N9, we considered scenarios where severe cases occurring in underrepresented, post-1968 birth cohorts were 50%, 33% or 25% as likely to be observed as cases occurring in older cohorts. We again used simulation to increase the number of cases in underrepresented cohorts by factors of 2, 3 or 4, respectively.

The number of cases added to each country-year depended on the number of cases observed in the same country-year in underrepresented cohorts for H5N1 (1918-1968), or H7N9 (1969-2015). This number was multiplied by the factor required to double, triple or quadruple the number of cases in these augmented birth cohorts. The probability that an added case was assigned to a particular birth year was proportional to the demographic age distribution across augmented birth years for the country and year of interest. For each virus and assumed relative detection probability, we generated 100 augmented data sets. We performed model fitting and

comparison on each augmented data set to determine whether HA imprinting would remain a factor in the best model, and to quantify the value of parameter H_m in these best models. Representative trials are shown in Fig. 1-S12.

We found that both H5N1 and H7N9 were robust to 'perfectly bad' age-biased reporting at the 50% reporting level: the DAH model remained the selected model in all 100 trials for H5N1, with a median H_m parameter estimate of 0.54; similarly, the DEAH model remained the selected model in all 100 trials for H7N9, with a median H_m parameter estimate of 0.54. For H7N9, even larger, 'perfectly bad' biases did not change the core finding. At the 33% and 25% levels, model selection still supported HA imprinting in 99% and 85% of trials, respectively (though the preferred model switched from DEAH to DAH). For H5N1, at the 33% relative detection level, DRH remained the best model in 76% of trials (with a weak H_m parameter estimate), but in the remaining 24/100 trials, HA imprinting effects were not included in the best model. At 25% relative detection, only 16/100 best models included HA imprinting effects

In reality, it seems highly unlikely that case ascertainment would depend on birth year instead of age, that 1968 would coincidentally act as a key turning point separating some middle-aged adults from others, or that ascertainment of H5N1 and H7N9 cases would pivot in opposite directions around 1968. Furthermore, it seems unlikely that age or birth-year specific differences in detection of *severe* cases (the focus of our study) would differ by a factor of two or more. Thus, given the fact that our core results are robust to case ascertainment biases 3-fold or more, even with bias parameters specifically designed to degrade the imprinting signal, we are confident that plausible biases would not be large enough to challenge our study's core findings.

Binomial exact test for mortality

One-sided binomial exact tests showed that census-excess H5N1 mortality was significantly less likely to occur in cohorts born before 1968 (estimated probability = 0.06, CI=0.00-0.19, $p < 1e^{-6}$). For H7N9, census-excess mortality was significantly more probable in the same birth years (estimated probability = 0.94, CI=0.83-1.00, $p < 1e^{-7}$). As introduced in the main text, the same test revealed similar patterns for the incidence of H5N1 (estimated probability = 0.00, CI=0.00-0.08, $p < 1e^{-10}$) and H7N9 (estimated probability = 0.93, CI=0.84-1.00, $p < 1e^{-9}$).

Analysis of novel subtypes other than H5N1 and H7N9

We searched the literature and avian influenza reports for clinically significant human cases of zoonotic IAV (other than H5N1 and H7N9) in which the year and country of the case was known and the age of the infected individual was reported (n=28). We excluded cases where the clinical manifestation was limited to conjunctivitis.

To examine whether the data were better explained by the Demography (D) or the Demography + Hemagglutinin imprinting (DH) model (described in sections 2.1 and 2.4 above), we performed a simple-versus-simple hypothesis test using the likelihood ratio as the test statistic. The null distribution of the test statistic (the distribution of likelihood ratio values generated under the assumption that the D model is true) was approximated using 250,000 simulated data sets. The quantile score of the true data's likelihood ratio in this distribution was used to generate the p-value reported in the main text.

Parameter identifiability

We designed our family of multinomial models to allow for elevated risk of severe disease in young children and adults, via the parameters A_c and A_e respectively, to ensure that we accounted for all known age-related effects before testing our hypothesis of HA imprinting. However, a challenge arises in our study because there are very few H5N1 cases observed in the elderly, and few H7N9 cases observed in children (see Fig. 1-2A, B). Thus, we have little statistical power to discern possible age-based risk effects in those groups. As a consequence, our results show elevated risk in age groups where we do see cases (i.e. in children for H5N1, and in the elderly for H7N9), but age-specific effects are not detected in age groups where cases do not frequently occur (Table 1-S2). This leads to an effect where the age-based risk appears to act in concert with HA imprinting. It is thus prudent to consider the possibility that the age-based risk parameters (A_c and A_e) and matched-imprinting protection parameter (H_m) are not perfectly identifiable.

We performed three analyses to verify that our central findings are not meaningfully affected by this potential issue with parameter identifiability. First, we plotted two-dimensional likelihood profiles for the parameter pairs of concern (figures not shown). These profiles show only weak positive correlations between the parameters H_m and A_c (for H5N1) and H_m and A_e (for H7N9). This indicates that identifiability is not a major concern. Second, from these profiles, we computed marginal 95% confidence intervals, and found values only slightly different from the univariate confidence intervals reported in Table 1-1 in the main text. For H5N1, the univariate CI on A_c was 1.83-2.57, and the marginal CI from the bivariate analysis was 1.75-2.65. For H7N9, the univariate CI on A_e was 1.74-2.51, and the marginal CI from the bivariate analysis was 1.68-2.58. Again, the small differences between univariate confidence

intervals and marginal, bivariate confidence intervals indicate that identifiability is not a major issue for these parameters.

Third, as a final check, we combined H5N1 and H7N9 data into a single model, and constrained parameters H_m, A_c and A_e to take the same values for both viruses (see details above in section 7). We then computed the maximum likelihood estimates for all three parameters, using the combined data set. The combined data set contained large numbers of cases in both old and young age groups, and gave us more power to estimate age-specific risk effects. The consensus estimates for A_c (1.78, 95% CI 1.53-2.07) and A_e (1.91, 95% CI 1.64-2.23) were statistically indistinguishable from the estimates of A_c (using H5N1 data) and A_e (using H7N9 data) presented in the main text analysis.

ACKNOWLEDGEMENTS

M.A. is supported by the National Science Foundation Graduate Research Fellowship (DGE-1144087). M.W. is supported by the David and Lucile Packard Foundation. J.O.L-S. is supported by the National Science Foundation (EF-0928690), the Research and Policy for Infectious Disease Dynamics (RAPIDD) program of the Science and Technology Directorate, Department of Homeland Security, and Fogarty International Center, National Institutes of Health. The content is solely the responsibility of the authors and does not necessarily represent the official views of the National Institutes of Health. The authors declare no competing financial interests.

SUPPLEMENTARY FIGURES AND TABLES

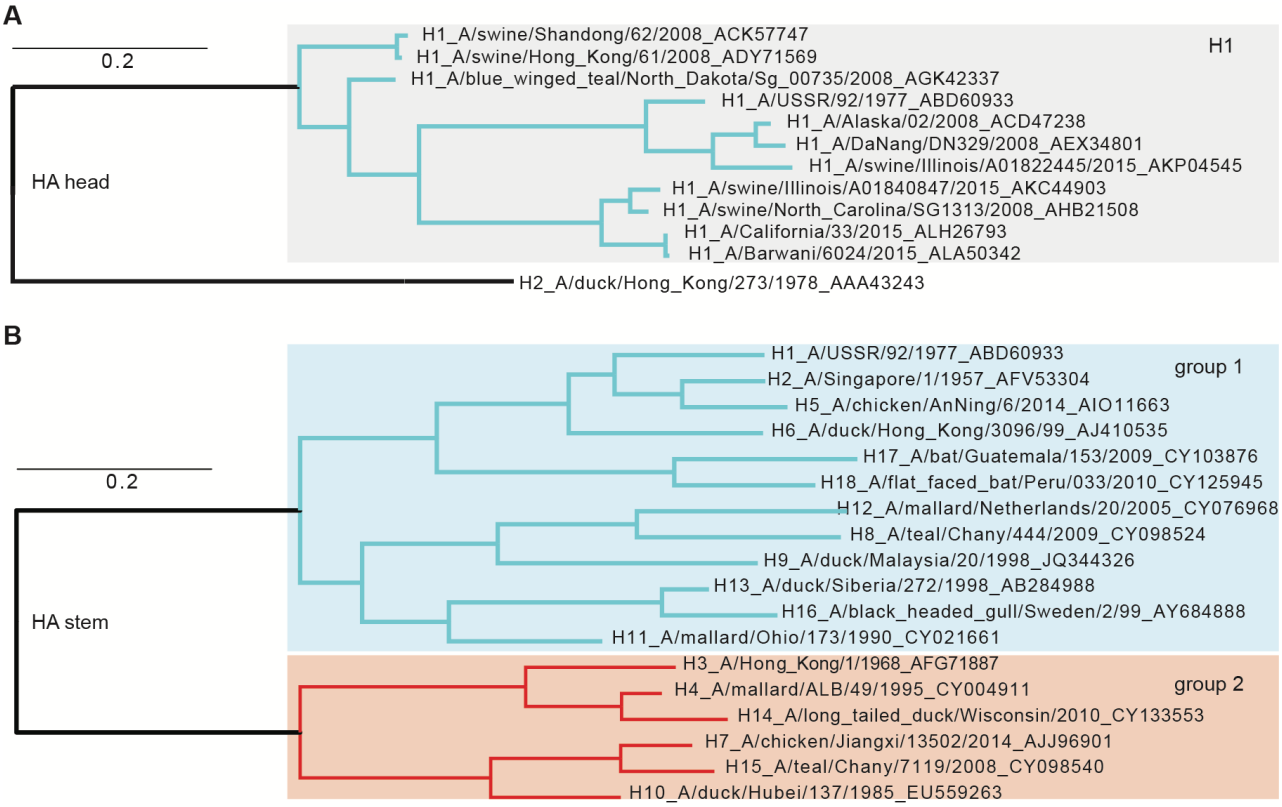

C

		group 1												group 2					
		H1	**H2**	H5	H6	H8	H9	H11	H12	H13	H16	H17	H18	**H3**	H4	H7	H10	H14	H15
group 1	**H1**		95.6	94.3	93.0	84.8	86.3	88.6	85.1	86.1	85.8	88.6	87.0	80.3	80.0	78.5	79.7	79.6	77.2
	H2	95.6		97.8	92.7	85.7	85.7	88.6	85.1	86.1	85.4	89.8	89.8	80.6	80.3	79.7	80.4	80.2	77.5
	H5	94.3	97.8		91.2	84.6	84.3	86.8	84.0	85.3	84.3	89.3	90.9	78.3	77.7	77.7	78.3	78.8	76.4
	H6	93.0	92.7	91.2		86.7	83.2	88.3	85.4	86.1	84.8	86.7	86.0	79.4	79.7	80.1	81.0	80.2	79.1
	H8	84.8	85.7	84.6	86.7		90.2	87.3	91.4	88.3	88.3	85.4	84.8	76.8	77.5	77.5	77.2	76.7	76.9
	H9	86.3	85.7	84.3	83.2	90.2		88.6	90.5	87.0	88.0	83.8	84.8	78.4	79.0	77.2	76.3	78.6	76.3
	H11	88.6	88.6	86.8	88.3	87.3	88.6		87.0	93.4	94.3	88.0	87.3	80.4	81.3	79.8	81.7	80.6	78.5
	H12	85.1	85.1	84.0	85.4	91.4	90.5	87.0		87.0	88.3	85.7	85.4	78.7	79.7	77.5	76.3	78.6	76.9
	H13	86.1	86.1	85.3	86.1	88.3	87.0	93.4	87.0		97.5	87.0	85.8	77.2	79.1	79.5	79.2	78.7	79.2
	H16	85.8	85.4	84.3	84.8	88.3	88.0	94.3	88.3	97.5		87.7	86.1	75.9	79.6	78.2	79.2	78.7	77.6
	H17	88.6	89.8	89.3	86.7	85.4	83.8	88.0	85.7	87.0	87.7		94.0	78.1	79.7	78.2	78.5	79.9	77.5
	H18	87.9	89.8	90.9	86.0	84.8	84.8	87.3	85.4	85.8	86.1	94.0		77.8	78.7	77.2	77.5	78.3	75.9
group 2	**H3**	80.3	80.6	78.3	79.4	76.8	78.4	80.4	78.7	77.2	75.9	78.1	77.8		93.9	86.0	87.9	93.6	86.7
	H4	80.0	80.3	77.7	79.7	77.5	79.0	81.3	79.7	79.1	79.7	79.7	78.7	93.9		87.6	87.9	97.4	87.3
	H7	78.5	79.7	77.7	80.1	77.5	77.2	79.8	77.5	79.5	78.2	78.2	77.2	86.0	87.6		93.0	88.8	96.5
	H10	79.7	80.4	78.3	81.0	77.2	76.3	81.7	76.3	79.2	79.2	78.5	77.5	87.9	87.9	93.0		87.5	93.3
	H14	79.6	80.2	78.8	80.2	76.7	78.6	80.6	78.6	78.7	78.7	79.9	78.3	93.6	97.4	88.8	87.5		88.5
	H15	77.2	77.5	76.4	79.1	76.9	76.3	78.5	76.9	79.2	77.6	77.5	75.9	86.7	87.3	96.5	93.3	88.5	

Supplementary Figure 1-S1. Phylogenetic and sequence analyses of HA amino acids.

(**A**) Maximum likelihood phylogenetic tree of H1 HA globular head amino acid sequences. (**B**) HA stem domain amino acid tree. Both trees are drawn at the same scale. (**C**) Heat map showing pairwise similarities between HA stem domain amino acid sequences (same strains as in plot **B)**. The number in each cell is the percent similarity (BLOSUM62 cost matrix) for the relevant pair of sequences, with darker colors indicating higher similarity. Pairwise comparisons for H5 and H7 versus H1, H2, and H3 (the variants that have circulated in human populations since 1918) are depicted in red. Each HA subtype's stem domain is more similar to the other subtypes within its group than to any subtype in the opposing group, consistent with the observed imprinting pattern operating within, but not between, HA groups.

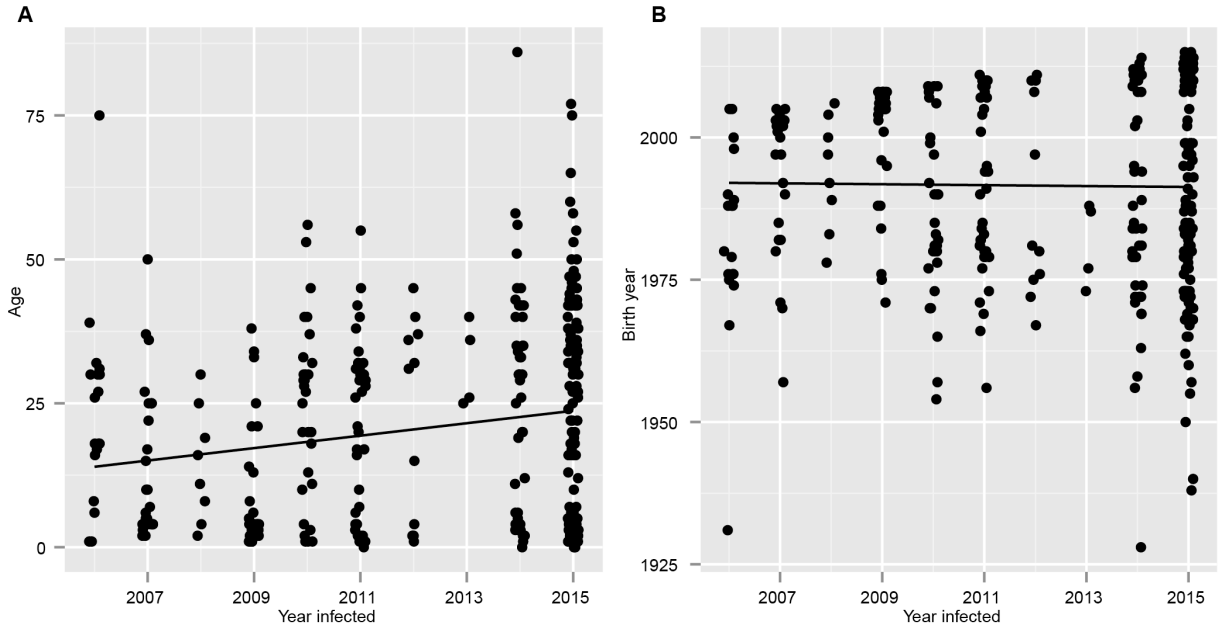

Supplementary Figure 1-S2. Trends in age and birth year of H5N1 cases over time.

For 361 H5N1 cases observed in Egypt from 2006-2015, (**A)** Spearman's rank correlation showed a significant positive association (p = 0.0003, one-sided test) between patient age and year of case observation. Points are jittered around the case observation year, and a least-squares trend line is shown. (**B)** Using the same test, no significant association was found for patient birth year. In support of the HA imprinting hypothesis, these results show that birth year is a more consistent predictor of severe infection risk than age-specific risk factors.

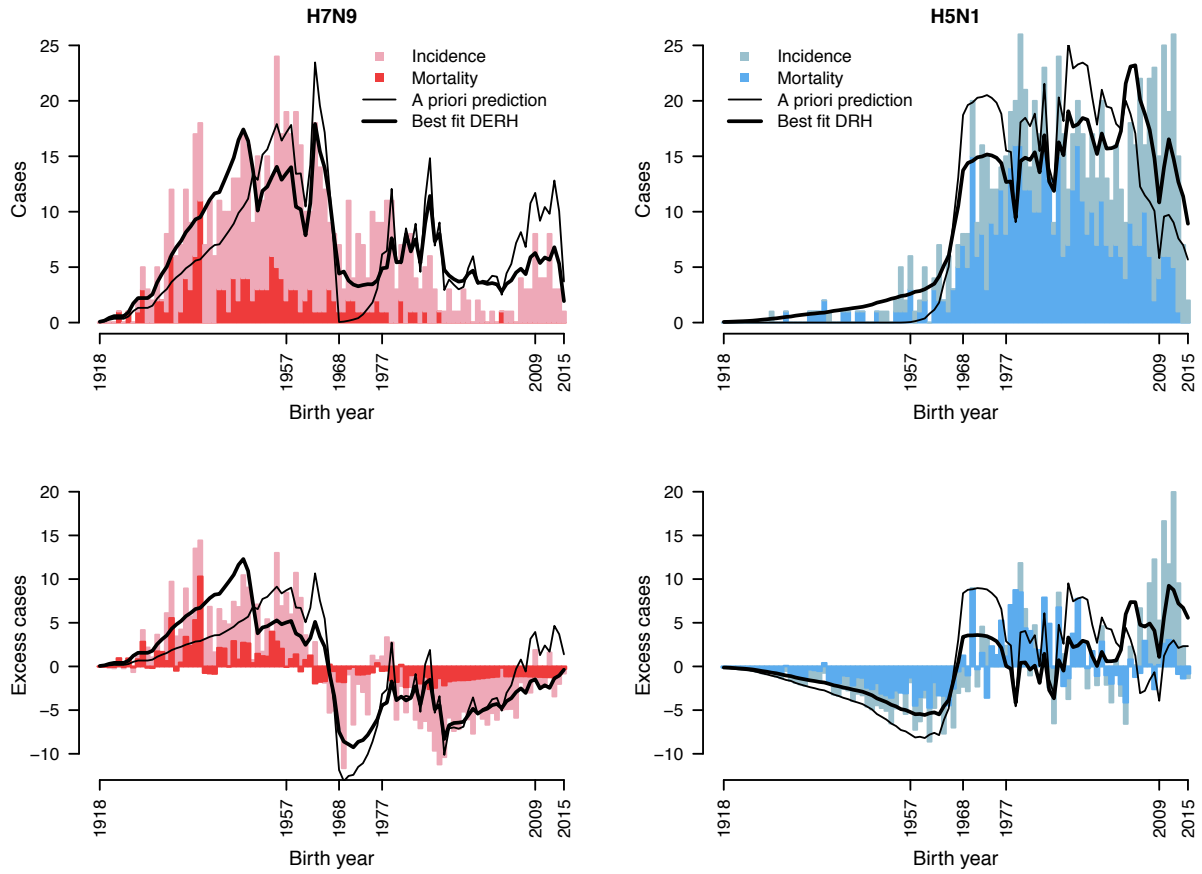

Supplementary Figure 1-S3. Model fits to observed data.

H7N9 and H5N1 data (bars) are shown with predictions from the best model fit (bold line). For comparison with Fig. 1-2, *a priori* predictions based on demography and HA imprinting alone (thin line) are also shown.

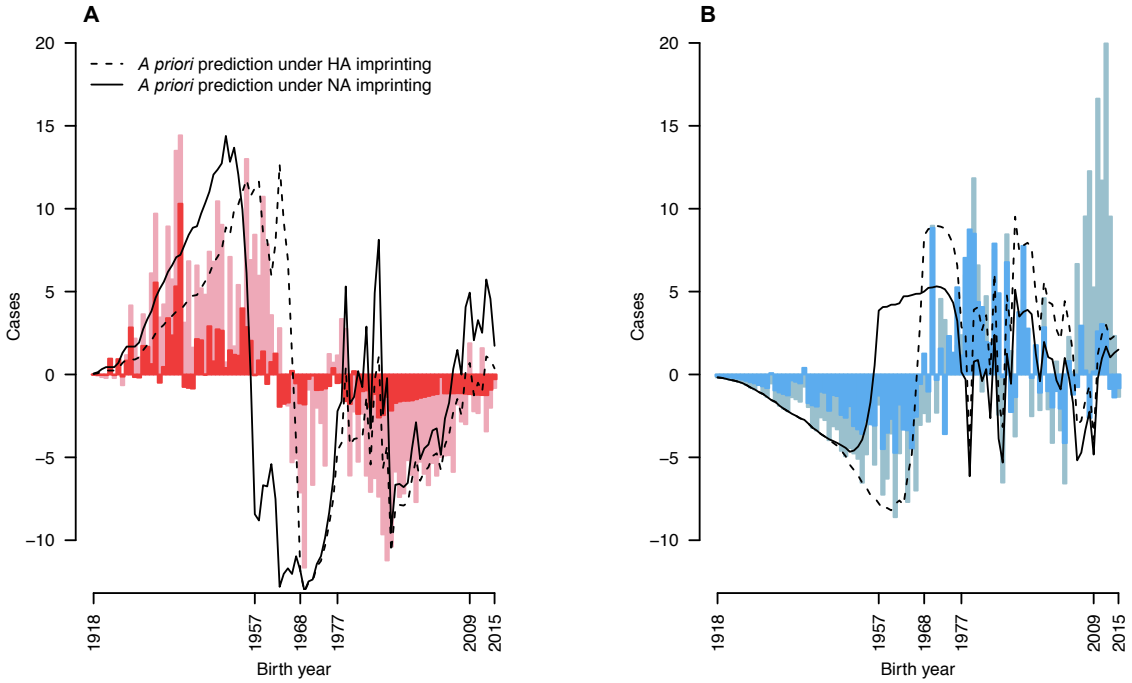

Supplementary Figure 1-S4. Comparison of NA and HA imprinting hypotheses to data.

(**A**) H7N9. (**B**) H5N1. Bars show incidence (light colors) and mortality (dark colors) normalized to demography as in Figure 1-2C, D. Overlaid lines show the *a priori* prediction based on HA imprinting (dashed line) or NA imprinting (solid line). During the period from 1957 to 1968 the NA imprinting prediction clearly fails to match observed incidence of excess severe infection or death from H7N9 or H5N1. Moreover, our modeling analysis indicates HA imprinting, not NA imprinting, is the dominant effect driving H5N1 and H7N9 severity patterns (see Table 1-S2).

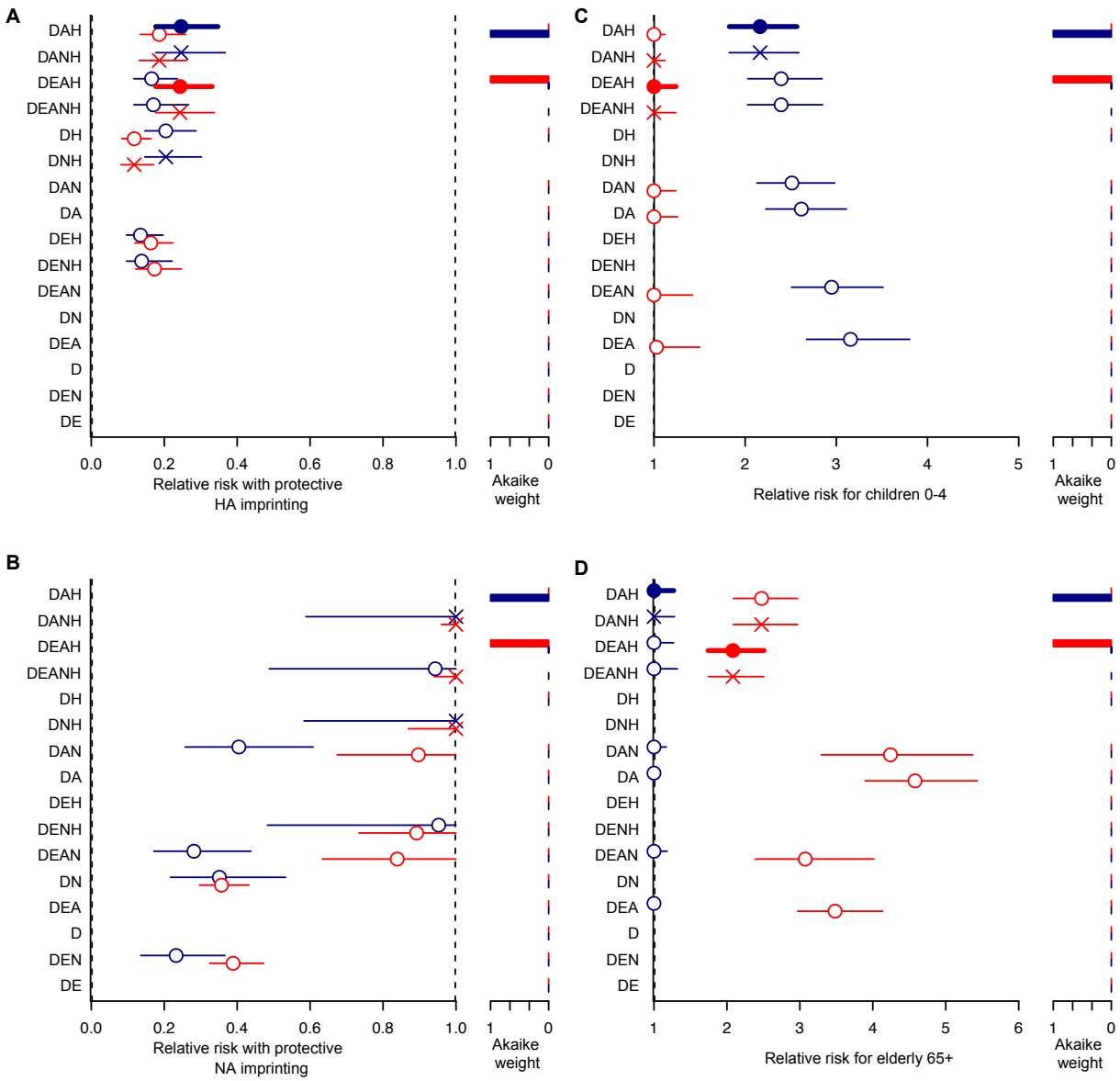

Supplementary Figure 1-S5. Parameter estimates for all models of H5N1 and H7N9 incidence. Maximum likelihood estimates and 95% likelihood profile CIs for parameters (with the 95% threshold determined using likelihood ratios) (**A**) H_m (**B**) N_m (**C**) A_c and (**D**) A_e, as fit to H5N1 (blue) and H7N9 (red) incidence data. Parameters and model abbreviations are described in Table 1-S1, and Methods. Demography, D, is included in all models. Additional tested factors include poultry exposure risk, E, age-based risk of severe morbidity in children and the elderly, A, NA imprinting, N, and HA imprinting, H. Dashed lines indicate boundary values imposed on parameters. Models are listed from top to bottom in

order of decreasing model support, as fit to H5N1 data. Bar plots at right show Akaike weights, and the best model is shown with a filled symbol and bold line; all preferred models have definitive statistical support with Akaike weights > 0.99 (Table 1-S2). In some cases, the MLE for parameter N_m was 1, indicating no NA imprinting effect, and the model with added factor N was identical to the model containing all the same factors except N. These degenerate models are represented with X's, and were excluded from Akaike weight calculations.

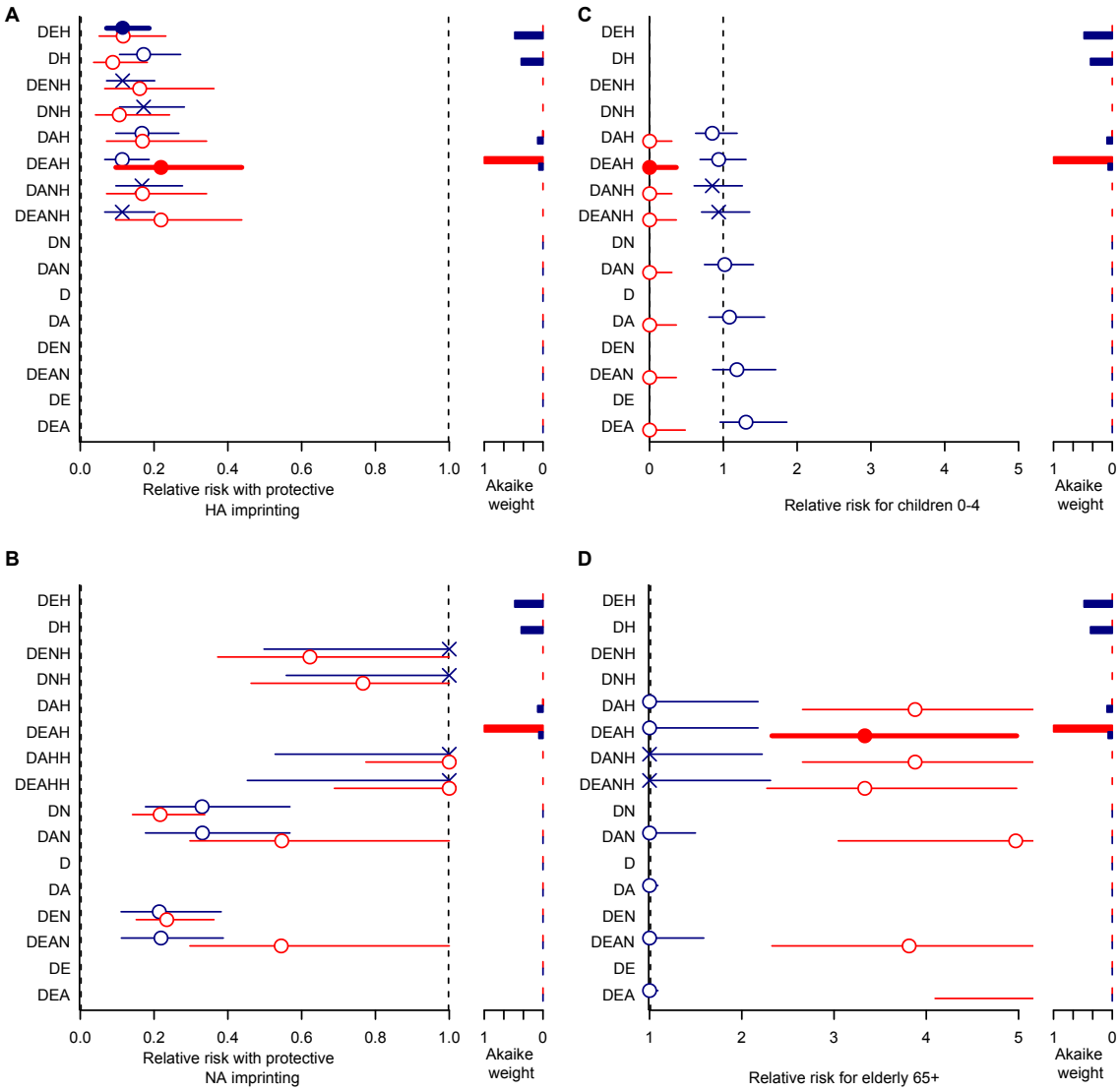

Supplementary Figure 1-S6. Parameter estimates for all models of H5N1 and H7N9 mortality. Maximum likelihood estimates and 95% likelihood profile CIs for parameters (**A**) H_m (**B**) N_m (**C**) A_c and (**D**) A_e, as fit to H5N1 (blue) and H7N9 (red) mortality data. Parameters and model abbreviations are described in Table 1-S1, and Methods. Formatting is as in Fig. 1-S5. For H7N9, which is less pathogenic in birds and humans than H5N1, DEAH is the definitive preferred model for both infection and mortality, with Akaike weights > 0.99 in both cases. However, for H5N1, which is more pathogenic in birds and humans, no single mortality model is definitively preferred. Rather, we found some statistical support (Akaike weights > 0.05) for all mortality models that include HA imprinting (Table 1-S2).

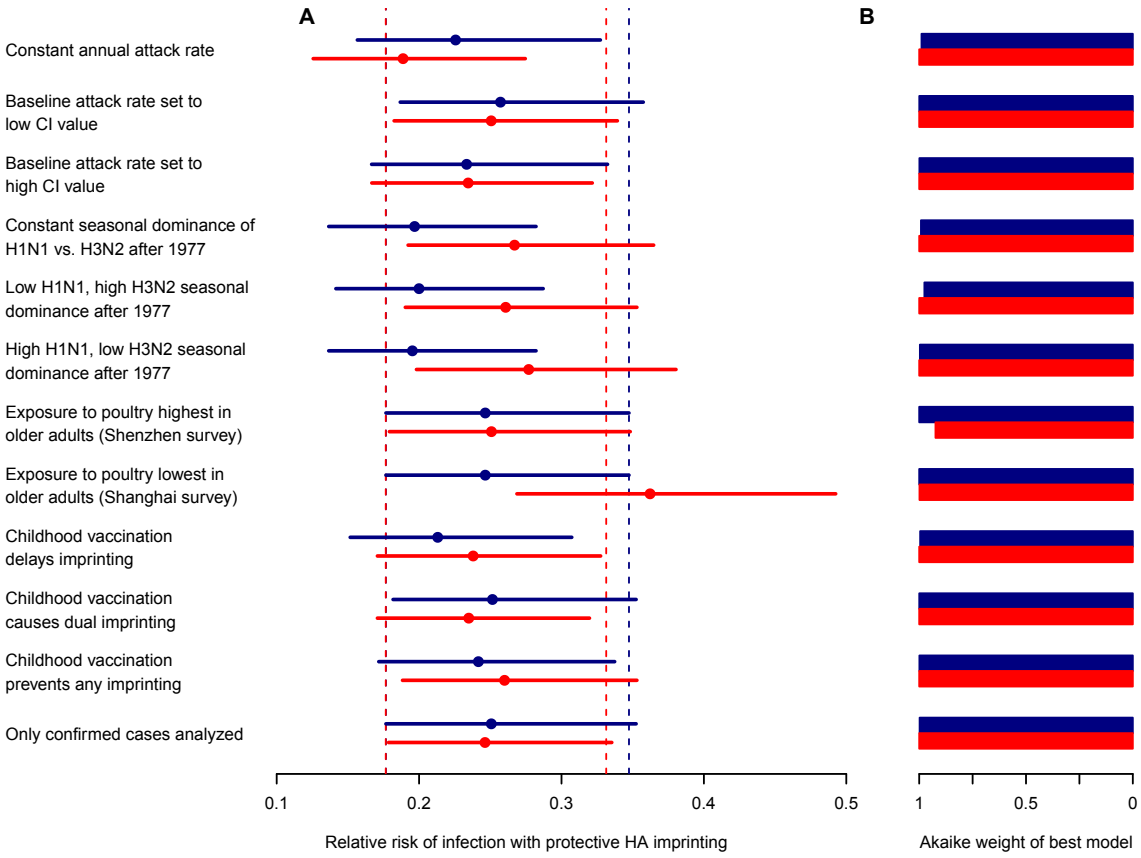

Supplementary Figure 1-S7. Sensitivity analyses.

We tested the robustness of H_m parameter estimates (Table 1-S1) and model selection results for twelve variations on our standard model formulation (Methods). **(A)** Maximum likelihood estimates and 95% likelihood profile CIs for parameter H_m, as fit to incidence data using the best incidence model for each subtype (DAH for H5N1, in blue, and DEAH for H7N9, in red). Dashed lines show 95% CIs on H_m estimates from the preferred model, as presented in the main text analysis. **(B)** Akaike weights for models DAH (H5N1, blue) and DEAH (H7N9, red). These models remain strongly supported throughout all sensitivity analyses, with Akaike weights > 0.98 in all cases but one. The lowest Akaike weight was 0.92.

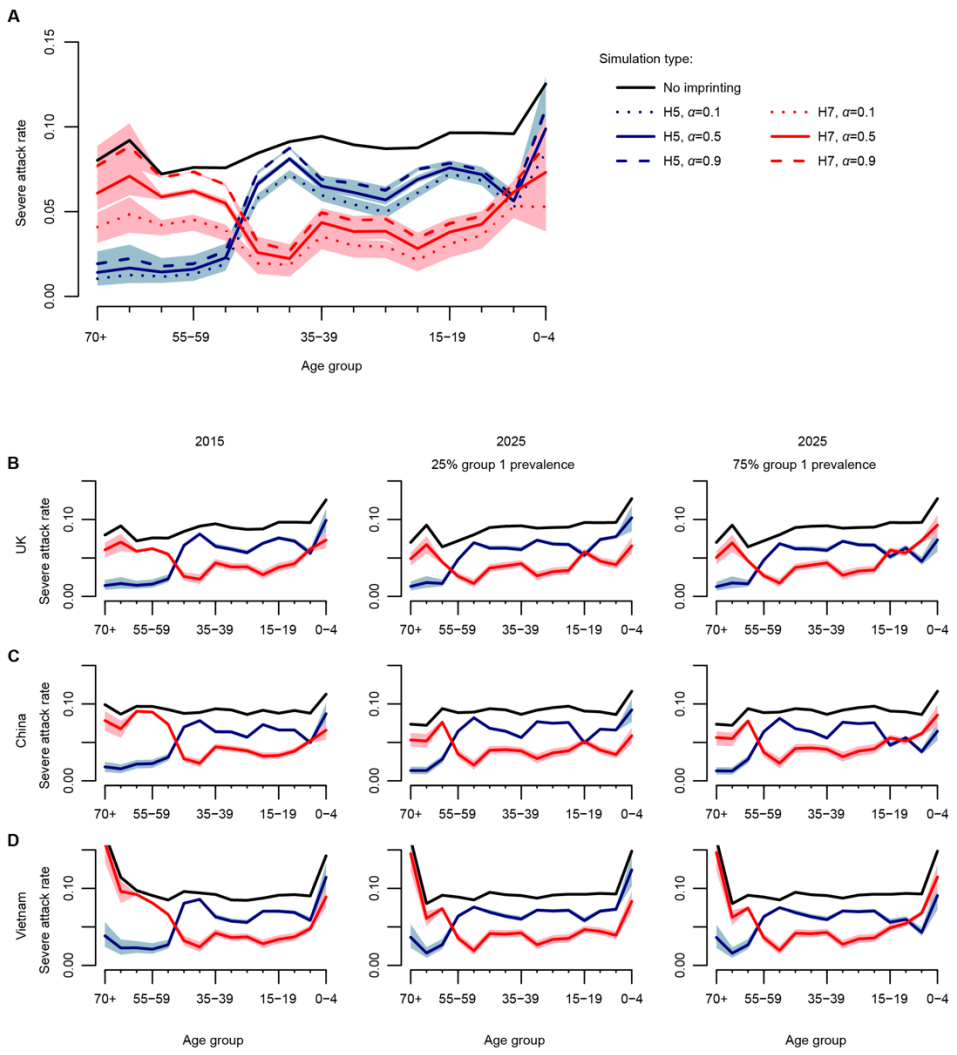

Supplementary Figure 1-S8. Projected age-structured severe attack rates during hypothetical future H5 (blue) and H7 (red) IAV pandemics.

Simulations assume country-specific demography and age-structured mixing, HA imprinting, and age-based risk groups (Supplementary Text). Colored lines show the average, and shaded regions include 95% of 100 simulated outcomes. For comparison, the severe attack rate in an IAV pandemic with no HA imprinting is also shown (black). All simulations use R_0 = 2.5. (**A)** Illustration of how changing the infectiousness of partially protected individuals (α), relative to unprotected individuals, affects the age-structured severe attack rate in a 2015 UK IAV pandemic. (**B-D)** Results for three countries in 2015 and 2025 when α=0.5. Two scenarios are considered for seasonal influenza circulation between 2015 and 2025: 25% group 1 IAV and 75% group 1 IAV.

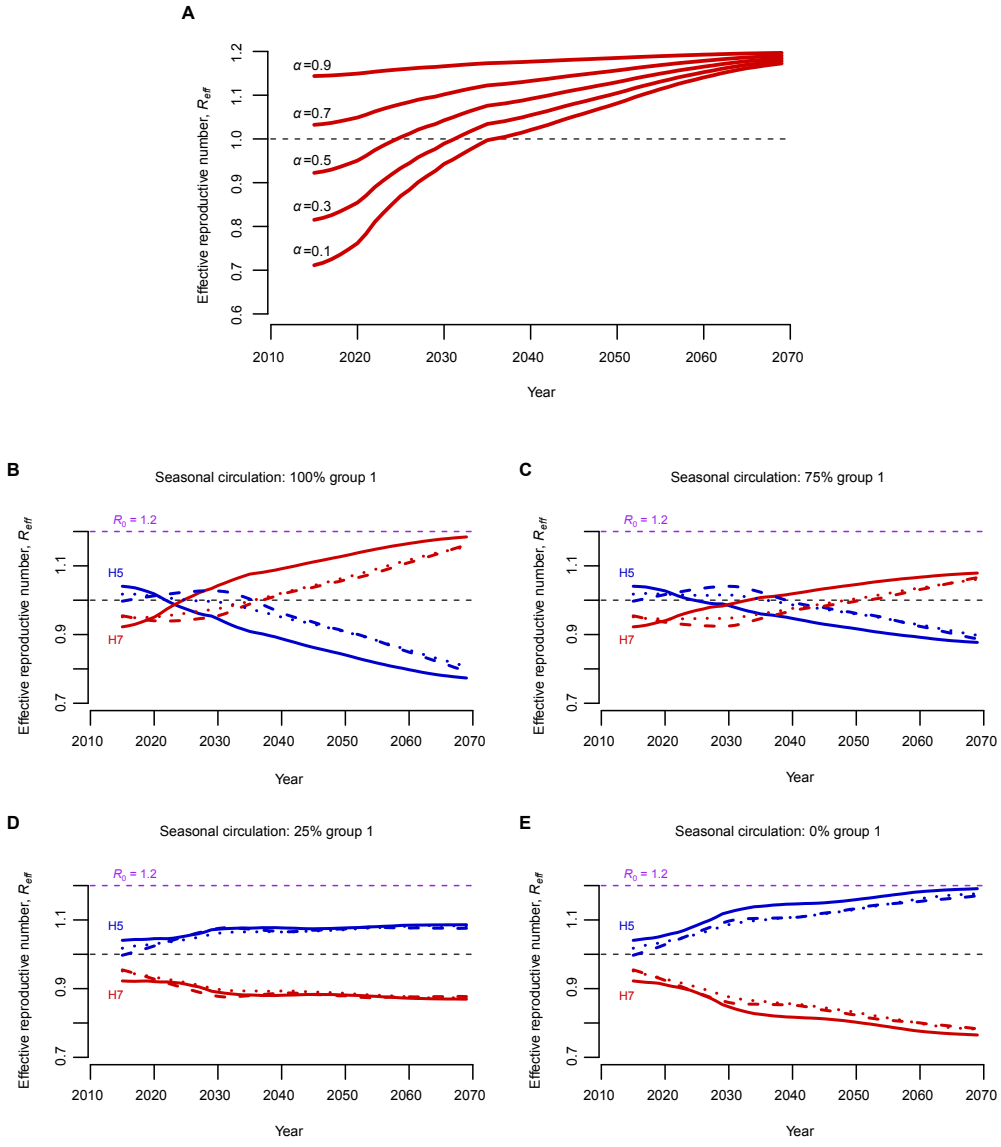

Supplementary Figure 1-S9. Projections of R_{eff} through time.

(**A)** Projections of R_{eff} for an H7 IAV with R_0 = 1.2 under different assumptions regarding the infectiousness of protected individuals (α). Projections are in the UK assuming 100% group 1 seasonal circulation after 2015. (**B-E)** Projections of how the R_{eff} for a hypothetical H5 (blue) and H7 (red) IAV with R_0 = 1.2 and α=0.5 would change through time in the UK (solid line), China (dashed line), and Vietnam (dotted line) under four different post-2015 seasonal group 1 IAV circulation scenarios. Although general trends are consistent across countries, different demographic age structures and mixing patterns result in notable differences in the exact R_{eff} trajectory of each country.

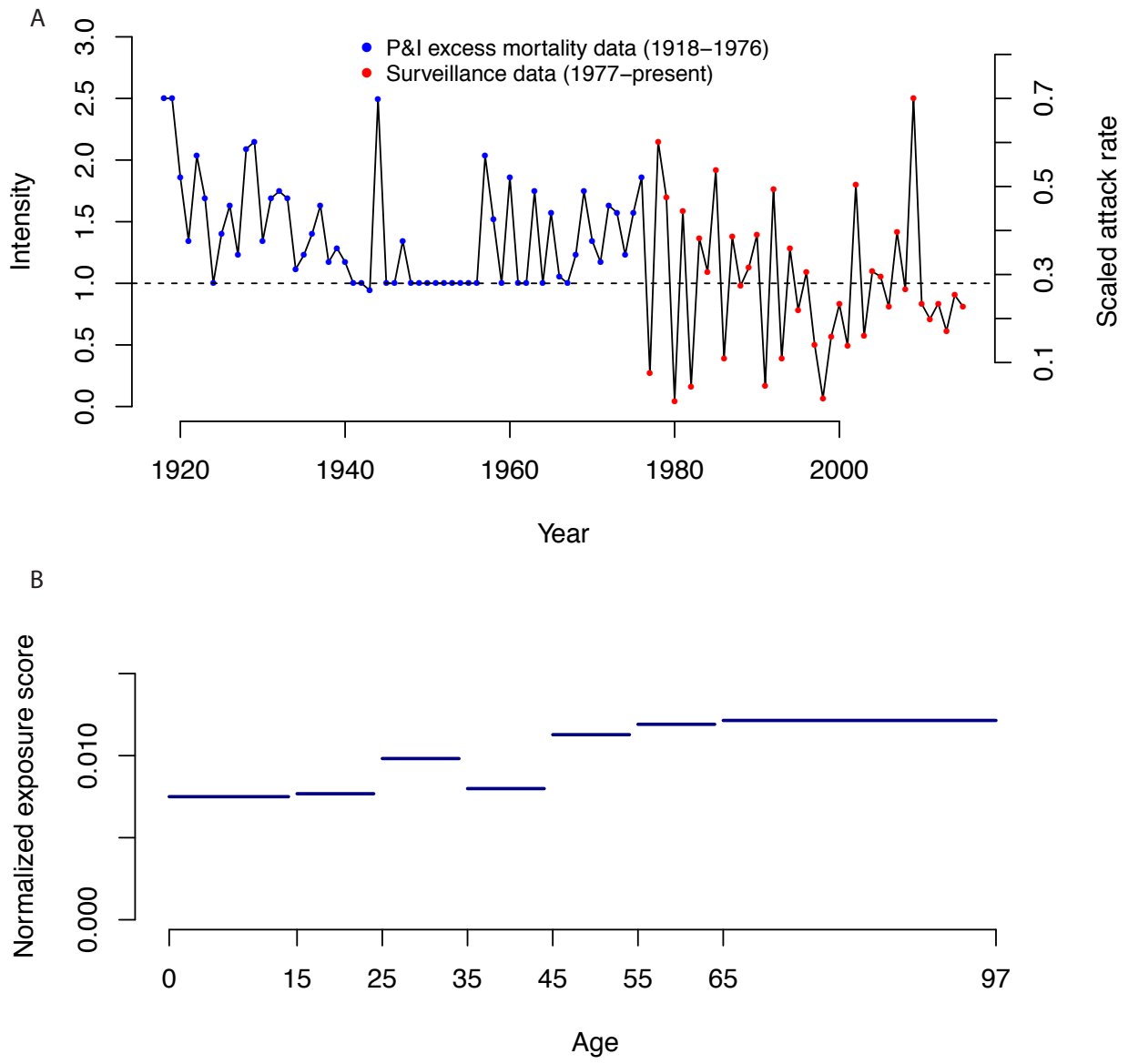

Supplementary Figure 1-S10. Model inputs.

(A) Index representing annual intensity of seasonal influenza circulation from 1918-2015. Right axis shows scaled annual attack rates on naïve children, which correspond to the intensity scores at left. As described in Supplementary Text, section 4, this index modulates the annual attack rate on children in reconstructions of HA and NA imprinting patterns. Blue points spanning 1918-1976 represent pneumonia & influenza excess mortality data, and hence are restricted to non-negative values. **(B)** Index of poultry exposure frequency by age group in humans, described in Methods. This index informs factor E in model comparison.

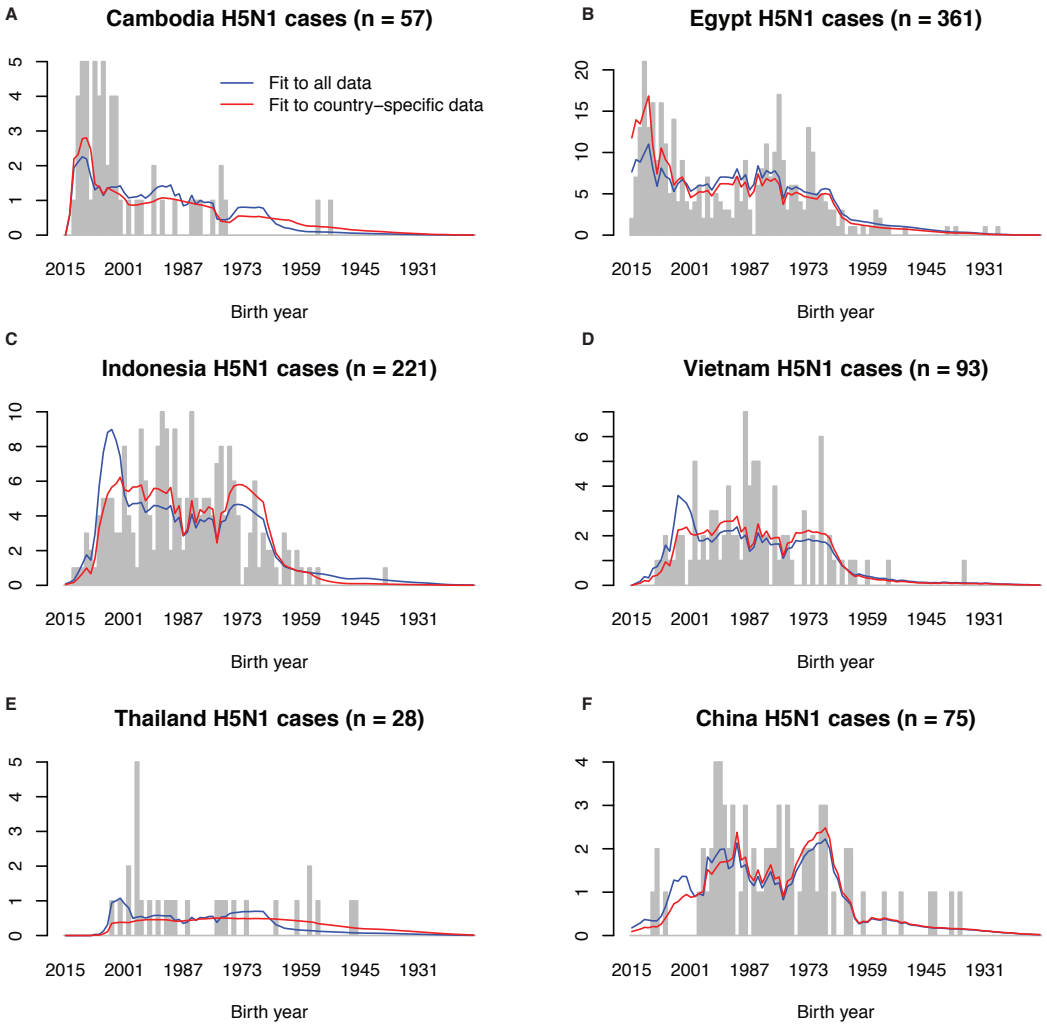

G

	N	Best model	H_m (95% CI)	N_m (95% CI)	A_c (95% CI)	A_e (95% CI)
Cambodia	57	DR			3.25 (1.72-5.61)	1.00 (1.00-2.15)
China	75	D**H**	0.24 (0.10-0.50)			
Egypt	361	DER**H**	0.20 (0.11-0.33)		3.80 (3.02-4.80)	1.00 (100-2.15)
Indonesia	221	DN**H**	0.19 (0.07-0.39)	0.24 (0.02-1.00)		
Thailand	28	D				
Vietnam	93	D**H**	0.16 (0.41-0.43)			

Supplementary Figure 1-S11. Country-specific model fits and model comparison results.

(A-F) Birth year distribution of cases from the country of interest (bars) with overlaid predictions from the best model fit to country-specific data (red), or fit to all data (blue). **(G)** Results of model comparison and maximum likelihood estimation for country-specific data. For Cambodia and Thailand, the second best models (DRH and DH) included HA imprinting effects, and were statistically indistinguishable from the best model with ΔAIC of 0.47 and 0.45.

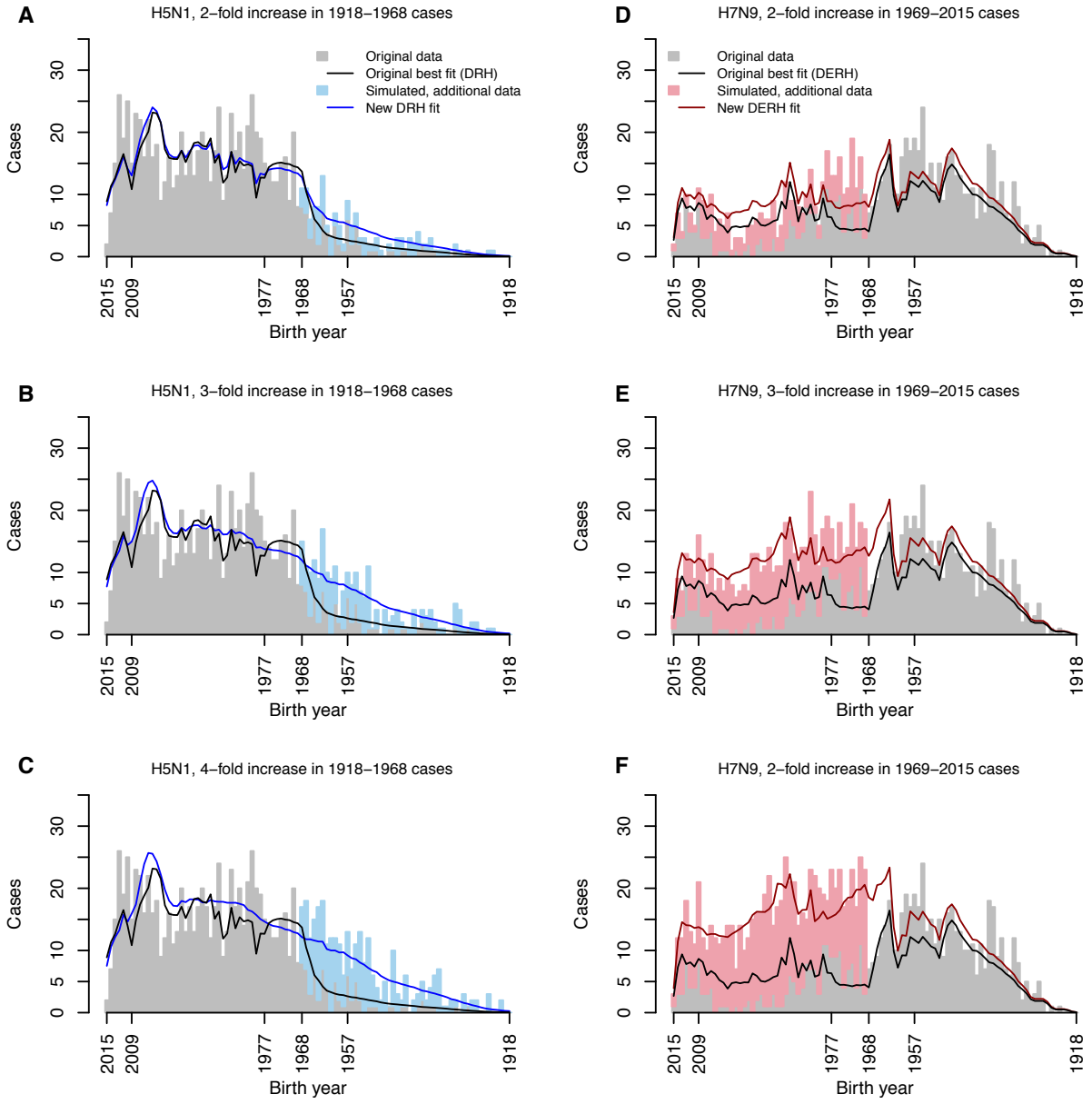

Supplementary Figure 1-S12. Robustness to biased case ascertainment.

Panels show results of representative simulations showing effects of a worst-case-scenario case ascertainment bias based on birth year (as described in Supplementary Text section 7). We increased the number of cases observed in underrepresented birth cohorts (1918-1968 for H5N1, 1969-2015 for H7N9) by 2-fold **(A, D)**, 3-fold **(B, E)**, or 4-fold **(C, F)** to systematically degrade the strongest signal of HA imprinting in the data. Even with these simulated, 'perfectly bad' biases, our core results were robust up

to the 3-fold level for H5N1 and the 4-fold level for H7N9. Note that the gap between model predictions and observed case numbers for H7N9 for birth years leading up to 1968 **(E, F)** arises from lags in imprinting: many individuals born just before the 1968 pandemic actually did imprint on the group 2 1968 virus, but were not included in our data augmentation scheme. Because the estimated protective effect of imprinting is weakened under 3-fold and 4-fold scenarios, the best fit models in these scenarios do not capture the partially protected status of these cohorts.

Supplementary Table 1-S1. Summary of model factors and free parameters.

Model factors		
Abbreviation	Model factor	Description
D	Demography	Demography modulates the probability, p_{cyi}, that an infection occurs in a particular birth year, i, based on the proportion of the population in country c, in year y, that was born in that year. Demography serves as the null model, and is included as a factor in all models tested.
E	Exposure to poultry	Exposure to poultry is a factor that modulates p_{yci} based on age-specific poultry exposure rates, as informed by data collected in China.
A	Age-based risk	Age-based risk is a factor that allows children ages 0-4, or the elderly ages 65+ to experience elevated risk of severe morbidity, mortality, or increased case ascertainment. This factor modulates p_{yci} via parameters A_c and A_e, as described below.
H	HA imprinting	HA imprinting is a factor that allows those with protective HA imprinting to experience decreased risk of severe infection or mortality, relative to all others. This factor modulates p_{yci} via parameter H_m as described below.
N	NA imprinting	NA imprinting is a factor that allows those with protective NA imprinting to experience decreased risk of severe infection or mortality, relative to all others. This factor modulates p_{yci} via parameter N_m as described below.

Model parameters			
Parameter	Description	Constraints	Interpretation of constraints
H_m	Relative susceptibility of those with group-matched (protective) first hemagglutinin exposures.	$0 \le H_m \le 1$	0 indicates full protection 1 indicates no additional protection
N_m	Relative susceptibility of those with group-matched (protective) first neuraminidase exposures.	$0 \le N_m \le 1$	0 indicates full protection 1 indicates no additional protection
A_c	Relative risk of severe infection/case detection bias for young children (ages 0-4)	$A_c \ge 1$*	1 indicates no elevated risk >1 indicates elevated risk
A_e	Relative risk of severe infection/case detection bias for the elderly (ages 65+)	$A_e \ge 1$	1 indicates no elevated risk >1 indicates elevated risk

*For models analyzing mortality risk, we changed this constraint to: $A_c \ge 0$, allowing the data to indicate whether young children were more or less likely to die from their infections than the reference age group (see Methods).

Supplementary Table 1-S2. Incidence and mortality model results.

	H_m (95% CI)	N_m (95% CI)	A_c (95% CI)	A_e (95% CI)	ΔAIC	Akaike weight
H5N1 incidence						
DAH	0.25 (0.18-0.35)		2.16 (1.83-2.57)	1.00 (1.00-1.27)	0	1.00
DANH*	0.25 (0.18-0.37)	1.00 (0.59-1.00)	2.16 (1.82-2.59)	1.00 (1.00-1.28)	2	
DEAH	0.17 (0.12-0.24)		2.39 (2.03-2.84)	1.00 (1.00-1.27)	15.35	4.65E-04
DEANH	0.17 (0.12-0.27)	0.94 (0.49-1.00)	2.39 (2.03-2.85)	1.00 (1.00-1.32)	17.32	1.74E-04
DH	0.20 (0.15-0.29)				69.81	9.50 E-16
DNH*	0.20 (0.15-0.30)	1.00 (0.58-1.00)			71.18	
DAN		0.40 (0.26-0.61)	2.51 (2.13-2.98)	1.00 (1.00-1.17)	73.58	1.05E-16
DA			2.62 (2.23-3.11)	1.00 (1.00-1.06)	96.34	1.20E-21
DEH	0.13 (0.10-0.20)				103.31	3.69E-23
DENH	0.14 (0.10-0.22)	0.95 (0.48-1.00)			105.29	1.37E-23
DEAN		0.28 (0.17-0.44)	2.95 (2.51-3.51)	1.00 (1.00-1.18)	136.99	1.79E-30
DN		0.35 (0.22-0.53)			172.30	3.84E-38
DEA			3.16 (2.67-3.80)	1.00 (1.00-1.05)	182.33	2.56E-40
D					203.81	5.52E-45
DEN		0.23 (0.14-0.37)			269.81	2.57E-59
DE					331.46	1.06E-72
H7N9 incidence						
DEAH	0.24 (0.18-0.33)		1.00 (1.00-1.24)	2.08 (1.74-2.51)	0	1.00
DEANH*	0.24 (0.18-0.34)	1.00 (0.94-1.00)	1.00 (1.00-1.24)	2.08 (1.74-2.51)	2	
DAH	0.19 (0.13-0.26)		1.00 (1.00-1.12)	2.47 (2.09-2.97)	42.87	4.90E-10
DANH*	0.19 (0.13-0.26)	1.00 (0.96-1.00)	1.00 (1.00-1.12)	2.47 (2.09-2.97)	44.87	
DEH	0.16 (0.12-0.22)				61.59	4.23E-14
DENH	0.17 (0.12-0.25)	0.89 (0.73-1.00)			62.26	3.02E-14
DEA			1.03 (1.00-1.50)	3.48 (2.97-4.14)	106.94	6.00E-24
DEAN		0.84 (0.63-1.00)	1.00 (1.00-1.42)	3.07 (2.39-4.02)	107.63	4.24E-24
DH	0.12 (0.08-0.16)				138.40	8.83E-31
DNH*	0.12 (0.08-0.17)	1.00 (0.87-1.00)			140.40	
DA			1.00 (1.00-1.26)	4.58 (3.89-5.43)	193.47	9.72E-43
DAN		0.90 (0.67-1.00)	1.00 (1.00-1.24)	4.24 (3.29-5.37)	194.97	4.60E-43
DEN		0.39 (0.32-0.47)			195.62	3.33E-43
DE					297.51	2.49E-65
DN		0.36 (0.30-0.43)			344.49	1.57E-75
D					466.22	5.76E-102
H5N1 mortality						
DEH	0.11 (0.07-0.19)				0.00	0.48
DH	0.17 (0.11-0.27)				0.53	0.37
DENH*	0.11 (0.07-0.20)	1.00 (0.50-1.00)			2.00	
DNH*	0.17 (0.11-0.28)	1.00 (0.56-1.00)			2.53	
DAH	0.17 (0.10-0.27)		0.85 (0.62-1.19)	1.00 (1.00-2.18)	3.41	0.09
DEAH	0.11 (0.07-0.19)		0.94 (0.68-1.31)	1.00 (1.00-2.18)	3.82	0.07
DANH*	0.17 (0.10-0.28)	1.00 (0.53-1.00)	0.85 (0.60-1.26)	1.00 (1.00-2.22)	5.41	
DEANH*	0.11 (0.07-0.20)	1.00 (0.45-1.00)	0.94 (0.70-1.36)	1.00 (1.00-2.31)	5.82	
DN		0.33 (0.18-0.57)			69.22	4.44E-16
DAN		0.33 (0.18-0.57)	1.02 (0.74-1.41)	1.00 (1.00-1.50)	73.21	6.06E-17
D					87.98	3.76E-20
DA			1.08 (0.80-1.56)	1.00 (1.00-1.09)	91.72	5.78E-21
DEN		0.21 (0.11-0.38)			104.04	1.22E-23
DEAN		0.22 (0.11-0.39)	1.18 (0.86-1.71)	1.00 (1.00-1.59)	106.93	2.88E-24
DE					143.27	3.69E-32
DEA			1.31 (0.96-1.86)	1.00 (1.00-1.09)	144.54	1.96E-32
H7N9 mortality						
DEAH	0.22 (0.10-0.44)		0.00 (0.00-0.36)	3.33 (2.33-4.98)	0	1.00
DEANH*	0.22 (0.10-0.44)	1.00 (0.69-1.00)	0.00 (0.00-0.36)	3.33 (2.27-4.98)	2	
DAH	0.17 (0.07-0.34)		0.00 (0.00-0.30)	3.88 (2.66-5.57)	12.05	2.41E-03
DANH*	0.17 (0.07-0.34)	1.00 (0.77-1.00)	0.00 (0.00-0.30)	3.88 (2.66-5.57)	14.05	
DEAN		0.54 (0.30-1.00)	0.00 (0.00-0.36)	3.81 (2.33-6.68)	20.34	3.83E-05
DEA			0.00 (0.00-0.48)	5.78 (4.10-8.24)	21.45	2.19E-05
DAN		0.55 (0.30-1.00)	0.00 (0.00-0.30)	4.97 (3.05-8.90)	40.94	1.29E-09
DA			0.00 (0.00-0.36)	7.51 (5.31-10.67)	42.03	7.47E-10
DENH	0.16 (0.07-0.36)	0.62 (0.37-1.00)			49.16	2.11E-11
DEH	0.12 (0.05-0.23)				51.14	7.84E-12
DEN		0.23 (0.15-0.36)			68.32	1.45E-15
DH	0.09 (0.04-0.18)				79.85	4.56E-18
DNH*	0.11 (0.04-0.24)	0.77 (0.46-1.00)			80.60	3.13E-18
DN		0.22 (0.14-0.34)			110.60	9.62E-25
DE					116.94	4.03E-26
D					165.02	1.46E-36

*Maximum likelihood model was identical to the model including all the same factors except N, and excluded from Akaike weight calculations.

REFERENCES

1. Y. Qin et al., Differences in the Epidemiology of Human Cases of Avian Influenza A(H7N9) and A(H5N1) Viruses Infection. Clin. Infect. Dis. 61, 563–71 (2015).

2. B. J. Cowling et al., Comparative epidemiology of human infections with avian influenza A H7N9 and H5N1 viruses in China: a population-based study of laboratory-confirmed cases. Lancet. 382, 129–37 (2013).

3. A. J. Kucharski, W. J. Edmunds, Cross-immunity and age patterns of influenza A(H5N1) infection. Epidemiol. Infect. 143, 1119–24 (2015).

4. M. R. Sandbulte et al., Cross-reactive neuraminidase antibodies afford partial protection against H5N1 in mice and are present in unexposed humans. PLoS Med. 4, e59 (2007).

5. C. Rivers, K. Lum, B. Lewis, S. Eubank, Estimating Human Cases of Avian Influenza A(H7N9) from Poultry Exposure. PLoS Curr. (2013). doi: 10.1371/currents.outbreaks.264e737b489bef383fbcbaba60daf928.

6. B. J. Cowling et al., Preliminary inferences on the age-specific seriousness of human disease caused by avian influenza A(H7N9) infections in China, March to April 2013. Euro Surveill. 18, 20475 (2013).

7. L. Wang et al., Human exposure to live poultry and psychological and behavioral responses to influenza A(H7N9), China. Emerg. Infect. Dis. 20 (2014).

8. J. Wrammert et al., Broadly cross-reactive antibodies dominate the human B cell response against 2009 pandemic H1N1 influenza virus infection. J. Exp. Med. 208, 181–93 (2011).

9. N. Pica et al., Hemagglutinin stalk antibodies elicited by the 2009 pandemic influenza virus as a mechanism for the extinction of seasonal H1N1 viruses. Proc. Natl. Acad. Sci. U. S. A. 109, 2573–8 (2012).

10. G.-M. Li et al., Pandemic H1N1 influenza vaccine induces a recall response in humans that favors broadly cross-reactive memory B cells. Proc. Natl. Acad. Sci. 109, 9047–52 (2012).

11. M. S. Miller et al., Neutralizing antibodies against previously encountered influenza virus strains increase over time: a longitudinal analysis. Sci. Transl. Med. 5, 198ra107 (2013).

12. F. Krammer et al., H3 stalk-based chimeric hemagglutinin influenza virus constructs protect mice from H7N9 challenge. J. Virol. 88, 2340–3 (2014).

13. A. H. Ellebedy et al., Induction of broadly cross-reactive antibody responses to the influenza HA stem region following H5N1 vaccination in humans. Proc. Natl. Acad. Sci. U. S. A. 111, 13133–8 (2014).

14. P. Palese, T. T. Wang, Why do influenza virus subtypes die out? A hypothesis. MBio. 2 (2011), doi:10.1128/mBio.00150-11.

15. T. Francis, On the Doctrine of Original Antigenic Sin. Proc. Am. Philos. Soc. 104, 572–578 (1960).

16. J. Lessler et al., Evidence for antigenic seniority in influenza A (H3N2) antibody responses in southern China. PLoS Pathog. 8, e1002802 (2012).

17. M. Smallman-Raynor & A.D. Cliff, Avian Influenza A (H5N1) Age Distribution in Humans. Emerg. Infect. Dis. 13 510-512 (2007).

18. M. Terajima, M. D. T. Co, F. A. Ennis, Age and different influenza viruses. Lancet. Infect. Dis. 14, 101 (2014).

19. M. Worobey, G.-Z. Han, A. Rambaut, Genesis and pathogenesis of the 1918 pandemic H1N1 influenza A virus. Proc. Natl. Acad. Sci. U. S. A. 111, 8107–8112 (2014).

20. A. Sauerbrei, R. Schmidt-Ott, H. Hoyer, P. Wutzler, Seroprevalence of influenza A and B in German infants and adolescents. Med. Microbiol. Immunol. 198, 93–101 (2009).

21. A. Sauerbrei et al., Prevalence of antibodies against influenza A and B viruses in children in Germany, 2008 to 2010. Eurosurveillance. 19, 1–8 (2014).

22. K. L. Laurie et al., Multiple infections with seasonal influenza A virus induce cross-protective immunity against A(H1N1) pandemic influenza virus in a ferret model. J. Infect. Dis. 202, 1011–20 (2010).

23. J. L. Schulman, E. D. Kilbourne, Induction of partial specific hetertypic immunity in mice by a single infection with influenza A virus. J. Bacteriol. 89, 170–4 (1965).

24. K. V Houser, M. B. Pearce, J. M. Katz, T. M. Tumpey, Impact of prior seasonal H3N2 influenza vaccination or infection on protection and transmission of emerging variants of influenza A(H3N2)v virus in ferrets. J. Virol. 87, 13480–9 (2013).

25. T. M. Wilkinson et al., Preexisting influenza-specific CD4+ T cells correlate with disease protection against influenza challenge in humans. Nat Med. 18, 274–280 (2012).

26. S. F. Andrews et al., Immune history profoundly affects broadly protective B cell responses to influenza. Sci. Transl. Med. 7, 316ra192–316ra192 (2015).

27. I. Kohler et al., Prevalence and predictors for homo- and heterosubtypic antibodies against influenza A virus. Clin. Infect. Dis. 59, 1386–1393 (2014).

28. J. Sui et al., Structural and functional bases for broad-spectrum neutralization of avian and human influenza A viruses. Nat. Struct. Mol. Biol. 16, 265–273 (2009).

29. C. J. Henry Dunand et al., Preexisting human antibodies neutralize recently emerged H7N9 influenza strains. 125, 1–14 (2015).

30. J. Mossong et al., Social contacts and mixing patterns relevant to the spread of infectious diseases. PLoS Med. 5, e74 (2008).

31. J. M. Read et al., Social mixing patterns in rural and urban areas of southern China. Proc. Biol. Sci. 281, 20140268 (2014).

32. P. Horby et al., Social contact patterns in Vietnam and implications for the control of infectious diseases. PLoS One. 6, e16965 (2011).

33. C. C. Dauer, R. E. Serfling, Mortality from Influenza. Am. Rev. Respir. Dis. 83, 15-28 (1961).

34. L. Simonsen, T. A. Reichert, M. A. Miller, The virtues of antigenic sin: consequences of pandemic recycling on influenza-associated mortality. Int. Congr. Ser. 1263, 791–794 (2004).

35. P. K. S. Chan, Outbreak of Avian Influenza A (H5N1) Virus Infection in Hong Kong in 1997. Clin. Infect. Dis. 34, S58–S64 (2002).

36. L. Fiebig et al., Avian influenza A(H5N1) in humans: New insights from a line list of World Health Organization confirmed cases, September 2006 to August 2010. Eurosurveillance. 16, 1–10 (2011).

37. A. Kucharski et al., Data from: Distinguishing between reservoir exposure and human-to-human transmission for emerging pathogens using case onset data. PLoS Curr. Outbreaks (2014). doi:10.5061/dryad.2g43n.

38. K. P. Burnham, D. R. Anderson, Model Selection and Multimodel Inference: A Practical Information-Theoretic Approach (Springer, New York, ed. 2, 2002).

39. US Census Bureau, International Programs, International Data Base (2015). [available at http://www.census.gov/population/international/data/idb/region.php?N= Results &T=10&A=separate&RT=0&Y=2013&R=-1&C=ID]

40. B. M. Coates, K. L. Staricha, K. M. Wiese, K. M. Ridge, Influenza A Virus Infection, Innate Immunity, and Childhood. JAMA Pediatr, 169, 956-63 (2015).

41. D. Cromer et al., The burden of influenza in England by age and clinical risk group: A statistical analysis to inform vaccine policy. J. Infect. 68, 363–71 (2014).

42. M.-A. Widdowson, A. S. Monto, Epidemiology of Influenza in Textbook of influenza, R. G. Webster, A. S. Monto, T. J. Braciale, R. A. Lamb, Eds. (John Wiley & Sons Ltd, Oxford, UK ed. 2, 2013), pp. 250–265.

43. R. Bodewes et al., Prevalence of antibodies against seasonal influenza A and B viruses in children in Netherlands. Clin. Vaccine Immunol. 18, 469–476 (2011).

44. K. M. Neuzil et al., Burden of interpandemic influenza in children younger than 5 years: a 25-year prospective study. J. Infect. Dis. 185, 147–52 (2002).

45. W. P. Glezen, Emerging infections: pandemic influenza. Epidemiol. Rev. 18, 64–76 (1996).

46. Global Influenza Surveillance and Response System, “FluNet” (2015). [available at www.who/int/flunet]

47. W. W. Thompson et al., Mortality associated with influenza and respiratory syncytial virus in the United States. JAMA. 289, 179–186 (2003).

48. A. Palache, V. Oriol-Mathieu, M. Fino, M. Xydia-Charmanta, Seasonal influenza vaccine dose distribution in 195 countries (2004-2013): Little progress in estimated global vaccination coverage. Vaccine. 33, 5598–605 (2015).

49. M. Kearse et al., Geneious Basic: An integrated and extendable desktop software platform for the organization and analysis of sequence data. Bioinformatics. 28, 1647–1649 (2012).

50. A. Stamatakis, RAxML-VI-HPC: maximum likelihood-based phylogenetic analyses with thousands of taxa and mixed models. Bioinformatics. 22, 2688–2690 (2006).

51. C. Fraser, D. A. T. Cummings, D. Klinkenberg, D. S. Burke, N. M. Ferguson, Influenza Transmission in Households During the 1918 Pandemic. Am. J. Epidemiol. 174, 505–514 (2011).

52. C. E. Mills, J. M. Robins, M. Lipsitch, Transmissibility of 1918 pandemic influenza. Nature. 432, 904–906 (2004).

53. C. Fraser et al., Pandemic Potential of a Strain of Influenza A (H1N1): Early Findings. Science. 324, 1557–1561 (2009).

54. C. Viboud et al., Transmissibility and mortality impact of epidemic and pandemic influenza, with emphasis on the unusually deadly 1951 epidemic. Vaccine. 24, 6701–6707 (2006).

55. L. F. White et al., Estimation of the reproductive number and the serial interval in early phase of the 2009 influenza A/H1N1 pandemic in the USA. Influenza Other Respi. Viruses. 3, 267–276 (2009).

56. Y. Yang et al., The Transmissibility and Control of Pandemic Influenza A (H1N1) Virus. Science. 326, 729–733 (2009).

57. B. J. Cowling, V. J. Fang, S. Riley, J. S. M. Peiris, G. M. Leung, Estimation of the serial interval of influenza. Epidemiology. 20, 344–347 (2009).

58. Public Health England. Influenza: the Green Book, chapter 19. Version 10. (2015). [found at https://www.gov.uk/government/publications/influenza-the-green-book-chapter-19]

59. Public Health England. The National Childhood Flu Immunisation Programme 2016/17: Information for healthcare practitioners. (2016). [found at https://www.gov.uk/government/uploads/system/uploads/attachment_data/file/540515/Childhood_flu_programme_information_for_healthcare_practitioners.pdf]

60. Public Health England. Seasonal influenza vaccine uptake amongst GP patients in England Provisional monthly data for 1 September 2014 to 31 January 2015. (2015). [found at https://www.gov.uk/government/uploads/system/uploads/attachment_data/file/407946/2903322_SeasonalFlu_GP_Jan2015_acc2.pdf]

61. Blank, Patricia R, Matthias Schwenkglenks, and Thomas D Szucs. 2008. “Influenza Vaccination Coverage Rates in Five European Countries during Season 2006/07 and Trends over Six Consecutive Seasons.” BMC Public Health 8: 272. doi:10.1186/1471-2458-8-272.

62. Public Health England. Seasonal flu vaccine uptake in children of primary school age: winter season 2015 to 2016. (2016). [found at https://www.gov.uk/government/statistics/seasonal-flu-vaccine-uptake-in-children-of-primary-school-age-winter-season-2015-to-2016]

63. J. T. Owusu et al., Seasonal influenza vaccine coverage among high-risk populations in Thailand, 2010-2012. Vaccine. 33, 742–7 (2015).

64. W. Kittikraisak et al., Influenza vaccination coverage and effectiveness in young children in Thailand, 2011-2013. Influenza Other Respi. Viruses. 9, 85–93 (2015).

65. L. Zhou et al., Seasonal influenza vaccination coverage rate of target groups in selected cities and provinces in China by season (2009/10 to 2011/12). PLoS One. 8, e73724 (2013).

66. J. T. F. Lau, P. K. H. Mo, Y. S. Cai, H. Y. Tsui, K. C. Choi, Coverage and parental perceptions of influenza vaccination among parents of children aged 6 to 23 months in Hong Kong. BMC Public Health. 13, 1026 (2013).

67. Centers for Disease Control and Prevention, Influenza Vaccination Coverage among Children Aged 6-23 Months - United states, 2008-09 Influenza Season (2010). [available at http://www.cdc.gov/flu/fluvaxview/coverage_6-23months.htm]

68. M. A. Allison et al., Influenza vaccine effectiveness in healthy 6- to 21-month-old children during the 2003-2004 season. J. Pediatr. 149, 755–762.e1 (2006).

69. J. Housworth, A. D. Langmuir, Excess mortality from epidemic influenza, 1957-1966. Am. J. Epidemiol. 100, 40–48 (1974).

70. D. R. Olson, L. Simonsen, P. J. Edelson, S. S. Morse, Epidemiological evidence of an early wave of the 1918 influenza pandemic in New York City. Proc. Natl. Acad. Sci. U.S.A. 102, 11059–11063 (2005).

71. G. R. Noble, in Basic and Applied Influenza Research, A. S. Beare, Ed. (CRC Press, Boca Raton, FL, 1982), pp. 11–50.

72. M. Gover, Influenza and Pneumonia Mortality in a Group of 90 Cities in the United States, August 1935-March 1943, with a Summary for August 1920-March 1943. Public Health Rep. 58, 1033–1061 (1943).

73. S. D. Collins, J. Lehmann, Trends and Epidemics of Influenza and Pneumonia. Public Health Rep. 66, 1487–1517 (1951).

74. D. W. Ailling, W. C. Blackwelder, C. H. Stuart-Harris, A study of excess mortality during influenza epidemics in the United States, 1968-1976. Am. J. Epidemiol. 113, 30–43 (1981).

Chapter 2: Childhood immune imprinting to influenza A shapes birth year-specific risk during seasonal H1N1 and H3N2 epidemics

ABSTRACT

Across decades of co-circulation in humans, influenza A subtypes H1N1 and H3N2 have caused seasonal epidemics characterized by different age distributions of infection and mortality. H3N2 causes the majority of cases in high-risk elderly cohorts, and the majority of overall deaths, whereas H1N1 causes incidence shifted towards young and middle-aged adults, and fewer deaths. These contrasting age profiles may result from differences in childhood exposure to H1N1 and H3N2 or from differences in evolutionary rate between subtypes. Here we analyze a large epidemiological surveillance dataset to test whether childhood immune imprinting shapes seasonal influenza epidemiology, and if so, whether it acts primarily via immune memory of a particular influenza subtype or via broader immune memory that protects across subtypes. We also test the impact of evolutionary differences between influenza subtypes on age distributions of infection. Likelihood-based model comparison shows that narrow, within-subtype imprinting is the strongest driver of seasonal influenza risk. The data do not support a strong effect of evolutionary rate, or of broadly protective imprinting that acts across subtypes. Our findings emphasize that childhood exposures can imprint a lifelong immunological bias toward particular influenza subtypes, and that these cohort-specific biases shape epidemic age distributions. As a result, newer and less "senior"

antibody responses acquired later in life do not provide the same strength of protection as responses imprinted in childhood. Finally, we project that the relatively low mortality burden of H1N1 may increase in the coming decades, as cohorts that lack H1N1-specific imprinting eventually reach old age.

AUTHOR SUMMARY

Influenza viruses of subtype H1N1 and H3N2 both cause seasonal epidemics in humans, but with different age-specific impacts. H3N2 causes a greater proportion of cases in older adults than H1N1, and more deaths overall. People tend to gain the strongest immune memory of influenza viruses encountered in childhood, and so differences in H1N1 and H3N2's age-specific impacts may reflect that individuals born in different eras of influenza circulation have been imprinted with different immunological risk profiles. Another idea is that H3N2 may be more able to infect immunologically experienced adults because it evolves slightly faster than H1N1, and can more quickly escape immune memory. We analyzed a large epidemiological data set and found the clearest signal that birth year-specific differences in childhood immune imprinting, not differences in evolutionary rate, explain differences in H1N1 and H3N2's age-specific impacts. These results can help epidemiologists understand how epidemic risk from specific influenza subtypes is distributed across the population, and predict how population risk may shift as differently imprinted birth years grow older. Further, these results provide immunological clues to which facets of immune memory become biased in childhood, and then later play a strong role in protection during seasonal influenza epidemics.

INTRODUCTION

Childhood influenza exposures leave an immunological imprint, which has reverberating, lifelong impacts on immune memory. Foundational work on original antigenic sin (1) and antigenic seniority (2) showed that individuals maintain the highest antibody titers against influenza strains encountered in childhood. But how these serological patterns map to functional immune protection, and shape birth year-specific risk during outbreaks, remains an active area of inquiry. One open question is the breadth of cross-protection provided by immune memory imprinted by influenza viruses encountered in childhood.

Many epidemiological studies highlight benefits from imprinting protection; every modern influenza pandemic has spared certain birth cohorts, presumably due to cross-protective memory primed in childhood (3–9). Recently, we showed that childhood imprinting also protects against novel, emerging avian influenza viruses (8,10). Childhood imprinting may additionally shape birth year-specific risk from seasonal influenza (11–13), but the importance of broadly protective immunity remains unclear in this context.

Recent studies have highlighted childhood imprinting's ability to shape multiple layers of influenza immune memory, both broad and narrow. Until recently, relatively narrow cross-protective immunity, which only protects against closely related antigenic variants of the same hemagglutinin (HA) subtype, has been considered the norm. Lymphocyte memory of variable epitopes on the HA head (i.e. sites at which hemagglutinin antigens of different subtypes show limited homology) drives this narrow, within-subtype protection, which is the main mechanism of protection from the inactivated influenza vaccine. But protection may also be driven by memory of other influenza antigens (e.g. neuraminidase, NA) (14–16), or by immune response to

conserved epitopes, many of which are found on the HA stalk (10,17–19). Antibodies that target conserved HA epitopes can provide broad protection across multiple HA subtypes in the same phylogenetic group (17,19,20), where HA group 1 contains hemagglutinin subtypes H1 and H2, while group 2 contains H3 (10,18,21). H1, H2 and H3 are the only HA subtypes that have circulated seasonally in humans since 1918.

Within-subtype cross-protection is known to shape seasonal influenza's epidemiology and evolution (22). But because this type of narrow immunity decays rapidly in the face of antigenic drift, it would not be expected to shape cohort-specific protection across an entire human lifetime (23,24). Conversely, broad, HA group-level immune memory arises when lymphocytes target conserved HA epitopes, and can play a strong role in defense against unfamiliar influenza strains (e.g. novel, avian or pandemic subtypes (10,17,19,20,25,26)). Broad, HA group-level responses are not traditionally thought to play a strong role in defense against familiar, seasonal influenza subtypes, but could plausibly be deployed against drifted seasonal strains whose variable HA epitopes have become unrecognizable. Because the conserved antigenic targets involved in broad, HA group-level protection are relatively stable over time, they could in theory, facilitate lifelong imprinting-related biases in immune memory (10,26). Thus, childhood immune imprinting may determine which birth cohorts are primed for effective defense against seasonal strains with conserved HA epitopes characteristic of group 1 or group 2, or with variable HA epitopes characteristic of a particular subtype (H1, H2, etc.). A similar line of reasoning may apply to immunity against NA, although much less attention has been paid to this antigen.

Since 1977, two distinct subtypes of influenza A, H1N1 and H3N2, have circulated seasonally in humans, with striking but poorly understood differences in their age-specific impact (8,11–13,27). These differences could be associated with childhood imprinting: older cohorts were almost certainly exposed to H1N1 in childhood (since it was the only subtype circulating in humans from 1918-1957), and now seem to be preferentially protected against modern seasonal H1N1 variants (8,11–13). Likewise, younger adults have the highest probabilities of childhood imprinting to H3N2, which is consistent with relatively low incidence of seasonal H3N2 in these cohorts (Fig. 2-1, 2-2). Alternatively, differences in the evolutionary dynamics of H1N1 and H3N2 could explain the observed age profiles. Subtype H3N2 exhibits slightly faster drift in its antigenic phenotype than H1N1, and as a result, H3N2 may be more able to escape pre-existing immunity and infect older, immunologically experienced adults, whereas H1N1 may be relatively restricted to infecting immunologically naïve children (28).

We analyzed a large data set on seasonal influenza incidence to test whether cohort effects from childhood imprinting primarily act against variable epitopes, only providing cross-protection against closely related HA or NA variants of the same subtype, or against more conserved epitopes, providing broad cross-protection across HA subtypes in the same phylogenetic group (Fig. 2-1A-B). We fitted a suite of models to data using maximum likelihood and compared models using AIC. In a separate analysis, we considered the hypothesis that differences in evolutionary rate of H1N1 and H3N2, rather than imprinting effects, shape differences in age distribution. Our results have implications for long-term projections of seasonal influenza risk in elderly cohorts (12), who suffer the heaviest burdens of influenza-

related morbidity and mortality, and whose imprinting status will shift through time as cohorts born during different inter-pandemic eras grow older.

THE DATA

The Arizona Department of Health Services (ADHS) provided a dataset containing 9,510 seasonal H1N1 and H3N2 cases from their statewide surveillance system. Cases of all ages were confirmed to subtype by PCR and/or culture, primarily from virologic testing at the Arizona State Public Health Laboratory. A smaller number of positive influenza tests were obtained through reporting by other clinical labs, which has been mandatory in Arizona since 2004 (29). Cases were observed across 22 years of influenza surveillance, from the 1993-1994 influenza season through the 2014-2015 season, although sample sizes increased dramatically after the 2009 pandemic (Table 2-1). The data included positive test results from patients in hospitals, long-term care facilities, correctional facilities, and outpatient clinics, and thus captured a range of case severities.

Following CDC standards, ADHS defines the influenza season as epidemiological week 40 (around early October) through week 39 of the following year (30). The 2008-2009 and 2009-2010 influenza seasons spanned the first and second wave, respectively, of the 2009 H1N1 pandemic. We did not analyze cases observed during this time period, because age distributions of infection and molecular drivers of immune memory differed during the 2009 pandemic from the normal, drivers of seasonal influenza's immuno-epidemiology of interest to this study (13,17,20). From the dataset of 9,510 seasonal cases (defined as any case observed outside the

2008-2009 or 2009-2010 season), we excluded 58 cases with birth years before 1918 (whose imprinting status could not be inferred unambiguously), and one case whose year of birth was recorded in error. Ultimately, we analyzed 9,541 cases.

Table 2-1. Confirmed cases in surveillance data from Arizona Department of Health Services.

Data representing the first and second waves of the 2009 H1N1 pandemic (2008-2009 and 2009-2010 seasons) were excluded.

Season	Confirmed H1N1	Confirmed H3N2
1993-94	0	101
1994-95	12	38
2002-03	71	8
2003-04	0	71
2004-05	0	131
2005-06	1	321
2006-07	212	28
2007-08	196	244
2010-11	472	1204
2011-12	595	348
2012-13	80	1578
2013-14	1475	151
2014-15	5	2109
Total	**3119**	**6332**

THE MODEL

Reconstructed imprinting patterns

We reconstructed birth year-specific probabilities of childhood imprinting to H1N1, H2N2 or H3N2 using methods described previously (10). These probabilities are based on patterns of first childhood exposure to influenza A and reflect historical circulation (Fig. 2-1A). Most individuals born between pandemics in 1918 and 1957 experienced a first influenza A virus (IAV) infection by H1N1, and middle-aged cohorts born between pandemics in 1957 and 1968 almost all were first infected by H2N2 (note that because the first influenza exposure may occur after the first year of life, individuals born in the years leading up to a pandemic have some probability of first infection by the new pandemic subtype, Fig. 2-1A). Ever since its emergence in 1968, H3N2 has dominated seasonal circulation in humans, and caused the majority of first infections in younger cohorts. However, H1N1 has also caused some seasonal circulation since 1977, and has imprinted a fraction of all cohorts born since the mid-1970s (Fig. 2-1A).

Reconstructions assumed children age 0-12 in the year of case observation might not yet have been exposed to any influenza virus. Interactions between imprinting and vaccination of naïve infants are plausible, but poorly understood (10,31). We did not consider childhood vaccination effects here; only a small percentage of individuals in the ADHS data were born at a time when healthy infants were routinely vaccinated against influenza.

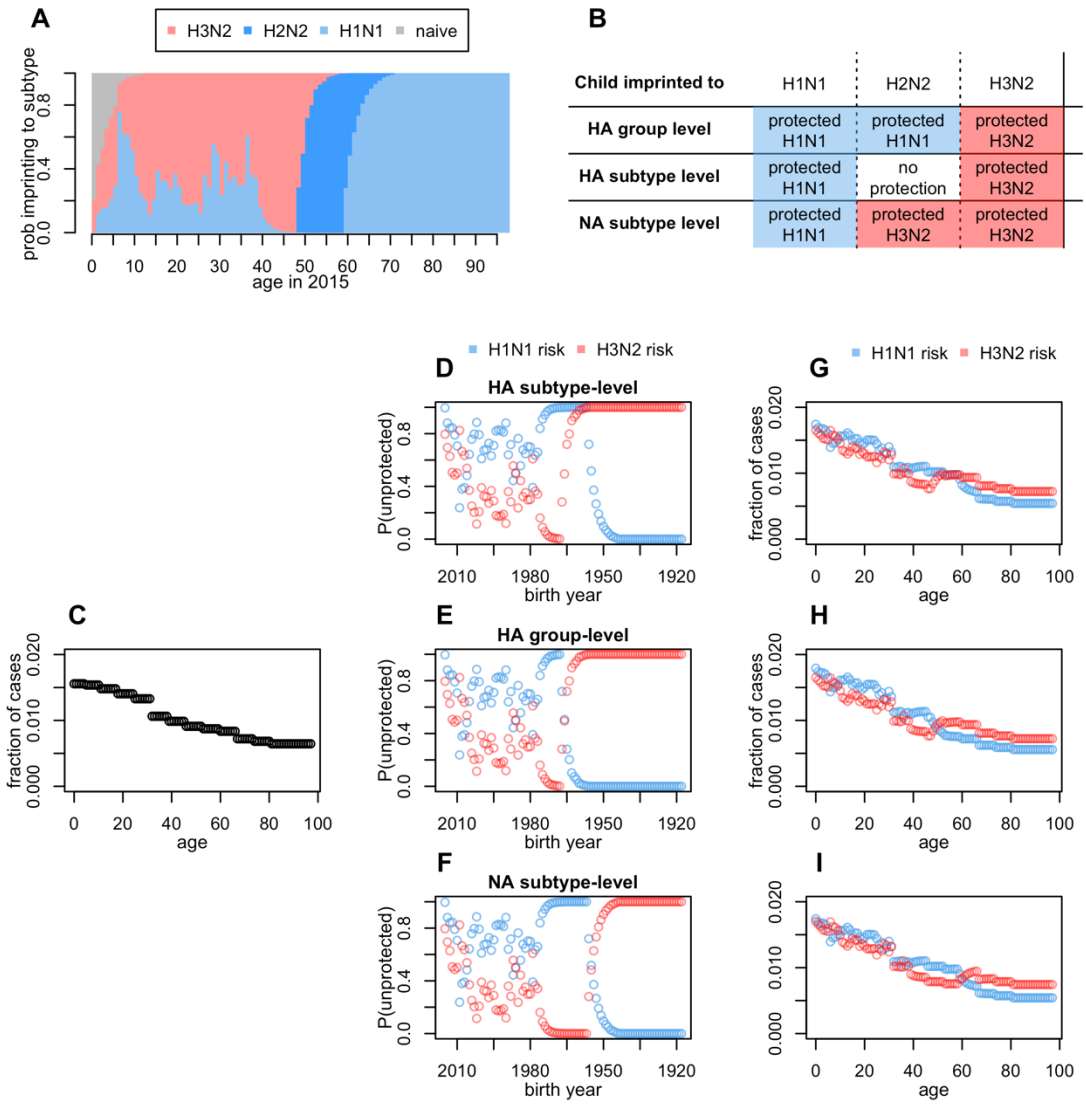

Figure 2-1. Model and expectations under different imprinting hypotheses.

(A) Reconstructed, birth year-specific probabilities of imprinting (representative example specific to USA for cases observed in 2015). Throughout the manuscript, group 1 HA subtypes are represented in blue and group 2 subtypes in red. **(B**) Expected imprinting protection against H1N1 or H3N2 under the three tested models. (**C**) Cartoon of age-specific risk curve. The shape of this curve is purely hypothetical, but each tested model fit a similar step function to data. (**D-F)** Fraction of each birth year unprotected by their childhood imprinting (from A) determines the shape of birth year-specific risk. (**G-I)** A linear combination of

age-specific risk (C), and birth year-specific risk (D-F) give the expected age distribution of H1N1 or H3N2 cases under each model.

Expected age distributions under alternate imprinting models

If HA subtype-level imprinting protection shapes seasonal influenza risk, primary exposure to HA subtype H1 or H3 in childhood should provide lifelong protection against modern variants of the same HA subtype. If imprinting protection acts primarily against specific NA subtypes, lifelong protection will be specific to N1 or to N2 (Fig. 2-1B). Alternatively, if broad HA group-level imprinting shapes seasonal influenza risk, then cohorts imprinted to HA subtype H1 or H2 (both group 1) should be protected against modern, seasonal H1N1 (also group 1), while only cohorts imprinted to H3 (group 2) would be protected against modern, seasonal H3N2 (also group 2) (Fig. 2-1B). Collinearities between the predictions of different imprinting models (Fig. 1D-I) were inevitable, given the limited diversity of influenza antigenic subtypes circulating in humans over the past century (reflected in Fig. 2-1A). Note that middle-aged cohorts, which were first infected by H2N2, are crucial, because they provide the only leverage to differentiate between imprinting at the HA subtype, NA subtype or HA group-level level (Fig. 2-1B).

Our approach distinguishes between age-specific risk factors of influenza infection related to health and social behavior, and birth year-specific effects related to imprinting. Specifically, age-specific risk could be influenced by medical factors like age-specific vaccine coverage, age-specific risk of severe disease, and immunosenescence, or by behavioral factors like age-assorted social mixing, and age-specific healthcare seeking behavior. These factors

should have similar impacts on any influenza subtype. In contrast, imprinting effects are subtype-specific. Thus, we fit a step function to characterize the shape of age-specific risk of any confirmed influenza infection. Simultaneously, we modeled residual, subtype-specific differences in risk as a function of birth year, to focus on the possible role of childhood imprinting in H1N1 or H3N2 infections. Each tested model used a linear combination of age-specific risk (Fig. 2-1C) and birth year-specific risk (Fig. 2-1D-F) to generate an expected distribution of H1N1 or H3N2 incidence (Fig. 2-1G-I). Note that for a given birth cohort, age-specific risk changed across progressive years of case observation (as the cohort got older), whereas birth year-specific risk was constant over time.

To test quantitatively whether observed subtype-specific differences in incidence were most consistent with imprinting at the HA subtype, NA subtype or HA group level, or with no contribution of imprinting, we fitted a suite of models to each data set using a multinomial likelihood and then performed model selection using AIC. AIC is used to compare the relative strength of statistical support for a set of candidate models, each fitted to the same data, and favors parsimonious models that fit the data well (32,33). Technical details are provided in the Methods.

Tested models

We fit a set of four models to the ADHS data set. The simplest model contained only age-specific risk (abbreviated A), and more complex models added effects from imprinting at the HA subtype level (S), at the HA group level (G), or at the NA subtype level (N): abbreviated AS, AG, and AN, respectively. The age-specific risk curve took the form of a step function, in which

relative risk was fixed to 1 in age bin 0-4, and one free parameter was fit to represent relative risk in each of the following 12 age bins: {5-10, 11-17, 18-24, 25-31, 32-38, 39-45, 46-52, 53-59, 60-66, 67-73, 74-80, 81+}. Within models that contained imprinting effects, two additional free parameters described the relative risk of confirmed H1N1 or H3N2 infection, given imprinting protection against that seasonal subtype.

Effect of influenza evolutionary rate on age profiles

We used publicly available data from *Nextstrain* (34,35), and from one previously published study (36), to calculate annual antigenic advance, which we defined as the antigenic distance between strains of a given lineage (pre-2009 H1N1, post-2009 H1N1 or H3N2) that circulated in consecutive seasons (Methods). The "antigenic distance" between two influenza strains is used as a proxy for similarity in antigenic phenotype, and potential for immune cross-protection. A variety of methods have been developed to estimate antigenic distance using serological data, genetic data, or both (35–37).

To assess the impact of antigenic evolutionary rate on the epidemic age distribution, we tested whether the proportion of cases in children increased in seasons associated with large antigenic changes. If the rate of antigenic drift is a strong driver of age-specific influenza risk, then the fraction of influenza cases observed in children should be negatively related to annual antigenic advance (28). In other words, strains that have not changed much antigenically since the previous season should be unable to escape pre-existing immunity in immunologically experienced adults, and more restricted to causing cases in immunologically naïve children; strains that have changed substantially will be less restricted to children.

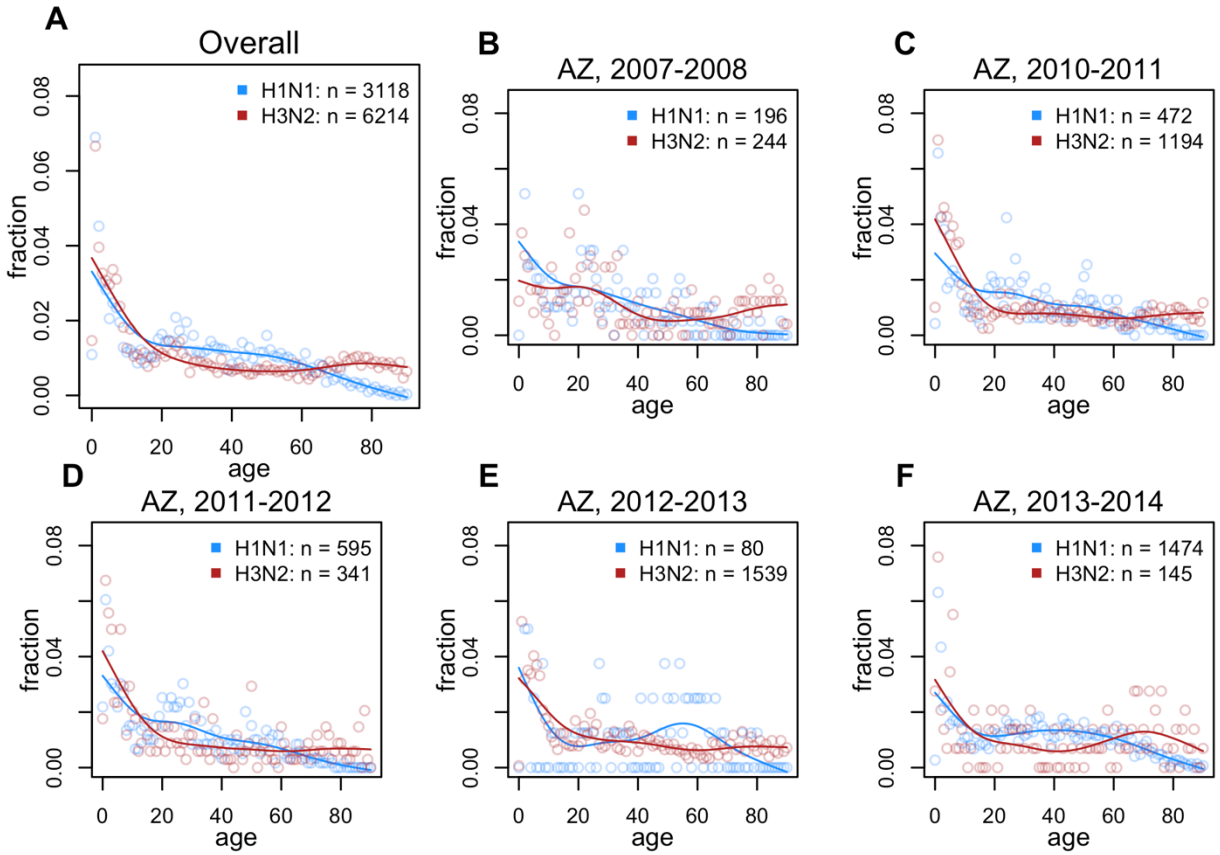

Figure 2-2. Observed age distributions, Arizona.

Points show fraction of confirmed H1N1 or H3N2 cases observed in each single year of age. Lines show a smoothing spline fit to observed distributions. **(A)** All confirmed cases in the data (aggregate across all seasons). (**B-G**) Age distributions from individual seasons in which both H1N1 and H3N2 circulated (seasons with ≥ 50 confirmed cases of each subtype are shown here. See Fig. 2-S1 for all seasons).

RESULTS

Subtype-specific differences in age distribution

Seasonal H3N2 epidemics usually caused more cases in older cohorts, while H1N1 caused a greater proportion of cases in young and middle-aged adults (Figs. 2-2, 2-S1, 2-S2). These patterns were apparent whether we compared H3N2 epidemic age distributions with those caused by the pre-2009 seasonal H1N1 lineage, or with the post-2009 lineage. Observed patterns are consistent with the predicted effects of cohort-specific imprinting (Fig. 2-1), and with previously reported differences in age distribution of seasonal H1N1 and H3N2 incidence (11–13,27). See Fig. 2-2 for seasons where H1N1 and H3N2 co-circulated in substantial numbers, and Figs. 2-S1, 2-S2 for the entire dataset and alternate smoothing parameters.

Imprinting model selection

The model containing NA subtype-level imprinting received the most statistical support, and the model containing HA subtype-level imprinting was the second most preferred in terms of AIC (Fig. 2-3, Table 2-2). The ADHS data showed a strong preference for NA subtype-level imprinting over HA subtype-level imprinting (ΔAIC=23.42), and effectively no statistical support for broad, HA group-level imprinting (ΔAIC=245.18), or for an absence of imprinting effects (ΔAIC=380.47). Visual assessment of model fits (Fig. 2-3 C-D) confirmed that models containing imprinting effects at the narrow, NA or HA subtype levels provided the best fits to data. The lack of support for the no-imprinting model supports the hypothesis that imprinting from the first exposure shapes lifelong seasonal influenza risk, just as it does avian-origin

influenza (10, 12). However, imprinting appears to act more narrowly against seasonal influenza than against avian influenza, providing cross protection only to a specific NA or HA subtype, instead of broader, HA group-level protection. This result is consistent with the idea that immunodominance of variable HA epitopes limits the breadth of immune cross protection deployed against familiar, seasonal influenza subtypes (19,20).

As expected (see Fig. 2-1 G-I), predictions from the two best models were highly collinear, except in their risk predictions among middle-aged, H2N2-imprinted cohorts (birth years 1957-1968), and some other minor differences arising from normalization across birth-years.

Fitted risk patterns

Fitted age-specific risk curves took similar forms in all tested models, with risk decreasing rapidly from birth through adolescence, and then decreasing much more slowly until the end of life (Fig. 2-2A shows the fitted curve from the best model). Estimates of imprinting parameters were less than one, indicating some reduction in relative risk of infection (Table 2-2). Within the best model, estimated reductions in relative risk from childhood imprinting were stronger for H1N1 (0.34, 95% CI 0.29-0.42) than for H3N2 (0.71, 95% CI 0.62-0.82). Table 2-2 shows parameter estimates and 95% profile confidence intervals from all models fitted.

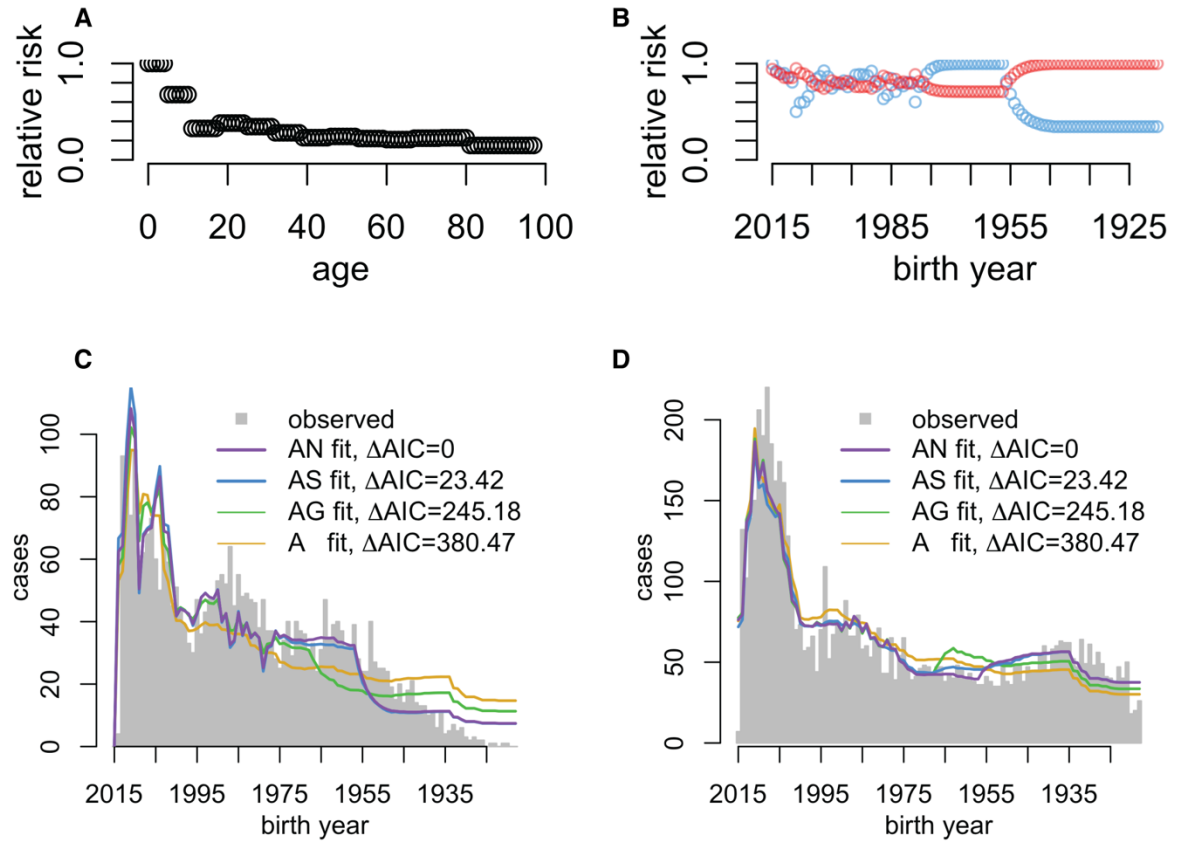

Figure 2-3. Model fits and model selection.

(A) Fitted effects of age and **(B)** imprinting from model AN, which provided the best fit to data**. (C-D)** Model fits to observed age distributions of H1N1 (**C)** and H3N2 **(D**) cases**.** Model name abbreviations indicate which factors were included: A = age-specific risk, N = NA subtype-level imprinting, S = HA subtype-level imprinting, G = HA group-level imprinting.

Table 2-2. Maximum likelihood parameter estimates and 95% profile confidence intervals from each model fit to ADHS data.

Model	AN	AS	AG	A
ΔAIC	0.00	23.42	245.18	380.47
H1N1 impr. protection	0.34 (0.29-0.42)	0.29 (0.24-0.35)	0.67 (0.58-0.78)	
H3N2 impr. protection	0.71 (0.62-0.82)	0.9 (0.78- >1)	0.69 (0.6-0.8)	
Ages 0-4	Reference group: Value fixed to 1			
Ages 5-10	0.68 (0.63-0.74)	0.66 (0.61-0.72)	0.66 (0.62-0.72)	0.62 (0.57-0.68)
Ages 11-17	0.33 (0.30-0.36)	0.31 (0.28-0.34)	0.33 (0.30-0.37)	0.30 (0.28-0.34)
Ages 18-24	0.38 (0.35-0.42)	0.36 (0.32-0.4)	0.39 (0.35-0.43)	0.35 (0.32-0.39)
Ages 25-31	0.34 (0.32-0.38)	0.33 (0.30-0.37)	0.34 (0.31-0.38)	0.31 (0.28-0.35)
Ages 32-38	0.28 (0.26-0.32)	0.26 (0.24-0.3)	0.28 (0.26-0.32)	0.26 (0.24-0.29)
Ages 39-45	0.23 (0.20-0.27)	0.21 (0.18-0.24)	0.24 (0.22-0.28)	0.21 (0.20-0.24)
Ages 46-52	0.24 (0.22-0.28)	0.21 (0.19-0.24)	0.24 (0.22-0.28)	0.23 (0.20-0.26)
Ages 53-59	0.22 (0.20-0.26)	0.20 (0.18-0.23)	0.20 (0.18-0.24)	0.20 (0.18-0.23)
Ages 60-66	0.21 (0.19-0.24)	0.22 (0.20-0.26)	0.19 (0.16-0.22)	0.18 (0.16-0.21)
Ages 67-73	0.22 (0.20-0.26)	0.25 (0.22-0.29)	0.20 (0.18-0.23)	0.19 (0.18-0.22)
Ages 74-80	0.23 (0.20-0.26)	0.25 (0.22-0.3)	0.20 (0.18-0.24)	0.20 (0.18-0.23)
Ages 81+	0.15 (0.14-0.18)	0.17 (0.15-0.2)	0.13 (0.12-0.16)	0.13 (0.12-0.15)

All estimated parameters represent the relative risk of confirmed infection, given the factors listed in the left-hand column. Model name abbreviations specific which factors were included. A = age-specific risk, N = NA subtype-level imprinting, S = HA subtype-level imprinting, G = HA group-level imprinting.

Effect of evolutionary rate

To test for effects of evolutionary rate on epidemic age distribution, we searched for decreases in the proportion of cases among children in seasons associated with antigenic novelty, when highly drifted strains might be more able to infect immunologically experienced adults. Consistent with this expectation, the data showed a slight negative but not significant association between annual antigenic advance and the fraction of H3N2 cases observed in children (Fig. 2-4A). However, note that no clear relationship emerged between antigenic novelty and the fraction of cases observed in children and adults older than 10 (Fig. 2-4A). These are the cohorts in which epidemiological data show the clearest differences between H1N1 and H3N2's age-specific impacts (Fig. 2-2); if rate of antigenic evolution is a dominant driver of age-specific differences in

incidence, we would have expected to see clearer evidence of evolutionary rate effects within adults cohorts, not just in the youngest children. The data contained too few influenza seasons with sufficient numbers of confirmed H1N1 cases to support meaningful Spearman correlation coefficients for either pre-2009 or post-2009 seasonal H1N1 lineages.

Furthermore, if evolutionary rate is the dominant driver of subtype-specific differences in epidemic age distribution, then when subtypes H1N1 and H3N2 show similar degrees of annual antigenic advance, their age distributions of infection should appear more similar. However, the data showed that differences in H1N1 and H3N2's age-specific impacts did not converge when lineages showed similar annual advance. When comparing the fraction of cases observed in specific age classes, H1N1 data consistently clustered separately from H3N2, with H1N1

consistently causing fewer cases at the extremes of age (children 0-10 and elderly adults 71-85), but more cases in middle-aged adults, regardless of antigenic novelty (Fig. 2-4A). Smoothed

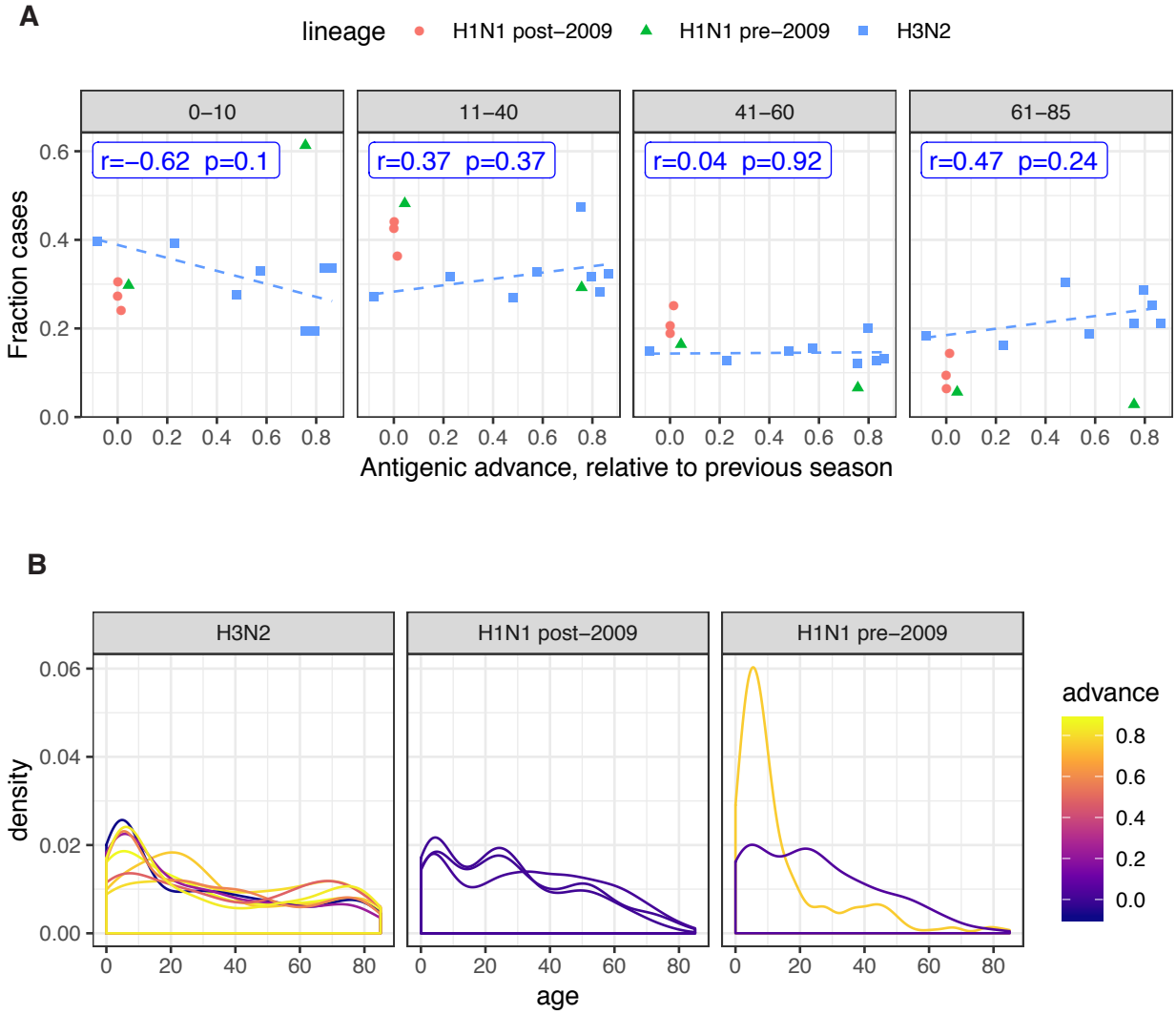

Figure 2-4. Effect of antigenic advance on age distribution.

(A) Relationship between annual antigenic advance and the fraction of cases observed in children (0-10), or in adult age groups. Each data point represents a single influenza season in which at least 100 confirmed cases of a given subtype were observed. Blue label shows Spearman correlation between the fraction of H3N2 cases observed in each age group and annual antigenic advance. Blue dashes show linear trend fitted using lm() in R. **(B)** Season-specific age distributions of infection, colored by antigenic advance since the previous season.

density plots showed no clear relationship between annual antigenic advance and age distribution (Fig. 2-4B). Overall, the data showed a weak, but not significant signal that incidence may be more restricted to young children when antigenic novelty is low, but the data did not show strong evidence that the magnitude of annual antigenic drift is a systematic driver of epidemic age distribution across the entire population.

DISCUSSION

We analyzed a large epidemiological surveillance dataset and found that seasonal influenza subtypes H1N1 and H3N2 cause different age distributions of infection, confirming previously reported patterns (11–13). We analyzed several possible drivers of these differences side-by-side, and found greatest support for the hypothesis that immunological imprinting leads to lasting protection against the NA or HA subtype of the first influenza strain encountered in childhood (11,12). The data did not support strong effects from broader HA group-level imprinting, as recently detected for novel zoonotic or pandemic viruses (8,10), or from differences in rates of antigenic evolution (28). Our results suggest that the first childhood infection leaves a lifelong imprint of immune memory to seasonal influenza, and that this imprint is not erased even after decades of exposure to or vaccination against dissimilar influenza subtypes.

As additional evidence that birth year, rather than age, drives subtype-specific differences in seasonal influenza risk, we note that H3N2's impacts have not always been focused in elderly

cohorts. When H3N2 first emerged in 1968, it caused little or no excess mortality in the elderly, putatively because those who were elderly in 1968 had been exposed, as children or young adults, to an H3 virus that had circulated in the late 1800s (6,8). Meanwhile, H1N1-imprinted cohorts (those ~10-50 years old at the time of the H3N2 pandemic), experienced considerable excess mortality in the H3N2 pandemic (6), and continue to experience excess H3N2 morbidity and mortality today as elderly adults ((11–13,27), Fig. 2-2). In short, comparing data from H3N2's emergence in 1968 to its seasonal circulation today shows impacts that have remained consistent with respect to birth year, but that have shifted with respect to age.

In model comparison, the data showed the strongest support for effects from childhood imprinting to NA. Although NA is not as intensively studied as HA, these results emphasize the increasingly recognized importance of both antigens as drivers of protection against seasonal influenza (14–16). Realistically, some combination of effects from both HA and NA subtype-level imprinting probably shape seasonal influenza risk. The models containing NA and HA subtype-level imprinting produced very similar fits to data and emerged as the top two models in terms of AIC. Unfortunately, collinearities between predictions of the simple, single-antigen models considered here arose inevitably from influenza's limited diversity of circulation in humans over the past century. These collinearities prevented us from testing more complicated models of combined effects from imprinting to HA and NA, or to other antigens such as internal proteins. Because analysis of population-level data can support only a limited scope of inference, deeper insights into the respective roles of HA, NA and other influenza antigens as drivers of cohort effects will most likely need to come from focused immunological cohort studies in which individual histories of influenza infection are known, such as those recently funded by the

National Institutes of Health (38). Alternatively, the development of immunological biomarkers for diagnosis of imprinting status in individual patients could substantially increase the power of epidemiological inference, which (as in this study) currently relies instead on probabilistic reconstructions of imprinting histories according to birth year.

Small sample sizes may have limited our power to detect a statistically significant relationship between annual antigenic advance and epidemic age distribution. The data did show a weak trend supporting the idea that in seasons where antigenic advance is low, the seasonal influenza cases may be more restricted to the youngest, immunologically naïve children (28). But the data did not reveal a clear relationship between antigenic advance and the fraction of cases occurring in adult age groups, the same age groups where epidemiological data reveals distinct subtype-specific differences in incidence proportion. This lack of clear signal is consistent with growing recognition that existing methods to map antigenic distance, which rely heavily on hemagglutination inhibition (HI) assays performed in laboratory ferrets, do not always capture realistic patterns of cross-reactivity in humans (reviewed in 39,40). Further, glycosylation of HA can cause antigenic escape in large subsets of the human population, yet such posttranslational modifications may be perceived as neutral in existing antigenic maps (40,41). Moreover, existing metrics of evolutionary and antigenic advance are based on properties of HA (34–36), but our epidemiologic data support an equal if not stronger role of NA. We speculate that a clearer relationship between epidemic age distribution and antigenic drift might emerge if antigenic distance measures were able to incorporate cohort-specific variation in immune history, and impacts from multiple antigens.

While our results provide some valuable new clues about the underlying immune drivers of imprinting protection against seasonal influenza, we can only speculate as to the exact mechanism. Traditionally, narrow, within-subtype influenza immunity is thought to decay quickly in the face of antigenic drift. Signals of rapid drift are largely based on HI data, which measures antibody responses to just a handful of immunodominant, variable epitopes found near the receptor-binding domain on the HA head. These epitopes accumulate substitutions rapidly, and so strains that circulated more than 14 years apart rarely show measurable cross-protective HI titers (36). The short timescale of immune memory to variable HA head epitopes stands in contrast to patterns observed in our study and others (11–13), where within-subtype immune memory imprinted in childhood appears to persist for an entire human lifetime, remaining evident even in the oldest cohorts in the data. Thus, we speculate that within-subtype imprinting protection arises via different immune mechanisms than the well-studied antibody responses measured by the HI assay.

One possibility is that within-subtype imprinting protection is driven by antibody responses to intermediately conserved epitopes, which might remain stable over time, but lack structural homology across different HA and NA subtypes. We rule out a strong role from antibody responses against the best-studied conserved epitopes (e.g. those on the stalk), which tend to provide broader, cross-subtype protection (10,17,19) than supported by model comparison. But recent studies show that B cell memory shifts to focus on conserved influenza epitopes as we grow older, presumably because a lifetime of exposures to drifted, seasonal H1N1 or H3N2 variants repeatedly back-boosts memory of unchanged epitopes (23,24). Repeat

boosting of intermediately conserved HA or NA antigens could explain the longevity of subtype-level imprinting protection.

Another potential explanation supported by recent immunological data (26), is that the memory B cell clones developed during the first childhood influenza exposure later adapt via somatic hypermutation to “follow” antigenic targets as they drift over time. Thus, the first influenza exposure in life may fill a child's memory B cell repertoire with clones that will serve in the future, not as final products but as prototypes that can be rapidly and effectively tailored to recognize drifted influenza strains of the same subtype. The adaptability of the B cell repertoire would not be detectable in traditional HI panels, which are collected using sera from ferrets exposed to a single influenza variant, and do not reflect the development of the human B cell repertoire across repeated, seasonal influenza exposures. A final possibility is that cellular immunity (e.g. CD4+ T cell memory), which would not be captured in serological assays, plays an underappreciated role in imprinting protection.

Signals of imprinting protection are anomalously strong in the current cohort of elderly adults, as reflected by higher estimates of imprinting protection to H1N1 than H3N2. For nearly four decades from 1918-1957, H1N1 persisted as the only strain circulating in humans. The oldest subjects in our data were born slightly after its emergence in 1918, and would not have encountered an influenza virus of any subtype but H1N1 until after age 30. Decades of early-life exposures to H1N1 variants may have reinforced and expanded the breadth of H1N1-specific immune memory in these oldest cohorts. But this strong protection against H1N1 seems to come at a cost; even after decades of seasonal H3N2 exposure, and vaccination, older cohorts have evidently failed to develop equally strong protection against H3N2. Antigenic similarity between

H1N1 strains that circulated earlier in the 20th century (which caused imprinting in older cohorts), and modern H1N1 lineages that emerged in 1977 and in 2009, may also have amplified the strength and longevity of H1N1 protection (4,42). One additional consideration is that HA group 1 antigens appear to induce narrower immune responses than structurally distinct HA group 2 antigens, which may be better able to induce cross-group responses (21). Perhaps elderly cohorts imprinted to group 1 antigens have been trapped in narrower responses that offer exceptional protection against strains similar to that of first exposure but relatively poor adaptability to other subtypes.

Given that cohorts born after 1968 have had much more varied early life exposures to both H1N1 and H3N2, it is unclear whether equally strong, subtype-specific biases in protection will persist when post-1968 birth cohorts eventually become elderly. Determining the precise immune mechanism(s) responsible for subtype-level imprinting is necessary to project long-term shifts in influenza-related incidence, and possibly in mortality. The vast majority of influenza-related deaths occur in adults over age 65, and H3N2 has caused many times the number of fatalities in high-risk elderly cohorts as seasonal H1N1, even in the post-2009 pandemic period (12,27,43). These patterns may arise because H3N2 is intrinsically more virulent than H1N1, but we speculate that imprinting protection, which currently limits the incidence of clinically-attended H1N1 infection in the elderly, may also explain these differences. In the future, cohorts imprinted to H2N2 (born c. 1950-1968) will become elderly, and would expect protection against H3N2 via NA subtype-level imprinting, while HA H2-level imprinting would not be of much use against any currently circulating seasonal subtype. If future elderly cohorts continue to show strong subtype-specific biases from imprinting, our results would corroborate the idea that

mortality from H1N1 may increase in the future (8,12) as protection in the elderly shifts toward other subtypes. On the other hand, future generations of elderly adults, especially those born after H1N1 and H3N2 began to co-circulate in 1977, may show a greater ability to act as immunological generalists, with effective defenses against multiple influenza subtypes.

One limitation of this study was that we could not model the impact of seasonal influenza vaccination explicitly, as the vaccination status of subjects in the ADHS data was unknown. We note that the influenza vaccine contains both an H1N1 and H3N2 strain, and so on average, influenza vaccination should protect individuals similarly against both subtypes. However, we also acknowledge that influenza vaccine effectiveness varies by season, age group, and subtype, in ways that are poorly understood and difficult to measure (44). These asynchronous and multi-dimensional shifts in vaccine effectiveness may contribute to variability in H1N1 and H3N2's age distributions across influenza seasons.

Another limitation of this study was the low number of confirmed cases available in the pre-2009 era. To separate age-specific risk effects from birth year-specific cohort effects, the greatest power will come from large data sets collected continuously over decades, so that individual birth cohorts can be followed as they become considerably older. We emphatically echo earlier calls (45) for more systematic sharing of single year-of-age in influenza surveillance data, standardization of sampling effort, and reporting of age-specific denominators, which could substantially boost the scientific community's ability to link influenza's genetic and antigenic properties with epidemiological outcomes.

Altogether, this analysis confirms that the epidemiological burden of H1N1 and H3N2 is shaped by cohort-specific differences in childhood imprinting (8,11,12,46). The finding that such

imprinting acts at the HA or NA subtype level informs prediction of the future epidemiological impact of specific seasonal subtypes in high-risk elderly cohorts. The lack of support for broader, HA group-level imprinting effects emphasizes the consequences of immunodominance of influenza's most variable epitopes, and the difficulty of deploying broadly protective memory B cell responses against familiar, seasonal strains. Overall, these findings further our understanding of how antigenic seniority shapes cohort-specific risk during epidemics. The fact that elderly cohorts show relatively weak immune protection against H3N2, even after living through decades of seasonal exposure to or vaccination against H3N2, suggests that antibody responses acquired in adulthood do not provide the same strength of immune protection as responses primed in childhood. Immunological experiments that consider multiple viral exposures, and cohort studies in which individual histories of influenza infection are tracked from birth, promise to illuminate how B cell and T cell memory develop across a series of early life exposures. In particular, these studies may provide clearer insights than epidemiological data into which influenza antigens, epitopes and immune effectors play the greatest role in immune imprinting, and how quickly subtype-specific biases become entrenched across the first or the first few exposures.

MATERIALS AND METHODS

Estimation of age from birth year in ADHS data

The data contained three variables, influenza season, birth year and confirmed subtype. For most cases, birth year was extracted directly from the reported date of birth in patient medical records, but age was not known. We estimated patient age at the time case observation

using the formula [year of observation]-[birth year]. To ensure that the minimum estimated age was 0, the second year in the influenza season of case observation was considered the calendar year of observation (e.g. 2013 for the 2012-2013 season).

Splines

In Figure 2-2, smoothing splines were fit to aid visual interpretation of noisy data. We fit splines using the command *smooth.spline(x = AGE, y = FRACTIONS, spar = 0.8)* in R version 3.5.0. Variables *AGE* and *FRACTIONS* were vectors whose entries represented single years of age, and the fraction of cases observed in the corresponding age group. The smoothing parameter 0.8 was chosen to provide a visually smooth fit. Alternative smoothing parameter choices (0.6 & 1.0) are shown in Figs. 2-S1, 2-S2. Although the choice of smoothing parameter changed the shape of each fitted spline, qualitative differences between splines fitted to H1N1 or H3N2 were robust.

Model formulation

For each unique season in which cases were observed, define p as a vector whose entries represent the expected probability that a randomly drawn H1N1 or a randomly drawn H3N2 case was observed in an individual of age a. Each model defined, p as a linear combination of age-specific risk, birth year-specific risk (i.e. imprinting effects). All tested models were nested within the equation:

$$p = A * \mathbf{1}_{H1N1}(I_{H1N1}) * \mathbf{1}_{H3N2}(I_{H3N2}) \quad (2\text{-}1)$$

To include risk factors that only modulated risk from one subtype, we included indicator functions $\mathbf{1}_{H1N1}$ and $\mathbf{1}_{H3N2}$, which took value 1 if p described the expected age distribution of H1N1 or H3N2 cases, respectively, and 0 otherwise.

Age-specific risk (A)

Age-specific risk was defined as a step function, in which relative risk was fixed to value 1 in an arbitrarily chosen age bin, and then z-1 free parameters, denoted r_2 to r_z, were fit to describe relative risk in all other age bins. Below, $\mathbf{1}_i$ are indicator functions specifying whether each vector entry is a member of age bin i. To obtain the predicted fraction of cases observed in each single year of age, we normalized the risk distribution so that predicted risk across all age groups summed to 1.

$$A = norm(\mathbf{1}_1 + \mathbf{1}_2 r_2 + \cdots \mathbf{1}_z r_z) \tag{2-2}$$

Imprinting (I)

An indicator function defined whether a given prediction vector described risk of confirmed H1N1 or H3N2 infection. Let f_{IHxNy} be vectors describing the fraction of cases of each birth year that were protected against strain *HxNy* by their childhood imprinting. We defined r_{IHxNy} as free parameters describing the risk of confirmed *HxNy* infection, given imprinting protection. Finally, the factor describing the effect of imprinting (I) was defined as:

$$I_{HxNy} = \mathbf{1}_{HxNy} * [f_{IHxNy} r_{IHxNy} + (1 - f_{IHxNy})] \tag{2-3}$$

Likelihood

We used equations 1-3 to generate predicted case age distributions (p) for each influenza season (s) in which cases were observed in the data. Then, the likelihood was obtained as a product of multinomial densities across all seasons. If n_s represents the total number of cases observed in a given season, $x_{0cs}, \ldots x_{mcs}$ each represent the number of cases observed in each single year of age/single year of birth, and if $p_{0cs} \ldots p_{mcs}$ each represent entries in the model's predicted age/birth year-distribution of cases, then the likelihood is given by:

$$\mathcal{L} = \prod_s \frac{n_s!}{x_{0s}! \ldots x_{ms!}} p_{0s}^{x_{0s}} \ldots p_{ms}^{x_{ms}} \quad (2\text{-}4)$$

Model fitting and model comparison

We fit models containing all possible combinations of the above factors to influenza data from each season in the data. We simultaneously estimated all free parameter values using the optim() function in R. We calculated likelihood profiles and 95% profile confidence intervals for each free parameter. Confidence intervals were defined using the method of likelihood ratios (32).

Antigenic advance

We obtained antigenic distance estimates from *Nextstrain (nextstrain.org)*(34,47), and from source data from Figure 3 in Bedford et al. (36). *Nextstrain* calculates antigenic distance using genetic data from GISAID (48), and using methods described by Neher et al. (35). We analyzed "CTiter" estimates from *Nextstrain*, which correspond to Neher et al.'s "tree model"

method. We repeated analyses using estimates from the similar "substitution model" method and verified that our choice of antigenic distance metric did not meaningfully impact our results (results not shown). Datasets from *Nextstrain* and Bedford et al. both contained redundant antigenic distance estimates for the H3N2 lineage, but only Bedford et al. analyzed the pre-2009 H1N1 lineage, and only *Nextstrain* data analyzed the post-2009 H1N1 lineage. The antigenic distance estimates reported by Bedford et al. were roughly proportional to those reported on *Nextstrain*, but greater in absolute magnitude (35). To enable visualization of all three lineages on the same plot axes, we rescaled pre-2009 H1N1 estimates from Bedford et al. using the formula $d_{Nextstrain} = 0.47 d_{Bedford}$. The scaling factor was chosen so that directly-comparable H3N2 distance estimates obtained using each method spanned the same range (Fig. 2-S3). The *Nextstrain* data files used in this analysis are archived within our analysis code.

ACKNOWLEDGEMENTS

KG was supported by the National Institutes of Health (F31AI134017, T32-GM008185). JLS was supported by NSF grants OCE-1335657 and DEB-1557022, SERDP RC-2635, and DARPA PREEMPT D18AC00031. MW was supported by the David and Lucile Packard Foundation. The funders had no role in study design, data collection and analysist. This work does not necessarily represent the views of the US government or the NIH.

CODE AND DATA AVAILABILITY

All relevant data and code is publicly available and archived in the Zenodo repository at DOI: 10.5281/zenodo.3269906.

ETHICS STATEMENT

This study analyzed only existing epidemiological data, which was completely anonymized.

SUPPLEMENTARY FIGURES

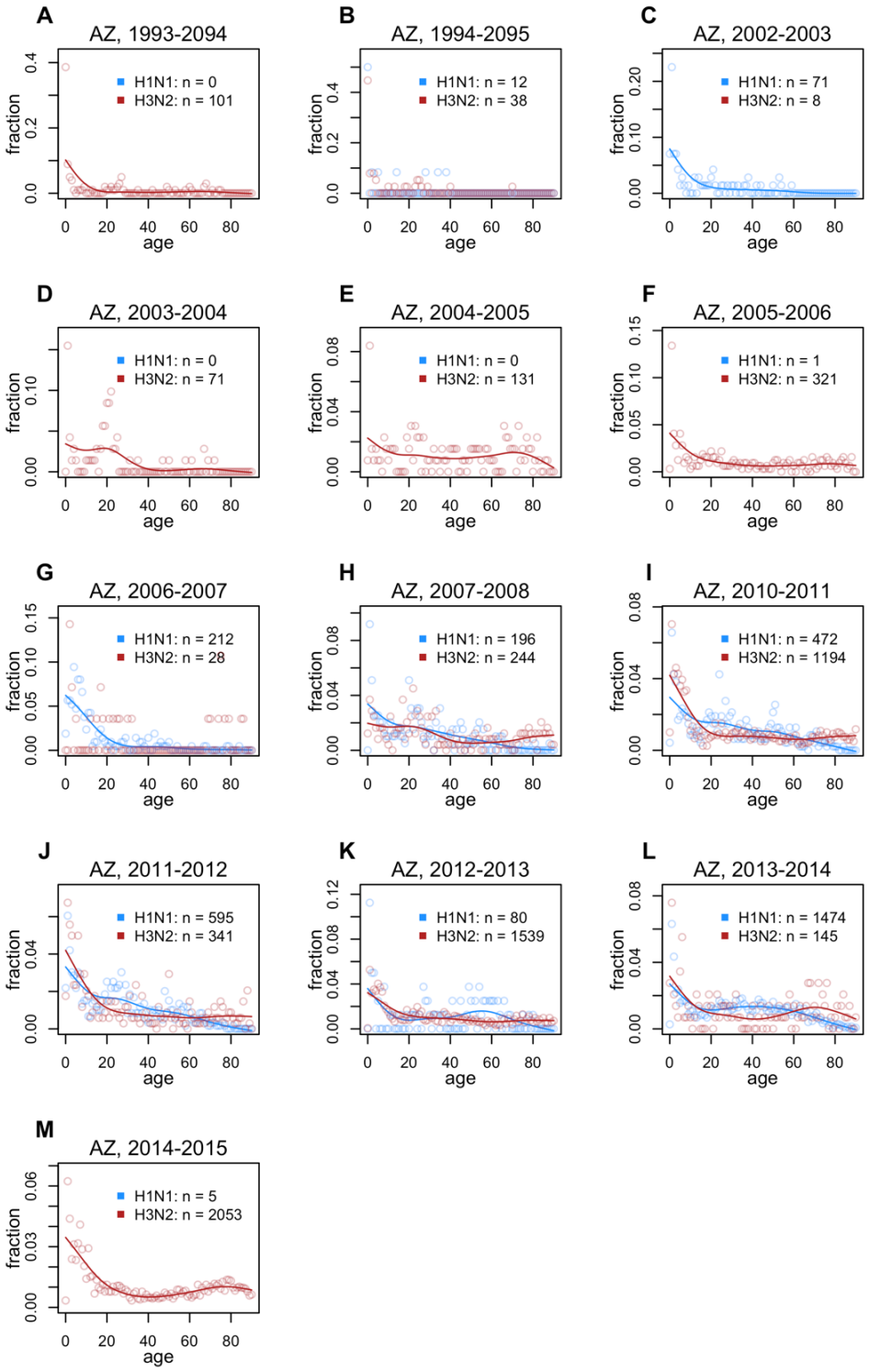

Supplementary Figure 2-S1. ADHS age distributions, all seasons.

Supplement to Fig. 2-2 showing observed age distributions from all influenza seasons. Observed case fractions (points) were only plotted if 10 or more cases of a given subtype were confirmed, to avoid extreme stretching of the y axis. Smoothing splines were only plotted if 50 or more cases of a given subtype were observed, as fits to fewer data points would not have been meaningful.

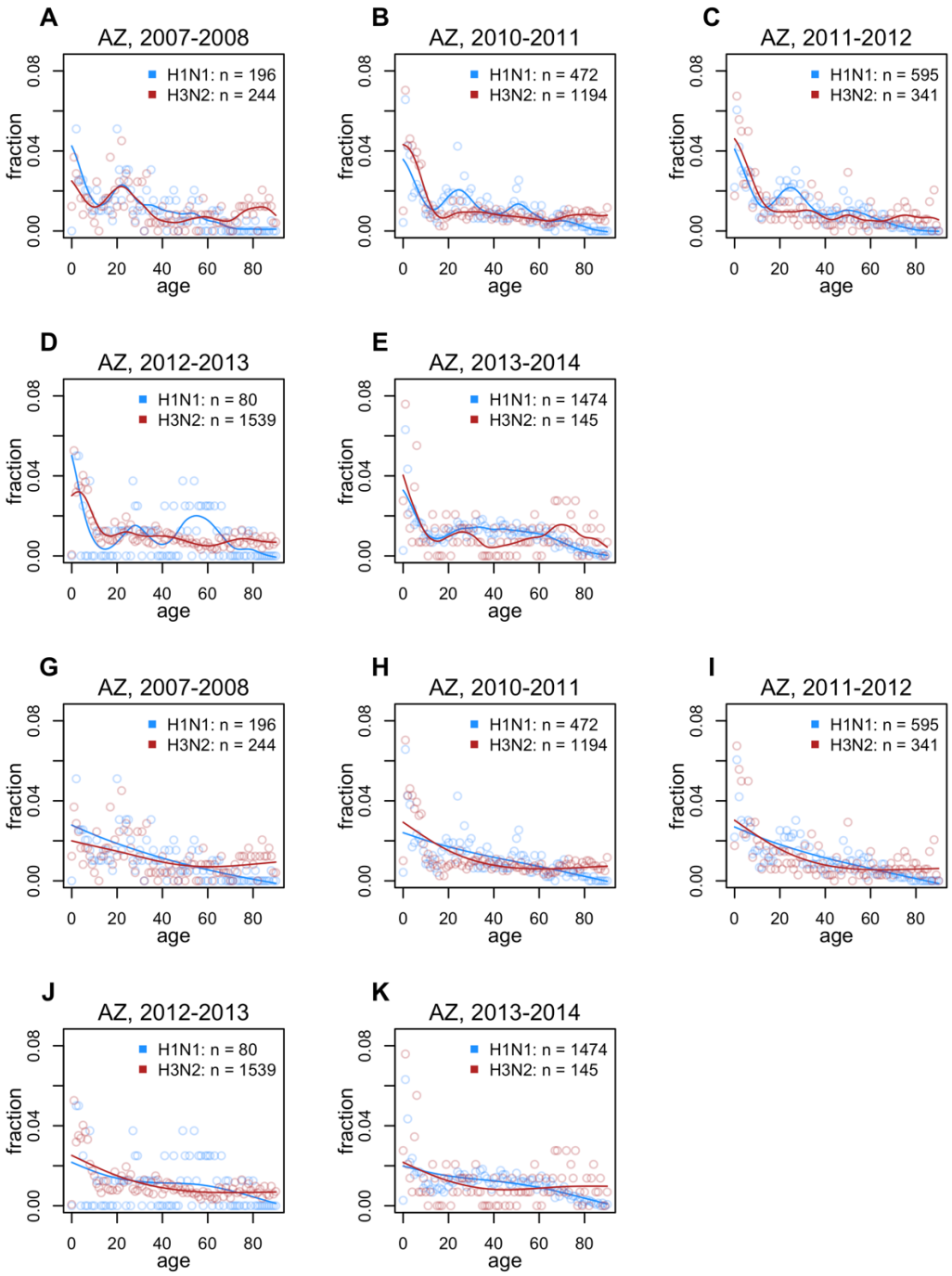

Supplementary Figure 2-S2. Alternate smoothing parameters, AZDHS data.

Supplement to Fig. 2-2, with smoothing parameters chosen to fit splines that are less (**A-F**), or more (**G-L**) smooth than the splines shown in the main text. Differences between H1N1 and H3N2's age-specific impacts remain evident, especially in the oldest cohorts, regardless of smoothness.

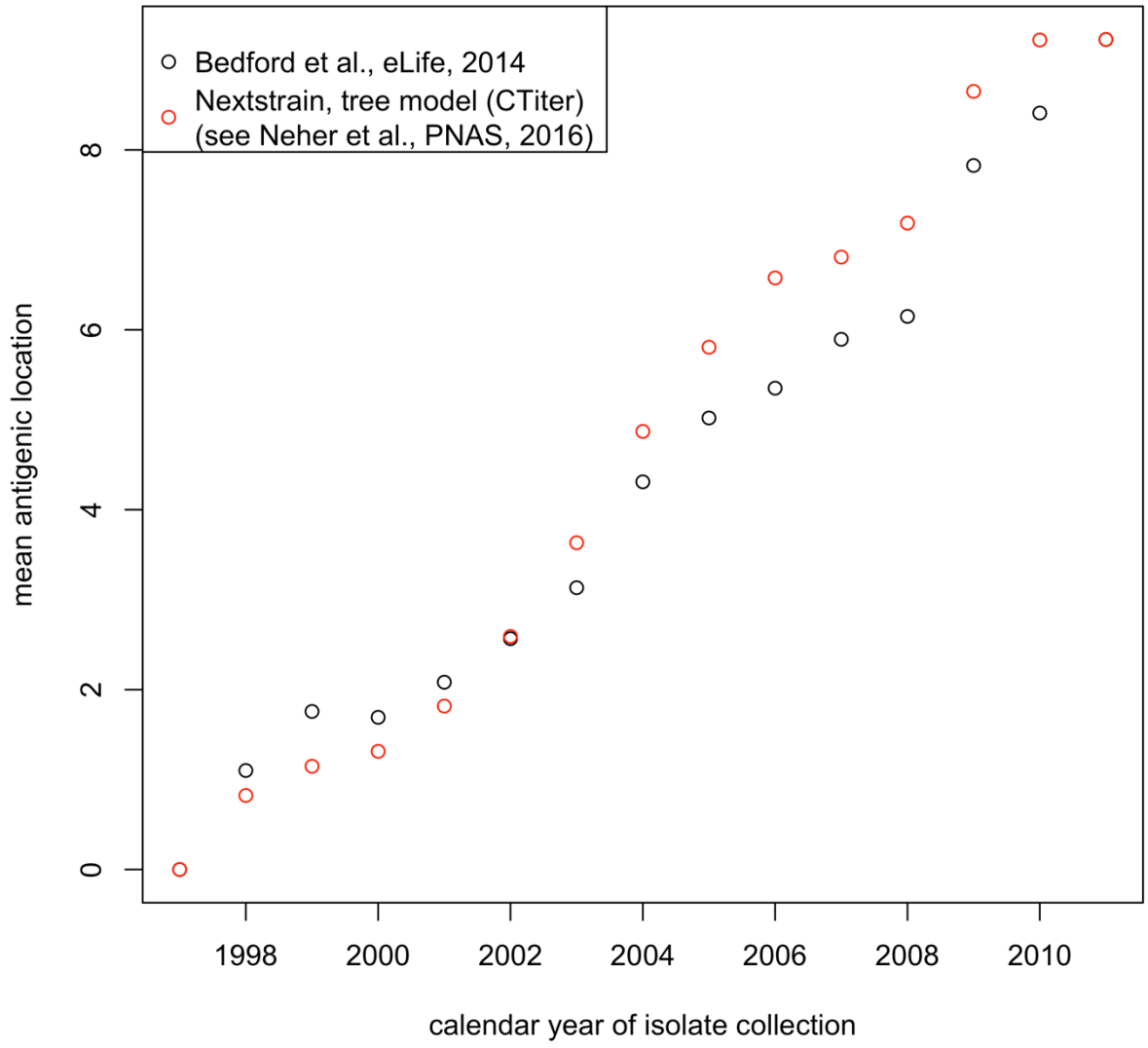

Supplementary Figure 2-S3. Comparison of rescaled antigenic distance estimates from the Bedford et al., and *Nextstrain* datasets.

Points represent average antigenic position of all isolates from a given calendar year.

REFERENCES

1. Francis T. On the Doctrine of Original Antigenic Sin. Proc Am Philos Soc. 1960;104(6):572–8.

2. Lessler J, Riley S, Read JM, Wang S, Zhu H, Smith GJD, et al. Evidence for Antigenic Seniority in Influenza A (H3N2) Antibody Responses in Southern China. PLOS Pathog. 2012 Jul 19;8(7):e1002802.

3. Xu R, Ekiert DC, Krause JC, Hai R, Crowe JE, Wilson IA. Structural Basis of Preexisting Immunity to the 2009 H1N1 Pandemic Influenza Virus. Science. 2010 Apr 16;328(5976):357–60.

4. Hancock K, Veguilla V, Lu X, Zhong W, Butler EN, Sun H, et al. Cross-Reactive Antibody Responses to the 2009 Pandemic H1N1 Influenza Virus. N Engl J Med Boston. 2009 Nov 12;361(20):1945–52.

5. Simonsen L, Spreeuwenberg P, Lustig R, Taylor RJ, Fleming DM, Kroneman M, et al. Global Mortality Estimates for the 2009 Influenza Pandemic from the GLaMOR Project: A Modeling Study. PLOS Med. 2013 Nov 26;10(11):e1001558.

6. Simonsen L, Reichert TA, Miller MA. The virtues of antigenic sin: consequences of pandemic recycling on influenza-associated mortality. Int Congr Ser. 2004 Jun 1;1263:791–4.

7. Ma J, Dushoff J, Earn DJD. Age-specific mortality risk from pandemic influenza. J Theor Biol. 2011 Nov 7;288:29–34.

8. Worobey M, Han G-Z, Rambaut A. Genesis and pathogenesis of the 1918 pandemic H1N1 influenza A virus. Proc Natl Acad Sci. 2014 Jun 3;111(22):8107–12.

9. Gagnon A, Miller MS, Hallman SA, Bourbeau R, Herring DA, Earn DJD, et al. Age-Specific Mortality During the 1918 Influenza Pandemic: Unravelling the Mystery of High Young Adult Mortality. PLoS ONE [Internet]. 2013 Aug 5 [cited 2019 Apr 4];8(8). Available from: https://www.ncbi.nlm.nih.gov/pmc/articles/PMC3734171/

10. Gostic KM, Ambrose M, Worobey M, Lloyd-Smith JO. Potent protection against H5N1 and H7N9 influenza via childhood hemagglutinin imprinting. Science. 2016 Nov 11;354(6313):722–6.

11. Khiabanian H, Farrell GM, George KS, Rabadan R. Differences in Patient Age Distribution between Influenza A Subtypes. PLOS ONE. 2009 Aug 31;4(8):e6832.

12. Budd AP, Beacham L, Smith CB, Garten RJ, Reed C, Kniss K, et al. Birth Cohort Effects in Influenza Surveillance Data: Evidence that First Influenza Infection Affects Later Influenza-Associated Illness. J Infect Dis [Internet]. [cited 2019 May 20]; Available from: https://academic.oup.com/jid/advance-article/doi/10.1093/infdis/jiz201/5485579

13. Lemaitre M, Carrat F. Comparative age distribution of influenza morbidity and mortality during seasonal influenza epidemics and the 2009 H1N1 pandemic. BMC Infect Dis. 2010 Jun 9;10(1):162.

14. Huang QS, Bandaranayake D, Wood T, Newbern EC, Seeds R, Ralston J, et al. Risk Factors and Attack Rates of Seasonal Influenza Infection: Results of the Southern Hemisphere Influenza and Vaccine Effectiveness Research and Surveillance (SHIVERS) Seroepidemiologic Cohort Study. J Infect Dis. 2019 Jan 9;219(3):347–57.

15. Cowling BJ, Sullivan SG. The Value of Neuraminidase Inhibition Antibody Titers in Influenza Seroepidemiology. J Infect Dis. 2019 Jan 9;219(3):341–3.

16. Memoli MJ, Shaw PA, Han A, Czajkowski L, Reed S, Athota R, et al. Evaluation of Antihemagglutinin and Antineuraminidase Antibodies as Correlates of Protection in an Influenza A/H1N1 Virus Healthy Human Challenge Model. mBio [Internet]. 2016 Apr 19 [cited 2019 May 31];7(2). Available from: https://www.ncbi.nlm.nih.gov/pmc/articles/PMC4959521/

17. Wrammert J, Koutsonanos D, Li G-M, Edupuganti S, Sui J, Morrissey M, et al. Broadly cross-reactive antibodies dominate the human B cell response against 2009 pandemic H1N1 influenza virus infection. J Exp Med. 2011 Jan 17;208(1):181–93.

18. Pica N, Hai R, Krammer F, Wang TT, Maamary J, Eggink D, et al. Hemagglutinin stalk antibodies elicited by the 2009 pandemic influenza virus as a mechanism for the extinction of seasonal H1N1 viruses. Proc Natl Acad Sci U S A. 2012;109(7):2573–8.

19. Krammer F. Novel universal influenza virus vaccine approaches. Curr Opin Virol. 2016 Apr;17:95–103.

20. Andrews SF, Huang Y, Kaur K, Popova LI, Ho IY, Pauli NT, et al. Immune history profoundly affects broadly protective B cell responses to influenza. Sci Transl Med. 2015 Dec 2;7(316):316ra192-316ra192.

21. Zost SJ, Wu NC, Hensley SE, Wilson IA. Immunodominance and Antigenic Variation of Influenza Virus Hemagglutinin: Implications for Design of Universal Vaccine Immunogens. J Infect Dis. 2019 Apr 8;219(Supplement_1):S38–45.

22. Grenfell BT, Pybus OG, Gog JR, Wood JLN, Daly JM, Mumford JA, et al. Unifying the Epidemiological and Evolutionary Dynamics of Pathogens. Science. 2004 Jan 16;303(5656):327–32.

23. Henry C, Zheng N-Y, Huang M, Cabanov A, Rojas KT, Kaur K, et al. Influenza Virus Vaccination Elicits Poorly Adapted B Cell Responses in Elderly Individuals. Cell Host Microbe. 2019 Mar;25(3):357-366.e6.

24. Age-specific differences in the dynamics of protective immunity to influenza | Nature Communications [Internet]. [cited 2019 May 6]. Available from: https://www.nature.com/articles/s41467-019-09652-6

25. Miller MS, Gardner TJ, Krammer F, Aguado LC, Tortorella D, Basler CF, et al. Neutralizing Antibodies Against Previously Encountered Influenza Virus Strains Increase over Time: A Longitudinal Analysis. Sci Transl Med. 2013 Aug 14;5(198):198ra107-198ra107.

26. Tesini BL, Kanagaiah P, Wang J, Hahn M, Halliley JL, Chaves FA, et al. Broad Hemagglutinin-Specific Memory B Cell Expansion by Seasonal Influenza Virus Infection Reflects Early-Life Imprinting and Adaptation to the Infecting Virus. J Virol. 2019 Apr 15;93(8):e00169-19.

27. Thompson WW, Shay DK, Weintraub E, Brammer L, Cox N, Anderson LJ, et al. Mortality associated with influenza and respiratory syncytial virus in the United States. JAMA. 2003 Jan 8;289(2):179–86.

28. Bedford T, Riley S, Barr IG, Broor S, Chadha M, Cox NJ, et al. Global circulation patterns of seasonal influenza viruses vary with antigenic drift. Nature. 2015 Jul;523(7559):217–20.

29. Arizona Department of Health Services. 2015–2016 Influenza Summary [Internet]. [cited 2019 May 23]. Available from: https://www.azdhs.gov/documents/preparedness/epidemiology-disease-control/flu/surveillance/2015-2016-influenza-summary.pdf

30. National Notifiable Diseases Surveillance System, Division of Health Informatics and Surveillance, National Center for Surveillance, Epidemiology and Laboratory Services.

MMWR Week Fact Sheet [Internet]. [cited 2019 May 23]. Available from: https://wwwn.cdc.gov/nndss/document/MMWR_Week_overview.pdf

31. Erbelding EJ, Post DJ, Stemmy EJ, Roberts PC, Augustine AD, Ferguson S, et al. A Universal Influenza Vaccine: The Strategic Plan for the National Institute of Allergy and Infectious Diseases. J Infect Dis. 2018 Jul 2;218(3):347–54.

32. Bolker BM. Ecological Models and Data in R. Princeton University Press; 2008. 409 p.

33. Burnham KP, Anderson DR. Model Selection and Multimodel Inference: A Practical Information-Theoretic Approach [Internet]. 2nd ed. New York: Springer-Verlag; 2002 [cited 2019 Apr 16]. Available from: https://www.springer.com/us/book/9780387953649

34. Hadfield J, Megill C, Bell SM, Huddleston J, Potter B, Callender C, et al. Nextstrain: real-time tracking of pathogen evolution. Bioinformatics. 2018 Dec 1;34(23):4121–3.

35. Neher RA, Bedford T, Daniels RS, Russell CA, Shraiman BI. Prediction, dynamics, and visualization of antigenic phenotypes of seasonal influenza viruses. Proc Natl Acad Sci. 2016 Mar 22;113(12):E1701–9.

36. Bedford T, Suchard MA, Lemey P, Dudas G, Gregory V, Hay AJ, et al. Integrating influenza antigenic dynamics with molecular evolution. Losick R, editor. eLife. 2014 Feb 4;3:e01914.

37. Smith DJ, Lapedes AS, Jong JC de, Bestebroer TM, Rimmelzwaan GF, Osterhaus ADME, et al. Mapping the Antigenic and Genetic Evolution of Influenza Virus. Science. 2004 Jul 16;305(5682):371–6.

38. RFA-AI-18-010: Impact of Initial Influenza Exposure on Immunity in Infants (U01 Clinical Trial Not Allowed) [Internet]. [cited 2019 Apr 15]. Available from: https://grants.nih.gov/grants/guide/rfa-files/RFA-AI-18-010.html

39. Morris DH, Gostic KM, Pompei S, Bedford T, Łuksza M, Neher RA, et al. Predictive Modeling of Influenza Shows the Promise of Applied Evolutionary Biology. Trends Microbiol. 2018 Feb 1;26(2):102–18.

40. Cobey S, Hensley SE. Immune history and influenza virus susceptibility. Curr Opin Virol. 2017 Feb 1;22:105–11.

41. Linderman SL, Chambers BS, Zost SJ, Parkhouse K, Li Y, Herrmann C, et al. Potential antigenic explanation for atypical H1N1 infections among middle-aged adults during the 2013–2014 influenza season. Proc Natl Acad Sci. 2014 Nov 4;111(44):15798–803.

42. Rozo M, Gronvall GK. The Reemergent 1977 H1N1 Strain and the Gain-of-Function Debate. mBio. 2015 Sep 1;6(4):e01013-15.

43. Dushoff J, Plotkin JB, Viboud C, Earn DJD, Simonsen L. Mortality due to Influenza in the United States—An Annualized Regression Approach Using Multiple-Cause Mortality Data. Am J Epidemiol. 2006 Jan 15;163(2):181–7.

44. Lewnard JA, Cobey S. Immune History and Influenza Vaccine Effectiveness. Vaccines. 2018 Jun;6(2):28.

45. Gagnon A, Acosta E, Miller MS. Reporting and evaluating influenza virus surveillance data: An argument for incidence by single year of age. Vaccine. 2018 Oct 8;36(42):6249–52.

46. Glezen WP, Keitel WA, Taber LH, Piedra PA, Clover RD, Couch RB. Age Distribution of Patients with Medically-Attended Illnesses Caused by Sequential Variants of Influenza A/H1N1: Comparison to Age-Specific Infection Rates, 1978–1989. Am J Epidemiol. 1991 Feb 1;133(3):296–304.

47. Sagulenko P, Puller V, Neher RA. TreeTime: Maximum-likelihood phylodynamic analysis. Virus Evol [Internet]. 2018 Jan 8 [cited 2019 Apr 12];4(1). Available from: https://www.ncbi.nlm.nih.gov/pmc/articles/PMC5758920/

48. Bogner P, Capua I, Lipman DJ, Cox NJ. A global initiative on sharing avian flu data. Nature. 2006 Aug;442(7106):981.

Chapter 3: Mechanistic dose-response modeling of animal challenge data shows that intact skin is a crucial barrier to leptospiral infection

ABSTRACT

Leptospirosis is a widespread and potentially life-threatening zoonotic disease caused by spirochetes of the *Leptospira* genus. Humans become infected primarily via contact with environmental reservoirs contaminated by the urine of shedding mammalian hosts. Populations in high transmission settings, such as urban slums and subsistence farming communities, are exposed to low doses of *Leptospira* on a daily basis. Under these conditions, numerous factors determine whether infection occurs, including the route of exposure and inoculum dose. Skin wounds and abrasions are risk factors for leptospirosis, but it is not known whether broken skin is necessary for spillover, or if low-dose exposures to intact skin and mucous membranes can also cause infection. To establish a quantitative relationship between dose, route, and probability of infection, we performed challenge experiments in hamsters and rats, developed mechanistic dose-response models representing the spatial dynamics of within-host infection and persistence, and fitted models to experimental data. Results show intact skin is a strong barrier against infection, and that broken skin is the predominant route by which low-dose environmental exposures cause infection. These results identify skin integrity as a bottleneck to spillover of *Leptospira* and underscore the importance of barrier interventions for preventing leptospirosis.

BACKGROUND

Much of the global burden of zoonotic disease is caused by familiar (and often neglected) zoonoses that remain difficult to control [1–3]. In particular, high-burden zoonotic pathogens including many zoonotic protozoans and helminths, nontyphoidal Salmonella spp., Leptospira spp., and Toxoplasma gondii, are difficult to control because they persist well in environmental reservoirs and have ample opportunities for spillover into humans.

For environmentally persistent zoonotic pathogens, a complicated suite of factors governs spillover risk. Understanding the interplay between these factors is a crucial first step toward reducing human incidence. Upstream factors include the level of environmental contamination (in turn governed by disease ecology in the animal host population [4]), and human exposures to contaminated environments. These upstream factors determine the dose and route of exposure, which interact with host physical and immune defenses to determine the probability that exposure leads to spillover [1]. Dose-response models quantify the relationship between the dose and the probability of infection, illness, or death, for a given route of exposure [5–7]. By fitting these models to data from outbreaks or challenge studies, we aim to quantify the infectivity of a given pathogen, and the impact of underlying biological factors such as host traits, susceptibility or immune factors.

Leptospirosis is an emerging and neglected disease caused by spirochetes of the genus *Leptospira.* In severe cases, leptospirosis can cause life-threatening symptoms including renal failure, hemorrhage and respiratory distress [8,9]. Leptospirosis is an environmentally-transmitted zoonosis with a worldwide distribution, but the major burden is in impoverished populations [10]. The spirochete can infect most mammalian hosts, and can be shed chronically

by asymptomatic carriers [8,11]. Humans become infected after exposure to water or soil contaminated by the urine of infected animals, and Norway rats (*Rattus norvegicus,* hereafter referred to as rats) are the primary reservoir species in many urban settings [12,13]. A colony of infected rats can shed on the order of one billion leptospires per day [14], but leptospires do not persist at high densities in soil and water [15]. Thus, low-dose environmental exposures most likely cause the majority of infections.

Skin wounds have been associated with high risk of leptospirosis in humans [16] and in rats [14,17]. In humans, broken skin may directly increase the probability of zoonotic spillover by increasing the susceptibility of human hosts [18]. In rats, broken skin may increase the probability of zoonotic spillover indirectly by helping maintain high prevalence and shedding in a key reservoir species, and in turn, higher levels of environmental contamination [17]. To quantify how skin integrity affects the probability of infection, given exposure to a particular dose, we conducted experimental infections in hamsters and rats, in which we introduced a range of inoculum doses through intact, shaved, or abraded skin, through the conjunctiva, and through the traditional intraperitoneal (IP) route. We then developed mechanistic dose-response models to quantify the protective effect of intact skin as a physical immune barrier against *Leptospira*.

METHODS

Experimental infections

All animals were infected with a virulent clinical isolate from Brazil [14,19], Leptospira interrogans serovar Copenhageni strain Fiocruz L1-130, with 4 and 8 passages in vivo and in vitro, respectively. Leptospires were cultivated in liquid Ellinghausen-McCullough-Johnson-

Harris (EMJH) medium [20] supplemented with 1% rabbit serum. The cultures were kept up to 7 days at 30°C, reaching a mid-log phase between 4 and 5 days of culture. Bacteria were counted in a Petroff-Hausser counting chamber (Fisher Scientific).

Experimental infections were performed with 3-week-old male Golden Syrian hamsters (Envigo). As previously described [21], groups of 3-4 hamsters were inoculated by intraperitoneal (IP) or conjunctival routes using different doses of strain Fiocruz L1-130, ranging from 101 to 108 and from 102 to 108 leptospires, respectively. For infections via the abraded skin route, groups of 4 hamsters were shaved over their flank one day before inoculation. On the day of challenge each animal amongst groups of 4 hamsters was anesthetized with isoflurane in an open-drop method, and an approximately 3-4 cm^2 area of the flank skin patch was abraded by gentle scraping with a surgical scalpel blade enough to damage the epidermis stratum corneum, adopting a methodology previously described [19]. A 50 mL volume of EMJH with the respective dose of leptospires was inoculated over the abraded area, followed by immediate application of a transparent film dressing (Tegaderm, 3M) to cover and keep the inoculum in place for 5 minutes. After removing the dressing, the area was gently washed with distilled water. A similar procedure was performed in groups of 4 hamsters for the “shaved skin”, without the abrading portion, and “intact skin”, without the shaving and abrading. For the latter procedure, the inoculum was performed over the fur on the animal flank.

Experimental infections were also performed using 3-week-old male Wistar rats (Envigo). Groups of 2-3 animals were inoculated by IP route or by abraded skin method as described above, using a dose range of 101 to 108 leptospires.

Hamsters were monitored twice daily, and rats were monitored 3 times per week up to 21-days post-infection. Endpoints in hamsters included signs of disease and death (19). Since infection is asymptomatic and causes persistent renal colonization in rats, we used lipL32-based qPCR [14] to evaluate presence of leptospiral DNA in their urine, as an endpoint. Surviving animals at the end of the experiment or moribund animals presenting with clinical signs of disease were immediately sacrificed by inhalation of CO2. LD50 (Lethal Dose, 50%, in hamsters) and CD50 (Colonization Dose, 50%, in rats) were calculated as described previously [22].

Mechanistic dose-response model

Once an infectious organism contacts a potential host (an event we term "exposure" or "inoculation"), infection is a multi-step process in which the infectious organism must cross physical immune barriers like the skin or mucous membranes (host entry), and then survive attacks from innate or adaptive immune effectors within the host (within-host invasion and persistence). Established dose-response models, such as the exponential and beta-Poisson models [5], treat infection as a one-step process, in which each organism in the inoculum has some probability of surviving both steps and contributing to infection. To study the specific impact of intact skin as a physical immune barrier against host entry, we built on established methods to develop a two-step dose-response model that treated host entry and within-host invasion and persistence as distinct stochastic processes (Figure 3-1).

First, based on the measured bacterial concentration in the inoculum stock solution, the expected number of organisms, d, in each inoculum was known. But the exact number of organisms introduced to the host, D_0, could have been slightly higher or lower than the expected

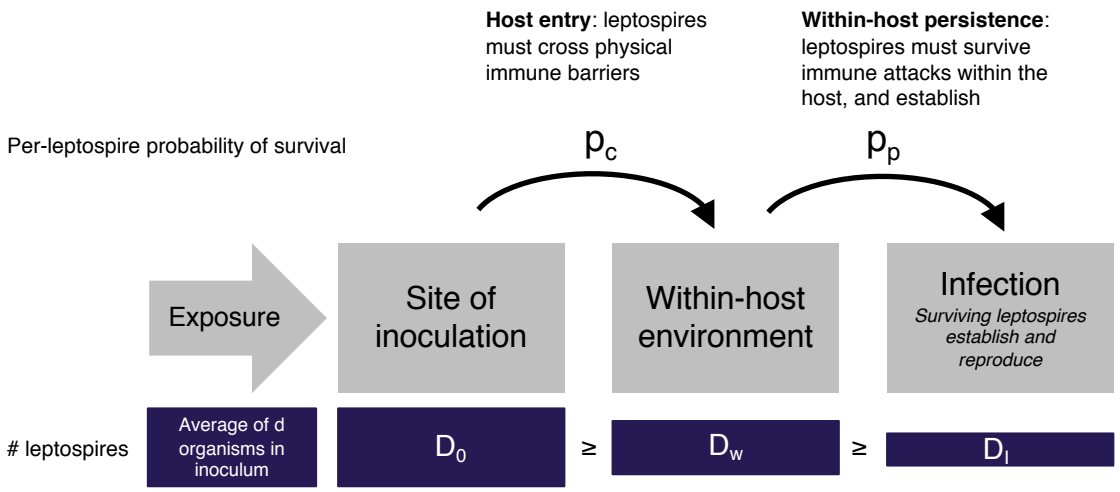

Figure 3-1. Model of infection process.

Organisms introduced via intraperitoneal (IP) inoculation bypass the 'host entry' process. Quantity d is known from the measured concentration of bacteria in the inoculum stock solution. Quantities D_0, D_w and D_I are not observable. The model probabilistically considers all possible values of these unknown quantities.

quantity d, and was not directly observable. Our models assumed the exact inoculum dose, D_0, followed a Poisson distribution with mean d.

Next, we assumed each infectious organism in D_0 had an equal and independent probability, p_c, of crossing physical immune barriers at the site of inoculation, and that D_w organisms successfully reached the within-host environment. Then, we assumed organisms that successfully entered the host had a second fixed and independent probability, p_p, of successfully invading and persisting as part of an established infection. D_I represented the number of organisms that survived both steps and became founders of an active infection. These assumptions imply the number of organisms successfully reaching the within-host environment, D_W, and the number of organisms establishing within the host, D_I, were both distributed binomially, with $P(D_W = k) \sim B(D_0, p_c)$ and $P(D_I = m) \sim B(D_W, p_p)$. We assumed that inoculations via the IP route bypassed physical barriers, such that $D_W = D_0$.

Finally, we assumed infection would occur if one or more organisms survived to establish and reproduce within the host, i.e. if $D_I > 0$. An alternative hypothesis holds that the minimum infecting dose might be greater than one, due to a need for cooperation or collective defense among pathogenic organisms. However, the single-organism hypothesis has received more scientific support than the threshold hypothesis in other systems [5], and infection occurred consistently in IP experiments with expected dose, d, of only 10 leptospires, which definitively rules out the existence of a high threshold for *Leptospira*.

Likelihood for IP inoculation experiments and estimation of p_p

Data from IP inoculation experiments enabled us to estimate p_p independently of the other unknown parameter, p_c. This step was necessary because parameters p_p and p_c occur as a product in the likelihood and hence are not identifiable (equation 6). The probability of infection after IP inoculation with dose d was:

$$P_I(d) = \sum_{D_I=1}^{\infty} \sum_{D_0=D_I}^{\infty} \left[\frac{d^{D_0} e^{-d}}{D_0!}\right] \left[\binom{D_0}{D_I} p_p^{D_I} (1-p_p)^{D_0-D_I}\right] \quad (3\text{-}1)$$

The first bracketed factor describes the Poisson probability that the inoculum contained exactly D_0 organisms, and the second bracketed factor describes the binomial probability that D_I of D_0 organisms survived to initiate infection. Finally, since D_0 and D_I were not observable, we sum across all possible combinations of D_0 and D_I values at which infection could have occurred. The above equation is identical in form to the exponential dose response model, which simplifies as described by Haas, Rose & Gerba [5]:

$$P_I(d) = 1 - e^{-dp_p} \quad (3\text{-}2)$$

We found maximum likelihood estimate (MLE), and 95% profile confidence interval of parameter p_p by fitting to data from IP infection trials. The likelihood was constructed from the binomial probability of observing I_d infected individuals out of N_d trials at a given dose, d:

$$\mathcal{L}\left(I_{dmin}, N_{dmin}, \ldots I_{dmax}, N_{dmax} | p_p\right) = \prod_d \binom{N_d}{I_d} I^{P_I(d)}(1-I)^{1-P_I(d)}$$

(3-3)

Likelihood for other routes of inoculation and estimation of p_c, basic model

After estimating p_p, we found maximum likelihood estimates of parameter p_c for each tested route of inoculation. For non-IP routes of inoculation, the probability of infection was similar to that in equation 1, but added an extra binomial factor to account for the probability of crossing physical immune barriers at the site of inoculation:

$$P_I(d) = \sum_{D_I=1}^{\infty} \sum_{D_w=D_I}^{\infty} \sum_{D_0=D_w}^{\infty} \left[\frac{d^{D_0} e^{-d}}{D_0!}\right] \left[\binom{D_0}{D_w} p_c^{D_w} (1-p_c)^{D_0-D_w}\right] \left[\binom{D_w}{D_I} p_p^{D_I} \left(1-p_p\right)^{D_w-D_I}\right]$$

(3-4)

We simplified equation 4 using a strategy similar to Haas, Rose and Gerba's approach to simplification of the standard exponential dose-response model [5]. First, the equation can be algebraically rearranged as follows:

$$P_I(d) = \sum_{D_I=1}^{\infty} \left[\frac{\left(dp_c p_p\right)^{D_I} e^{(-dp_c p_p)}}{D_I!}\right] \sum_{D_0=D_w}^{\infty} \left[\frac{d(1-p_c)^{(D_0-D_w)} e^{-d(1-p_c)}}{(D_0-D_w)!}\right] \sum_{D_w=D_I}^{\infty} \left[\frac{\left(dp_c\left(1-p_p\right)\right)^{D_w-D_I} e^{-dp_c(1-p_p)}}{(D_w-D_I)!}\right]$$

(3-5)

Above, each bracketed factor is a Poisson density, with means $dp_c p_p$, $d(1-p_c)$, or, $dp_c(1-p_p)$ respectively. The second two Poisson series conveniently sum to 1, and can be removed from the equation. The remaining part, $\sum_{D_I=1}^{\infty}\left[\frac{(dp_c p_p)^{D_I} e^{(-dp_c p_p)}}{D_I!}\right]$, can be re-written as the Poisson probability that D_I takes any value other than 0:

$$P_I(d) = 1 - e^{(-dp_c p_p)} \tag{3-6}$$

We substituted the definition of $P_I(d)$ from Equation 6 into the likelihood given in Equation 3. We then found maximum likelihood estimates and 95% profile confidence intervals of parameter p_c by fitting to data from each tested route of inoculation (intact skin, shaved skin, abraded skin and conjunctiva).

Likelihood for other routes of inoculation and estimation of α, β, mixture model

The basic model introduced above assumed the per-leptospire probability of crossing physical immune barriers at the site of inoculation, p_c, did not vary among individual subjects. This assumption was reasonable for inoculation of intact skin or the conjunctiva, in which there was minimal potential for random, host-to-host variation in the integrity of physical immune barriers. However, even when using a carefully controlled experimental procedure, imperceptible, random variation in the depth of abrasions could have caused host-level variation in the skin's resistance to leptospires. We developed a more complex model (referred to as the

mixture model) to test whether p_c varied meaningfully across hosts with abraded skin. Note that the mixture model is a two-step extension of the established Beta-Poisson dose response model described in [5].

In the basic model, p_c took a single, constant value for all hosts, whereas in the mixture model, probability p_c was treated as a random variable, with values in individual hosts following a Beta distribution, i.e. p_c~Beta(α, β). Fitted parameters α and β determined the shape of this distribution of p_c values, and in turn, characterized the shape of host-to-host variability in the abraded skin's resistance to leptospires. Under the mixture model, the dose-specific probability of infection was:

$$P_I(d) = 1 - \int_0^1 e^{(-dp_c p_p)} \left[\frac{(p_c)^{\alpha-1}(1-p_c)^{\beta-1}}{\mathrm{B}(\alpha,\beta)}\right] dp_c \qquad (3\text{-}7)$$

Above, the bracketed factor is the Beta(α, β) probability density describing the distribution of p_c values. We integrated across all possible p_c values to obtain the total probability of infection. The integral in equation 7 was solved numerically using the integrate() function in R.

The mixture model likelihood followed the same definition as in Equation 3, but with equation 7 specifying $P_I(d)$, and with two free parameters, α and β, replacing the single free parameter p_c.

Code Availability

All data analysis was performed in R [23], and all code used for data cleaning and import, data analysis, parameter estimation, and plotting is freely available at https://zenodo.org/badge/latestdoi/171368954.

RESULTS

Infection experiments

A summary of the animal experiments is provided in Table 3-1, whereas Table 3-S1 presents the full data with corresponding values of LD_{50} and CD_{50}. Our results are consistent with previous findings that *L. interrogans* strain Fiocruz L1-130 has a low LD_{50} (~10 bacteria) (17) when hamsters were infected by the IP route, while the strain had a lower CD_{50} (~10^3 bacteria) than previously reported (10^4 bacteria) when rats were infected by the IP route [24]. Of note, the abraded skin model showed similar results to IP route in hamsters and rats, with LD_{50} and CD_{50} between 10^2 and 10^3 leptospires. In contrast, the strain had an LD_{50} between 10^6 and 10^7 when hamsters were inoculated by the conjunctival route, which was similar to the LD_{50} observed when inoculations were administered on shaved intact skin. Furthermore, a high infecting inoculum dose (10^8 bacteria) was required to cause death in hamsters when inoculations were administered on un-shaved intact skin. Taken together, those results indicated that intact skin is a major barrier against leptospiral infection in both acute hamster and chronic

rat animal models for leptospirosis. Moreover, a simple abrasion of the epidermis reduced the LD_{50} by an average factor of 10^4.

Estimated probabilities of host entry and within-host invasion and persistence

We used data from IP infection trials to estimate p_p, the per-leptospire probability of surviving to establish within the host and contribute to infection, given that the organism had already survived to cross physical immune barriers at the site of inoculation. The maximum likelihood estimates were 0.21 (95% CI 0.12-0.36) in hamsters and 0.07 (95% CI 0.02-0.35) in rats (Table 3-2).

Table 3-1. Experimental outcomes.

		Hamsters			Rats		
Route	Dose	n	lethality	%	n	colonization	%
Intact skin	10^4	4	0	0.0			
	10^6	8	0	0.0			
	10^7	4	0	0.0			
	10^8	8	2	25.0			
Shaved skin	10^4	4	0	0.0			
	10^6	8	2	25.0			
	10^7	4	3	75.0			
	10^8	8	5	62.5			
Abraded skin	10^1	12	5	41.7	3	0	0.0
	10^2	12	8	66.7	5	0	0.0
	10^3	12	10	83.3	2	2	100.0
	10^4				6	6	100.0
	10^6				3	3	100.0
	10^8				4	4	100.0
Conjunctiva	10^2	4	0	0.0			
	10^3	4	0	0.0			
	10^4	8	0	0.0			
	10^5	12	0	0.0			
	10^6	24	9	37.5			
	10^7	20	14	70.0			
	10^8	36	36	100.0			
Intraperitoneal	10^1	24	21	87.5	2	1	50
	$5x10^1$	4	4	100.0			
	10^2	43	43	100.0	6	6	100.0
	$2.5x10^2$	12	12	100.0			
	10^3	19	19	100.0			
	10^4	28	28	100.0	3	3	100.0
	10^6	16	16	100.0	2	2	100.0
	10^8	3	3	100.0	6	6	100.0

Table 3-2. Maximum likelihood parameter estimates.

Route	Model	Parameter	Estimate	95% CI
	Hamsters			
IP	All	p_p	0.21	0.12 - 0.36
Intact	Basic	p_c	1.29 E^{-8}	$2.14E^{-9}$ - $4.17E^{-8}$
Shaved	Basic	p_c	9.54 E^{-8}	$4.57E^{-8}$ – $1.86E^{-7}$
Abraded	Basic	p_c	0.02	0.01 - 0.04
	Mixture	α	0.24	1.2E-3 – 0.95
		β	0.40	1.0E-3 – 8.47
Conjunctival	Basic	p_c	8.43 E^{-7}	$5.25E^{-7}$ - $1.35E^{-6}$
	Rats			
IP	All	p_p	0.07	0.02 - 0.35
Abraded	Basic	p_c	0.02	$1.4E^{-3}$ - 0.03
	Mixture	α	No unique solution*	
		β	No unique solution*	

*As explained in the Supplementary Text, this maximum likelihood estimate was defined as a limit, and did not take a single fixed value. The pair (α=1114.675, β= 50000.00) was used to approximate the MLE in Fig. 2B,D and Fig. 3E.

Next, we estimated p_c, the per-leptospire probability of success in host entry. Exact estimates and confidence intervals are reported in Table 3-2 and Fig. 3-2. Abraded skin showed the weakest resistance to leptospires. The estimated per-leptospire chance of crossing abraded skin was about one in fifty, whereas the estimated per-leptospire chances of crossing any intact barrier were never better than one in a million (conjunctiva), and for intact skin, about one in 77 million.

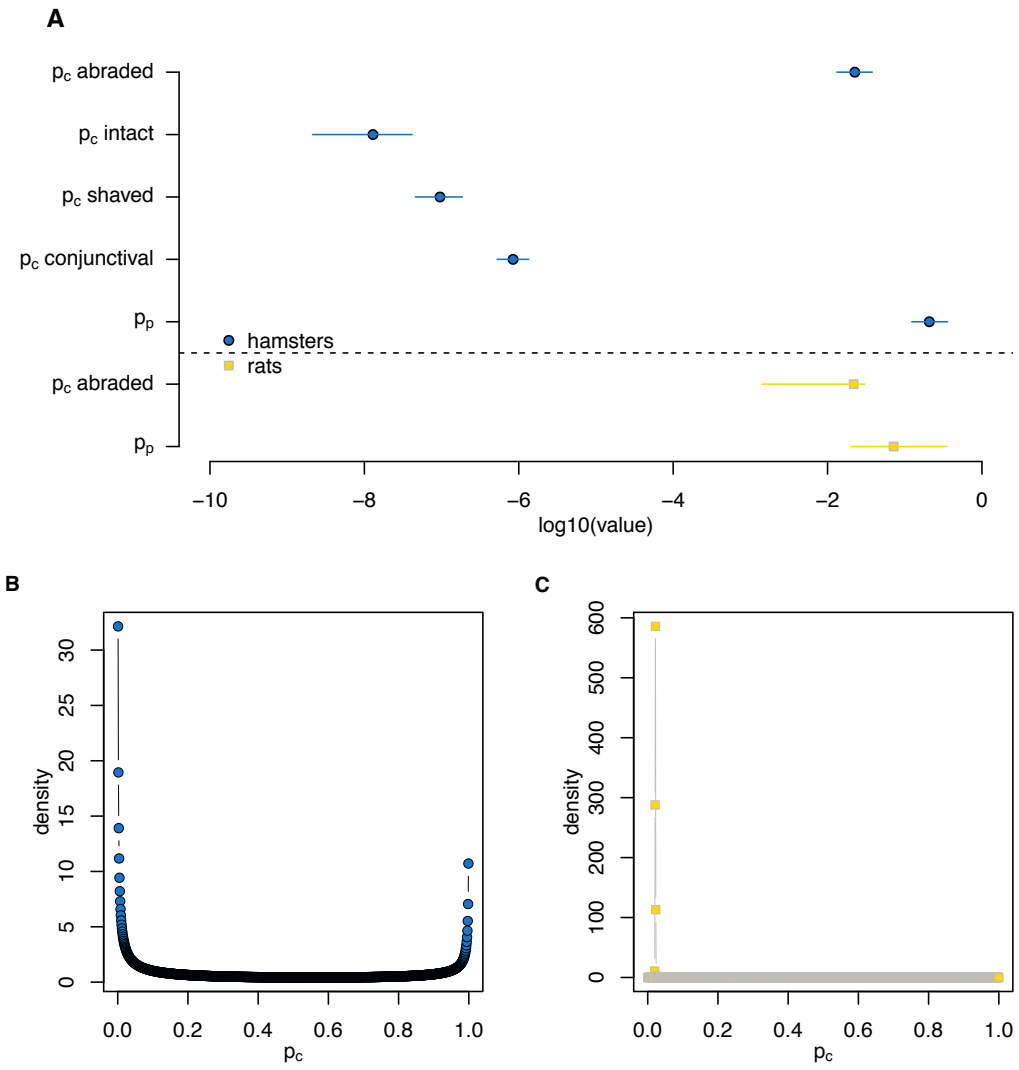

Figure 3-2. Fitted parameter values.

(A) Maximum likelihood point estimates from the basic model of p_p and p_c, with 95% profile confidence intervals. The left-hand side of the x axis represents probabilities closest to 0 (strongest immune barriers). (B) The mixture model returned a fitted distribution of p_c values, instead of a single point estimate. The distribution fitted to data from hamsters was strongly bimodal. (C) The distribution of p_c values fitted to data from rats asymptotically approached a Dirac delta function with all density at p_c= 0.02, corresponding to the estimate from the basic model (Supplementary Text).

Impact of host-specific variability in abrasion depth

Initially, we assumed the per-leptospire probability of crossing the skin or mucosa (p_c) would be roughly equivalent for all individuals of the same species. Thus, p_c took a single, fixed value in the basic model, which provided good fits to most experimental data (Fig. 3-3). The one notable exception was the basic model's poor fit to data from experimental inoculation of hamsters with abraded skin (Fig. 3-3C).

We hypothesized that the poor fit could have arisen if individual hamsters in fact showed different levels of resistance to leptospires, perhaps due to micro-anatomical differences in the depth of their abrasions in the lab. To test this hypothesis, we built a more complicated model (the mixture model), which incorporated the possibility of hamster-to-hamster variability in the abraded skin's resistance to leptospires. This mixture model provided a much better fit to the data (ΔAIC=25.47, Fig. 3-3C).

Within the mixture model, p_c did not take a single value. Instead, the model assumed p_c values followed a probability distribution from the Beta family, whose shape was determined by fitted parameters α and β (Table 3-2). This fitted distribution of p_c values can be interpreted as the distribution of individual hamsters' resistance to leptospires at abraded skin, with values closest to 1 representing the least resistance, (i.e. relatively severe abrasions).

The distribution of p_c values fitted to data from hamsters was bimodal, with the majority of density near extreme values 0 (does not cross abraded skin) and 1 (always crosses abraded skin) (Fig. 3-2B). The shape of this distribution suggests that even the narrow range of individual abrasion severity represented experimentally led to dramatic and measurable variation in the integrity of abraded hamster skin.

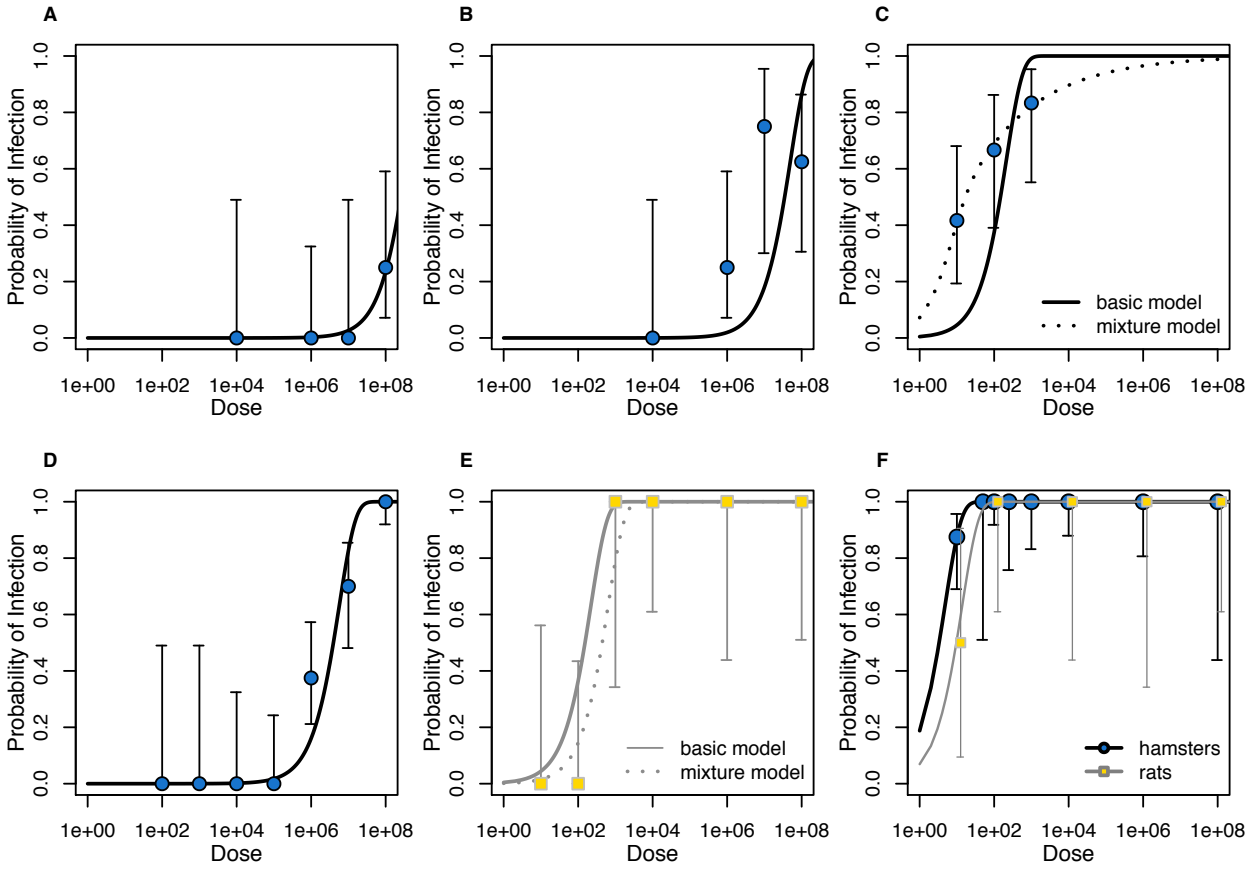

Figure 3-3. Model fits to data.

Curves represent model predicted probabilities of infection for each route of inoculation by dose, based on maximum likelihood estimates. Routes of inoculation and study species: A, hamsters, intact skin, B, hamsters, shaved skin, C, hamsters, abraded skin, D, hamsters, conjunctiva, E, rats, abraded skin, F, both species, IP inoculation. Points and vertical bars represent experimentally observed infection frequencies, and 95% binomial confidence intervals calculated using the Wilson method.

In contrast, data collected in rats showed no support for the mixture model over the basic model. In fact, when fitted to data from inoculation of abraded rat skin, the mixture model asymptotically approached the form of the basic model, with all density in the fitted distribution of p_c values concentrated in a spike near maximum likelihood point estimate from the basic model (Fig. 3-2C, Supplementary Text, Fig. 3-S1). The shape of this distribution suggests there was negligible rat-to-rat variability in abraded skin's resistance to leptospires.

Probabilities of infection given environmental exposure to a known dose

In natural settings, where hosts are likely to experience repeated, low-dose environmental exposures to *Leptospira*, probabilities of infection will depend on the route of exposure, as well as the intensity of environmental contamination. A comparison of probabilities of infection across various doses and various routes of exposure found that the probability that a low-dose exposure ($d<10^5$) causes an infection is ≥10% only when the exposure occurs via abraded skin (Figure 3-4). If exposure occurred via abraded skin, models predicted that an inoculum dose of a single leptospire had ≥10% probability of causing an infection in hamsters, while as few as 50 leptospires had ≥10% probability of causing an infection in rats (Figure 3-4). In comparison, inoculum doses $>10^5$ leptospires were necessary for a conjunctival exposure to have a ≥10% probability of causing an infection, and even higher doses were necessary given exposures at intact skin (Figure 3-4).

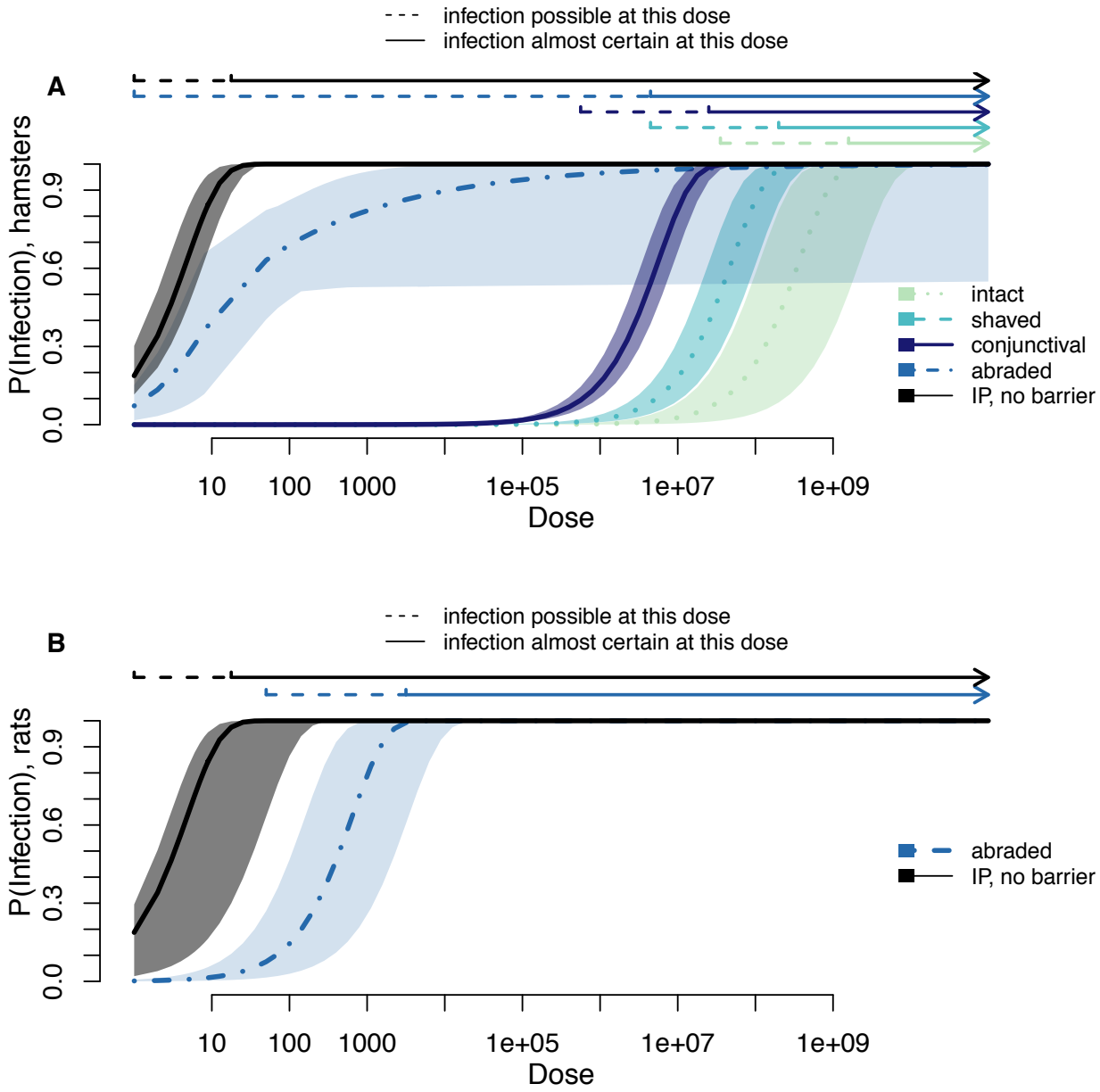

Figure 3-4. Model-estimated probabilities of infection, and confidence intervals for different routes of exposure.

(A) Estimates for hamsters, and (B) rats. The basic model was used to generate estimates, except for abraded skin in hamsters, where the best-fitting mixture model was used. Infection was considered possible for estimated probabilities of infection ≥ 0.1. Infection was considered almost certain for estimated probabilities of infection ≥ 0.975.

DISCUSSION

Our results provide experimental evidence that the relationship between broken skin and leptospirosis risk is causal, corroborating one previous study [19], and for the first time establish a quantitative relationship between dose and infection probability in the presence and absence of skin abrasions. Epidemiological studies previously associated broken skin with increased leptospirosis risk in humans [16] and in rats [14,17]. We showed the per-leptospire probability of crossing physical immune barriers at most sites of inoculation was many orders of magnitude lower than the probability that a leptospire establishes infection once it reaches the within-host environment. Thus, intact skin and mucous membranes are the primary and crucial line of immune defense against *Leptospira* infection.

Intact skin showed strong resistance to leptospires. The per-leptospire odds of crossing intact skin were about one in 77 million (intact skin p_c=1.29E^{-8}, Table 3-2, Fig. 3-2), and a dose of 10^8 leptospires was necessary to cause infection if the inoculum was experimentally introduced to intact skin (Table 3-1). For comparison, when physical immune barriers were absent (IP inoculation) or damaged (abraded skin), experimentally inoculated hosts became infected at doses as low as 10 leptospires. Parameter estimates from mechanistic dose-response models suggested that once leptospires cross physical immune barriers at the site of inoculation, they have excellent odds (better than one in 15, $p_p \geq 0.07$) of persisting within the host and establishing infection. Furthermore, although mucosa is often described as a major point of entry for leptospires, our data showed that conjunctival mucosa is still an efficient barrier, emphasizing the importance of abrasion for leptospiral transmission.

The mixture model, which allowed for individual variation in abraded skin's resistance to leptospires, fit the data from hamsters much better than the basic model. We were surprised to detect any measurable signal of individual variation in the resistance of abraded skin, as our experimental protocol would have allowed only imperceptible, microanatomical differences in abrasion depth across individuals. We suspect that hamsters' innate sensitivity to leptospirosis [25] may have helped magnify the impact of minor differences in abrasion severity. In contrast to results from hamsters, we found no signal of variation in the resistance of abraded skin across individual rats, a more resistant species (Fig. 3-2C, Supplementary Text). Fewer experimental replicates in rats may also have dampened any signal of individual variation.

Given the innate sensitivity of hamsters, we interpret the signal of microanatomical variation in abrasion severity as a model for the impact of real-world variation in the size and depth of wounds in more resistant species. Given the bimodal distribution of fitted p_c values (Figure 3-2B), the immunological impact of wounds does not appear to increase gradually with size and depth. Rather, the shape of the fitted distribution is consistent with the idea that some physiological threshold (in resistant species, perhaps breaking through the dermis, or damaging the microvasculature) distinguishes severe wounds from mild wounds. The fitted p_c distribution included considerable density near 1, indicating that severe wounds can render skin effectively useless as a barrier to infection. Even relatively mild abrasions showed surprisingly little resistance to leptospires. About 59% of p_c density fell at values greater than 0.1, which corresponds to a 10% chance or greater that leptospires successfully crossed abraded skin (Figure 3-2B).

Overall, these findings have clear implications for the epidemiology of zoonotic spillover transmission and the epidemiology and prevention of leptospirosis. If intact human skin is a similarly effective barrier to infection, then exposures at sites of broken skin may cause the majority of naturally occurring infections in humans. *Leptospira* do not survive at high concentration in experimentally inoculated soil or water [15] and recent field studies confirmed that the leptospiral concentration in environmental sources, although ubiquitous, is relatively low [12,13]. Thus, real-world environmental exposures to high doses are likely to be rare.

We propose that together, low infecting doses in the environment and the effectiveness of the intact skin barrier may not only limit the incidence of spillover, but may also limit the severity of infection when spillover does occur. Although leptospirosis can cause severe disease and death, most human cases are mild or asymptomatic [16,26]. In experimental animal models, exposure to higher doses and higher leptospiremia are associated with greater infection severity [21]. Thus, we speculate that the relatively high frequency of mild or asymptomatic cases in humans may be related to the high frequency of low-dose exposures in natural settings. Consistent with this hypothesis, severe cases or outbreaks are associated with floods and natural disasters (e.g., [27,28]), during which the risk of high-dose exposures, or overall exposure frequency may be elevated [12].

These results lend support to existing recommendations that using protective clothing and covering wounds and abrasions may dramatically reduce the risk of infection and symptomatic disease among people at high risk of *Leptospira* exposure [16]. Results suggest that covering even relatively mild skin abrasions may be beneficial. Follow-up studies should explore how

much healing time is required before damaged skin regains the ability to act as an effective barrier against infection.

One limitation of our analysis was that we did not test the impact of repeated or extended exposures. In theory, dose-specific probabilities of infection might be lower with repeated, low-dose exposures if hosts develop adaptive immunity, or up-regulate innate immunity over time [29]. Future experiments in rats, a resistant model for *Leptospira* infection, and a known maintenance species in urban settings, could clarify the impact of repeated exposures on dose-response relationships.

Practical and ethical constraints limited the number of experimental infections we performed, and the range of doses we were able to test. Ideally, the expected doses used in experimental infections would have spanned the full range of infection probabilities, from 0 to 1, for all tested routes of inoculation. However, our experience with these experiments shows that doses lower than 10 leptospires are impractical, and can yield experimental outcomes that are highly variable, biased or difficult to reproduce. We suspect this variability arises because with an expected dose, d <10, stochastic variation in the actual number of organisms in the inoculum has strong impacts on infection outcomes. Furthermore, doses greater than 10^8 are not relevant to the infecting doses found in the environment and responsible for spillover infections. For that reason, we made a technical and experimental decision to use 10 and 10^8 leptospires as standard dose limits in our experiments, which in turn made it difficult to characterize the full dose-response curve for certain routes of infection. However, uncertainty around parameter estimates (Fig. 3-2A) and model-predicted probabilities of infection (Fig. 3-4) was lowest in cases where

experimental data was available across the full range of infection probabilities (conjunctival inoculation in hamsters and abraded skin inoculation in rats).

Another major assumption of this analysis is that IP inoculation is the physiological equivalent of pathogens having penetrated the skin barrier. This assumption was motivated by previous work showing that leptospires introduced to abraded skin, or via IP injection enter the bloodstream and spread with comparable speed and efficiency [19,21]. But differences in the local immune environments, or unmodeled physical barriers such as the peritoneal membrane, could lead IP infection data to slightly overestimate, or to slightly underestimate the value of p_p for other routes of exposure. Hypothetically, a subcutaneous injection experiment could help resolve additional details of the pathogen-host interaction. Importantly, our core finding that abrasions dramatically decrease the skin's resistance to leptospires, follows from the relative estimates of p_c and is robust to this assumption.

This study analyzed new experimental data with a mechanistic mathematical model to quantify dose-infection relationships for *Leptospira interrogans*, a globally important environmentally transmitted zoonotic pathogen. For the first time, our results quantified the importance of intact skin and mucous membranes as immune barriers against infection and show that wounds or abrasions can increase the risk of infection by many orders of magnitude. Our approach builds on a growing trend in microbial dose-response research, where models increasingly aim to incorporate mechanistic details of the within-host infection process [6,29]. It also exemplifies the crucial role of the dose-response relationship in shaping zoonotic spillover risk [1], and highlights the benefit of dissecting barriers to spillover for guiding disease control and prevention measures.

ACKNOWLEDGEMENTS

KG was supported by the Cota Robles Foundation, and the National Institutes of Health (F31AI134017, T32-GM008185). CH was supported by Programa Ciências sem Fronteiras, CNPq, Brazil. AIK was supported by NIH grants R01AI052473, U01AI088752, R25TW009338, R01TW009504, and R01AI121207. JLS was supported by NSF grants OCE-1335657 and DEB-1557022, SERDP RC-2635, and DARPA PREEMPT D18AC00031. The content of the information does not necessarily reflect the position or the policy of the U.S. government, and no official endorsement should be inferred.

ETHICS STATEMENT

All animal protocols were approved by the Institutional Committee for the Use of Experimental Animals, Yale University (protocol # 2017-11424).

DATA, CODE AND MATERIALS

All experimental data, and relevant code are archived at https://zenodo.org/badge/latestdoi/171368954.

REFERENCES

1. Plowright RK, Parrish CR, McCallum H, Hudson PJ, Ko AI, Graham AL, Lloyd-Smith JO. 2017 Pathways to zoonotic spillover. *Nat. Rev. Microbiol.* **15**, 502–510. (doi:10.1038/nrmicro.2017.45)

2. Lloyd-Smith JO, George D, Pepin KM, Pitzer VE, Pulliam JRC, Dobson AP, Hudson PJ, Grenfell BT. 2009 Epidemic Dynamics at the Human-Animal Interface. *Science* **326**, 1362–1367. (doi:10.1126/science.1177345)

3. Maudlin Ian, Eisler Mark Charles, Welburn Susan Christina. 2009 Neglected and endemic zoonoses. *Philos. Trans. R. Soc. B Biol. Sci.* **364**, 2777–2787. (doi:10.1098/rstb.2009.0067)

4. Plowright, Raina. In press. Sampling to elucidate the dynamics of infections in reservoir hosts. *THIS ISSUE*

5. Haas CN, Rose JB, Gerba CP. 2014 *Quantitative microbial risk assessment*. Second edition. New York: John Wiley & Sons, Inc.

6. Haas CN. 2015 Microbial Dose Response Modeling: Past, Present, and Future. *Environ. Sci. Technol.* **49**, 1245–1259. (doi:10.1021/es504422q)

7. Lunn, Tamika. Dose-response and transmission: the nexus between reservoir hosts, environment, and recipient hosts. 2019. *Phil. Trans. B.* In press.

8. Bharti AR *et al.* 2003 Leptospirosis: a zoonotic disease of global importance. *Lancet Infect. Dis.* **3**, 757–771. (doi:10.1016/S1473-3099(03)00830-2)

9. Ko AI, Reis MG, Dourado CMR, Johnson WD, Riley LW. 1999 Urban epidemic of severe leptospirosis in Brazil. *The Lancet* **354**, 820–825. (doi:10.1016/S0140-6736(99)80012-9)

10. Costa F, Hagan JE, Calcagno J, Kane M, Torgerson P, Martinez-Silveira MS, Stein C, Abela-Ridder B, Ko AI. 2015 Global Morbidity and Mortality of Leptospirosis: A Systematic Review. *PLoS Negl. Trop. Dis.* **9**, e0003898. (doi:10.1371/journal.pntd.0003898)

11. Ko AI, Goarant C, Picardeau M. 2009 Leptospira: the dawn of the molecular genetics era for an emerging zoonotic pathogen. *Nat. Rev. Microbiol.* **7**, 736–747. (doi:10.1038/nrmicro2208)

12. Casanovas-Massana A *et al.* 2018 Spatial and temporal dynamics of pathogenic Leptospira in surface waters from the urban slum environment. *Water Res.* **130**, 176–184. (doi:10.1016/j.watres.2017.11.068)

13. Schneider AG *et al.* 2018 Quantification of pathogenic Leptospira in the soils of a Brazilian urban slum. *PLoS Negl. Trop. Dis.* **12**, e0006415. (doi:10.1371/journal.pntd.0006415)

14. Costa F, Wunder EA, De Oliveira D, Bisht V, Rodrigues G, Reis MG, Ko AI, Begon M, Childs JE. 2015 Patterns in Leptospira Shedding in Norway Rats (Rattus norvegicus) from Brazilian Slum Communities at High Risk of Disease Transmission. *PLoS Negl. Trop. Dis.* **9**, e0003819. (doi:10.1371/journal.pntd.0003819)

15. Casanovas-Massana A, Pedra GG, Wunder EA, Diggle PJ, Begon M, Ko AI. 2018 Quantification of Leptospira interrogans Survival in Soil and Water Microcosms. *Appl Env. Microbiol* **84**, e00507-18. (doi:10.1128/AEM.00507-18)

16. Phraisuwan P *et al.* 2002 Leptospirosis: Skin Wounds and Control Strategies, Thailand, 1999. *Emerg. Infect. Dis.* **8**, 1455–1459. (doi:10.3201/eid0812.020180)

17. Minter A, Himsworth CG, Byers KA, Childs JE, Ko AI, Costa F. 2019 Tails of Two Cities: Age and Wounding Are Associated With Carriage of Leptospira interrogans by Norway Rats (Rattus norvegicus) in Ecologically Distinct Urban Environments. *Front. Ecol. Evol.* **7**. (doi:10.3389/fevo.2019.00014)

18. McBride AJ, Athanazio DA, Reis MG, Ko AI. 2005 Leptospirosis. *Curr. Opin. Infect. Dis.* **18**, 376. (doi:10.1097/01.qco.0000178824.05715.2c)

19. Zhang Y, Lou X-L, Yang H-L, Guo X-K, Zhang X-Y, He P, Jiang X-C. 2012 Establishment of a leptospirosis model in guinea pigs using an epicutaneous inoculations route. *BMC Infect. Dis.* **12**. (doi:10.1186/1471-2334-12-20)

20. Johnson RC, Harris VG. 1967 Differentiation of Pathogenic and Saprophytic Leptospires. *J. Bacteriol.* **94**, 27–31.

21. Wunder EA *et al.* 2016 Real-Time PCR Reveals Rapid Dissemination of Leptospira interrogans after Intraperitoneal and Conjunctival Inoculation of Hamsters. *Infect. Immun.* **84**, 2105–2115. (doi:10.1128/IAI.00094-16)

22. Reed LJ, Muench H. 1938 A simple method of estimating fifty per cent endpoints. *Am. J. Epidemiol.* **27**, 493–497. (doi:10.1093/oxfordjournals.aje.a118408)

23. R Core Team. 2018 *R: A Language and Environment for Statistical Computing*. Vienna, Austria: R Foundation for Statistical Computing. See https://www.R-project.org/.

24. Athanazio DA, Silva EF, Santos CS, Rocha GM, Vannier-Santos MA, McBride AJA, Ko AI, Reis MG. 2008 Rattus norvegicus as a model for persistent renal colonization by pathogenic Leptospira interrogans. *Acta Trop.* **105**, 176–180. (doi:10.1016/j.actatropica.2007.10.012)

25. Silva ÉF *et al.* 2008 Characterization of virulence of Leptospira isolates in a hamster model. *Vaccine* **26**, 3892–3896. (doi:10.1016/j.vaccine.2008.04.085)

26. Ashford DA *et al.* 2000 Asymptomatic infection and risk factors for leptospirosis in Nicaragua. *Am. J. Trop. Med. Hyg.* **63**, 249–254. (doi:10.4269/ajtmh.2000.63.249)

27. Togami E, Kama M, Goarant C, Craig SB, Lau C, Ritter JM, Imrie A, Ko AI, Nilles EJ. 2018 A Large Leptospirosis Outbreak following Successive Severe Floods in Fiji, 2012. *Am. J. Trop. Med. Hyg.* **99**, 849–851. (doi:10.4269/ajtmh.18-0335)

28. Agampodi SB, Dahanayaka NJ, Bandaranayaka AK, Perera M, Priyankara S, Weerawansa P, Matthias MA, Vinetz JM. 2014 Regional Differences of Leptospirosis in Sri Lanka: Observations from a Flood-Associated Outbreak in 2011. *PLoS Negl. Trop. Dis.* **8**, e2626. (doi:10.1371/journal.pntd.0002626)

29. Pujol JM, Eisenberg JE, Haas CN, Koopman JS. 2009 The Effect of Ongoing Exposure Dynamics in Dose Response Relationships. *PLoS Comput. Biol.* **5**, e1000399. (doi:10.1371/journal.pcbi.1000399)